

A novel two-chamber setup for containment investigations with special focus on powder dustiness

Dissertation

with the aim of achieving a doctoral degree

at Faculty of Mathematics, Informatics and Natural Sciences

Department of Chemistry

Universität Hamburg

submitted by

Steffen Wirth

Hamburg 2025

Reviewer of the thesis:

Professor Dr. Dr. h.c. Claudia S. Leopold

Professor Dr. Ralph Holl

Thesis defence committee:

Professor Dr. Dr. h.c. Claudia S. Leopold

Professor Dr. Gerrit A. Luinstra

Priv. Doz. Dr. Christoph Wutz

Date of thesis defence:

11.07.2025

The experimental studies and the preparation of this thesis were carried out between November 2018 and May 2025 in the Department of Chemistry at the University of Hamburg, in the division of Pharmaceutical Technology, on the initiative and under the supervision of Professor Dr. Dr. h.c. Claudia S. Leopold.

Conference Contributions and Publications

The following contributions related to this work have been presented at conferences and published in journals.

Conference contributions - poster presentations

Wirth, S., Schöler, M., Leopold, C.S.

Investigation on the dustiness of a binary powder mixture with a newly developed two-chamber setup

12th PBP World Meeting, 2021, Vienna, Austria

Wirth, S., Schöler, M., Leopold, C.S.

Investigation on the dustiness of a binary powder mixture with a newly developed two-chamber setup

13th PBP World Meeting, 2022, Rotterdam, Netherlands

Wirth, S., Schöler, M., Leopold, C.S.

Investigation on the dustiness of a binary powder mixture with a newly developed two-chamber setup

AAPS PharmSci 360, 2022, Boston (MA), USA

List of publications

Title	Journal	Authors	Contribution of the work	Percentage	
A novel two-chamber setup for containment investigations with special focus on the dustiness of pharmaceutical powders depending on the airflow.	Pharmaceutics	Wirth, S.	Project plan, experiments, data analysis, publication	85.0 %	
	(doi.org/10.3390/pharmaceutics14112387)	Schöler, M.	Co-supervisor	2.5 %	
		Brügmann, J.	Technical support	2.5 %	
		Leopold, C.S.	Supervisor	10.0 %	
An investigation on the relationship between dust emission and air flow as well as particle size with a novel containment two-chamber setup.	Pharmaceutics	Wirth, S.	Project plan, experiments, data analysis, publication	87.5 %	
	(doi.org/10.3390/pharmaceutics16081088)	Schöler, M.	Co-supervisor	2.5 %	
		Leopold, C.S.	Supervisor	10.0 %	
Investigations on the dustiness of binary acetaminophen-lactose monohydrate powder blends.	Powder Technology	Wirth, S.	Project plan, experiments, data analysis, publication	85.0 %	
	(doi.org/10.1016/j.powtec.2024.120317)	Schöler, M.	Co-supervisor	2.5 %	
		Brügmann, J.	Technical support	2.5 %	
		Leopold, C.S.	Supervisor	10.0 %	

Table of contents

Conference Contributions and Publications	I
List of publications	I
List of abbreviations	IV
Zusammenfassung	VI
Abstract	VIII
1. Introduction	1
1.1 Relevance of highly potent active pharmaceutical ingredients	1
1.1.1 Highly potent active pharmaceutical ingredients (HPAPIs)	1
1.1.2 Containment	2
1.2 Handling of HPAPIs	2
1.2.1 Risks of dust containing HPAPIs during manufacturing	3
1.2.2 Dust generation during handling of HPAPIs	3
1.3 Fundamentals of containment and exposure control	3
1.3.1 Primary and secondary containment	4
1.3.2 Occupational exposure bands and occupational exposure limits	4
1.3.3 Requirements for the design of containment systems	7
1.3.4 Regulatory and legal requirements for containment systems	7
1.4 Mechanisms and influencing factors of dustiness	8
1.4.1 Material-related factors in dustiness	8
1.4.2 External factors affecting dustiness	11
1.5 Methods for determination of powder dustiness	12
1.5.1 Continuous Drop Test Apparatus	13
1.5.2 Heubach Dustmeter	15
1.5.3 Palas Dustview	16
1.5.4 UNC Dustiness Tester	17
1.5.5 Pros and cons of the methods for dustiness determination	18
1.6 Dustiness measurements in the pharmaceutical industry	19
1.6.1 Principle of IOM samplers	19
1.6.2 IOM samplers in pharmaceutical settings	20
1.7 Surrogate substances for dust analysis and containment validation	22
1.7.1 Reasons for the application of surrogate substances	22

1.7.2 Selection criteria for surrogate substances	23
1.7.3 Examples for surrogate substances	23
1.7.4 Performance tests with surrogates	25
1.7.5 Benefits and limitations of the surrogate substances	26
1.8 Computational Fluid Dynamics (CFD)	27
1.8.1 General applications of CFD in the pharmaceutical context	27
1.8.2 Applications of CFD in the context of containment	28
2. Aim of the work	29
3. Cumulative part of the dissertation	31
3.1 A novel two-chamber setup for containment investigations with special focus on the dustiness of pharmaceutical powders depending on the airflow	31
3.2 Investigation on the relationship between dust emission and air flow as well as particle size with a novel containment two-chamber setup	52
3.3 Investigation on the dustiness of binary acetaminophen - lactose monohydrate powder blends	71
Discussion	83
References	88
Appendix	102
Hazardous materials	102
List of figures	103
List of tables	104
Curriculum vitae	105
Acknowledgements	106
Declaration on oath / Eidesstattliche Versicherung	108

List of abbreviations

ACAM	Acetaminophen
ADC	Antibody-drug conjugate
ADE	Acceptable daily exposure
API	Active pharmaceutical ingredient
BW	Body weight
CFD	Computational fluid dynamics
DTS	Dustiness
EN ISO	European Norm for International Organization for Standardization
Eq.	Equation
EU	European Union
FAT	Factory Acceptance Test
GMP	Good Manufacturing Practice
HEPA	High efficiency particulate air filter
HPLC	High-performance liquid chromatography
HPAPI	Highly potent active pharmaceutical ingredient
ILO	International Labour Organization
IOM	Institute of Occupational Medicine
ISPE	International Society for Pharmaceutical Engineering
LM	α -Lactose monohydrate
LOD	Limit of detection
LOQ	Limit of quantification
OEB	Occupational exposure band

OEL	Occupational exposure limit
PK	Pharmacokinetic adjustment factor
PoD	Point of departure
PR	Pump rate
PTFE	Polytetrafluoroethylene
RP	Reversed-phase
RPM	Revolutions per minute
SAT	Site Acceptance Test
SD	Standard deviation
SEM	Scanning electron microscopy
t	Time
TCS	Two-Chamber setup
TGA	Thermogravimetric analysis
TPE	Thermoplastic elastomer
UFc	Compound uncertainty factor
UNC	University of North Carolina dustiness tester

Zusammenfassung

Die Bedeutung hochpotenter Wirkstoffe, die bereits in geringen Mengen pharmakologisch wirksam sind, hat in den letzten Jahren erheblich zugenommen. Daher sind eine sichere Handhabung und Verarbeitung essenziell, um das Personal, die Patienten sowie die Umwelt zu schützen. In drei Studien wurden mithilfe des neu entwickelten Zwei-Kammer-Systems Strategien zur Reduktion von Staubemissionen bei der Handhabung und Verarbeitung pharmazeutischer Pulver untersucht. Das System umfasst eine Emissions- und eine Detektionskammer, zwischen denen durch Druckdifferenzen verschiedene Strömungsbedingungen simuliert und die Partikelbewegung unter realistischen Bedingungen analysiert werden kann.

In der ersten Studie diente das Zwei-Kammer-System als Konzeptnachweis zur Untersuchung der Beziehung zwischen Staubemissionen und Druckdifferenzen von 0 - 4 Pa. Hierbei wurde mikronisiertes Paracetamol als Surrogatsubstanz verwendet. Eine Erhöhung der Druckdifferenz und der daraus resultierenden Erhöhung der Strömungsgeschwindigkeit führte zu einer signifikanten Reduktion der Staubemissionen. Allerdings reichten 4 Pa nicht aus, um Staubemissionen vollständig zu verhindern. Die Ergebnisse bestätigen die Präzision und Reproduzierbarkeit des Systems und zeigen, dass gezielte Strömungsbedingungen die Staubexposition effektiv reduzieren können.

In der zweiten Studie wurde das System für Druckdifferenzen von bis zu 12 Pa optimiert, um die Staubemissionen weiter zu reduzieren. Paracetamol wurde in sechs unterschiedlichen Partikelgrößen verwendet, um die Schwellenwerte der Druckdifferenzen zu bestimmen, bei denen Staubemissionen nicht mehr nachweisbar sind. Die Untersuchungen zeigten, dass Pulver mit groben Partikeln geringere Staubemissionen verursachten als Pulver mit feinen Partikeln. Die Luftgeschwindigkeit, die direkt aus der Druckdifferenz resultiert, korrelierte stark mit den Staubemissionen. Diese Erkennt-

nisse unterstreichen die Effektivität einer gezielten Drucksteuerung und etablieren das Zwei-Kammer-System als robustes Werkzeug zur Analyse von Strömungsbedingungen und Partikelverhalten. Die Ergebnisse stimmten mit etablierten Richtwerten überein und zeigten, dass gezielte Strömungsbedingungen die Staubexposition signifikant reduzieren können.

Die dritte Studie untersuchte binäre Mischungen aus Paracetamol und Laktose-Monohydrat mit unterschiedlichen Partikelgrößen und Mischungsverhältnissen. Die Mischungen zeigten im Vergleich zu reinem Paracetamol deutlich reduzierte Staubemissionen, insbesondere bei der Kombination von feinem Paracetamol mit grobem Laktose-Monohydrat. Diese Ergebnisse verdeutlichen, dass Partikelgröße und physikalische Eigenschaften der Hilfsstoffe in Pulvermischungen wesentliche Faktoren für die Staubemissionen sind.

Zusammenfassend liefern die Studien bedeutende Erkenntnisse, indem sie aufzeigen, dass durch die gezielte Steuerung von Strömungsbedingungen sowie die systematische Anpassung von Partikelgrößen und Mischungsverhältnissen Staubemissionen signifikant reduziert und der Schutz von Personal, Patienten und Produkten effektiv verbessert werden können.

Abstract

The importance of highly potent active pharmaceutical ingredients (HPAPIs), which exhibit pharmacological efficacy at low concentrations, has significantly increased in recent years. Consequently, safe handling and processing are essential to protect personnel, patients, and the environment. In three studies, strategies to reduce dust emissions while handling and processing pharmaceutical powders were investigated using a newly developed two-chamber setup. The setup comprises an emission chamber and a detection chamber, between which pressure differentials simulate various flow conditions and allow particle movement to be analysed under realistic scenarios.

In the first study, the two-chamber system was employed as a proof of concept to examine the relationship between dust emissions and pressure differentials (0 - 4 Pa). Micronised acetaminophen was used as a surrogate. An increase in pressure differentials and the resulting flow velocity led to a significant reduction in dust emissions. However, a pressure differential of 4 Pa was insufficient to prevent dust emissions completely. The results validate the precision and reproducibility of the system, demonstrating that controlled flow conditions may effectively reduce dust exposure.

The second study optimised the setup for pressure differentials up to 12 Pa. Acetaminophen in six particle size distributions was used to determine the pressure differential thresholds at which dust emissions are no longer detectable. The investigations revealed that powders with larger particles produced lower dust emissions than those with finer particles. Air velocity, directly resulting from the pressure differential, exhibited a strong correlation with dust emission. These findings underscore the efficacy of pressure control and establish the two-chamber system as a robust tool for analysing flow conditions and particle behaviour. The results aligned

with established benchmarks, confirming that controlled flow conditions can significantly reduce dust exposure.

The third study explored binary blends of acetaminophen and lactose monohydrate with varying particle sizes and mixing ratios. Compared to plain acetaminophen, the blends demonstrated markedly reduced dust emissions, particularly when fine acetaminophen was combined with coarse lactose monohydrate. These findings highlight that particle sizes and the physical properties of the components are critical factors influencing dust emissions.

In summary, the studies provide valuable insights, showing that control of flow conditions, along with systematic adjustments of particle sizes and mixing ratios, may significantly reduce dust emissions, thereby enhancing the protection of personnel, patients, and products.

1. Introduction

1.1 Relevance of highly potent active pharmaceutical ingredients

1.1.1 Highly potent active pharmaceutical ingredients (HPAPIs)

In recent years, the application of highly potent active pharmaceutical ingredients (HPAPIs) has attracted increasing interest in the pharmaceutical industry. HPAPIs are substances which may exert pharmacological effects on the human body because of their high potency, even in very small quantities [1–5]. They play an important role in modern therapeutic approaches and are applied throughout various therapeutic fields, such as oncology, neurology, endocrinology, and immunology. Typical examples are cytostatics, hormones, immunomodulators, kinase inhibitors, and antibody-drug conjugates (ADCs) [6–11]. Even HPAPIs that are still at the development stage play a crucial role in offering new therapeutic options [2,8,12].

However, the high pharmacological potential of HPAPIs presents considerable challenges. Even very small quantities may already cause unintended pharmacological effects and pose a significant health risk to the personnel involved in handling, present a hazard to patients because of possible cross-contamination, and negatively impact the environment. For this reason, the maximum possible care is required when processing HPAPIs and pharmaceutical manufacturing facilities need to be specially designed to prevent these hazards [1–3,5,7,13–16]. In addition, maintaining cost-efficient processes is an important factor. HPAPIs are often very expensive, with the loss of small quantities representing significant financial problems for the pharmaceutical manufacturer. Thorough manufacturing management and the implementation of efficient systems to prevent substance losses are therefore crucial for ensuring both product quality and profitability [2,3,5,13,17].

1.1.2 Containment

The term ‘containment’ refers to measures that reduce the spread of highly potent substances like HPAPIs. Special containment systems effectively minimise these risks in the event of possible exposure. Containment systems inhibit the release of HPAPIs into the surrounding environment, thereby minimising potential hazards associated with the health and safety of the operators and personnel [5].

Protective measures such as pressure differentials and air filtration systems for production processes and access restrictions prioritise safety in the manufacture of dosage forms and ensure a safe production environment [6,15,18–22]. The number of protective measures and the extent of protection depend on the potency and toxicity of the processed active pharmaceutical ingredients (APIs). Highly potent APIs require more demanding measures than less potent substances [5].

Interestingly, completely closed systems are difficult to realise: with modern analytical methods, even very low residues outside the protected areas are detectable [5]. The increasing number of HPAPIs underlines the importance of robust containment measures and the need for the permanent development of advanced containment concepts and improvement of safety standards. Such progress is required to effectively address the challenges associated with the handling of these highly potent substances [2,5,16,23].

1.2 Handling of HPAPIs

The safe handling of HPAPIs is an essential requirement to minimise the generation and spread of airborne particles during manufacturing, processing, or transport. The manufacturing of solid dosage forms typically involves the continuous generation of dust [16,18,19,24]. A containment system is crucial to maintain a controlled environment, preventing particle release and ensuring safe operations [20,21].

1.2.1 Risks of dust containing HPAPIs during manufacturing

Pharmaceutical dust is typically generated during mechanical processing such as transferring, grinding/pulverising, blending, granulating, and tableting of powder formulations [3,25–31]. Dust generation is a particularly critical issue with HPAPIs, as airborne particles are typically dispersed inadvertently and may enter the respiratory tract and thus the human body through inhalation [16,32–34]. In addition to inhalation exposure, dermal exposure may occur if HPAPIs are handled, which may also pose a hazard risk to the personnel [4,6,18,35,36].

1.2.2 Dust generation during handling of HPAPIs

The development of safe manufacturing processes requires special consideration when handling HPAPIs [16]. A profound insight into the mechanisms of dust generation and their multiple influencing factors is crucial. This knowledge enables a more precise risk assessment and the development of effective strategies to reduce dust emissions and ensure safe working and production conditions when working with HPAPIs [19].

1.3 Fundamentals of containment and exposure control

Containment is an integral part of quality management, which focuses on the systematic identification, control and communication of risks related to product quality [5,37–40]. European Union (EU) directives as well as national and international regulations, including the recommendations of the International Labour Organization (ILO), consider containment as essential for occupational health and safety. Effective containment ensures compliance with GMP (Good Manufacturing Practice) and consequently the safety of manufactured products [5,39,41,42].

1.3.1 Primary and secondary containment

The manufacturing of dosage forms containing high potency APIs requires coordinated strategies and measures to realise the requirements of a safe and effective manufacturing environment. These measures may be divided into two categories: primary and secondary containment measures [5].

Primary containment measures comprise the actual production equipment and include isolators, glove boxes and closed reactors that create physical barriers to prevent exposure at the source of airborne particles. Secondary containment measures provide an additional level of protection by ensuring the safety of the environment, implemented by facility pressurisation, single-pass airflow and high efficiency particulate air (HEPA) filtration [1,5,39,43–45]. In particular, the progress of isolator technologies has improved the precision and safety of such systems, making the handling of fine particles which show a high tendency to levitate possible [1].

1.3.2 Occupational exposure bands and occupational exposure limits

The occupational exposure bands (OEBs) and occupational exposure limits (OELs) are used to ensure safe handling of HPAPIs [38,46–49].

The OEBs characterise the toxicity potential of a drug substance [14]. They enable a simplified classification based on drug toxicity and are usually ranked on a scale of 1 - 5 or 1 - 6 [5,38,46]. OEBs serve as a categorical framework that classifies drug substances from low toxicity (OEB 1) to very high toxicity (OEB 5 or 6). The OEB classification helps to define appropriate containment measures, from standard precautions for low-risk drug substances to completely closed systems for high-risk APIs [20,38,39].

In contrast, OELs represent specific limit values that indicate which concentration of an active airborne API is considered safe over a defined time period, typically over

8 hours. These values are derived from toxicological and pharmacokinetic data as well as safety aspects and are specified in micrograms per cubic meter ($\mu\text{g}/\text{m}^3$) [37].

OELs may be as low as a few ng/m^3 for extremely hazardous APIs, reflecting their extreme toxicity and the resulting hazard risk [16,40,42].

The OEL is defined by the following equation:

$$\text{OEL} = \frac{\text{PoD} \cdot \text{BW}}{\text{UF}_c \cdot \text{PK} \cdot V} \quad (\text{Eq. 1})$$

where PoD stands for the point of departure: threshold between no effect and adverse effect ($\mu\text{g}/\text{kg}/\text{d}$); BW for body weight (kg); UF_c is the compound uncertainty factor: dimensionless factor incorporating uncertainties and variabilities, including inter- and intraspecies differences, extrapolation, and data quality; PK is the pharmacokinetic adjustment factor which includes the dosing path and the duration of exposure; and V is the volume of inhaled air per one day (m^3/d). The equation shows that even the smallest quantities of highly potent substances require strict control measures [5,11,38,50,51].

Because for many newly developed APIs, no specific OEL values exist, they are categorised based on OEBs. OEBs allow a classification of APIs into five categories which are summarised in Table 1 [5,40,52–54]:

Table 1: OEB classification system (modified from [5]).

OEB categories	OEL	Effect
OEB 1	$> 1000 \mu\text{g}/\text{m}^3$	Very low pharmacologic and toxic effect
OEB 2	$100\text{-}1000 \mu\text{g}/\text{m}^3$	Low pharmacologic and toxic effect
OEB 3	$10\text{-}100 \mu\text{g}/\text{m}^3$	Medium pharmacologic and toxic effect
OEB 4	$1\text{-}10 \mu\text{g}/\text{m}^3$	High pharmacologic and toxic effect
OEB 5	$< 1 \mu\text{g}/\text{m}^3$	Very high pharmacologic and toxic effect

APIs classified in OEBs 4 and 5 require the most rigorous protective measures, including closed systems and supplementary safety precautions. The concept of OEBs facilitates the allocation of safety measures, especially for substances without detailed toxicological data [5].

Another parameter for evaluating the work with potentially hazardous drug substances is the Acceptable Daily Exposure (ADE). The ADE values refer to a drug dose specific to an API that poses no significant risk for harmful effects, even with a daily exposure over the entire lifetime. In contrast to the OEL, which specifies the highest permitted concentration of a drug substance in the air at the workplace, the ADE describes the maximum daily dose of a drug substance that a person may absorb without health risk [51,55–57].

The ADE is calculated as shown below:

$$\text{ADE} = \frac{\text{PoD} \cdot \text{BW}}{\text{UF}_c \cdot \text{PK}} \quad (\text{Eq. 2})$$

For the abbreviations, please refer to Equation 1 [55,56,58].

In Figure 1, the relationships between the OEB categories and their corresponding OELs are illustrated. The ADEs, derived from the OELs, are also included in the figure.

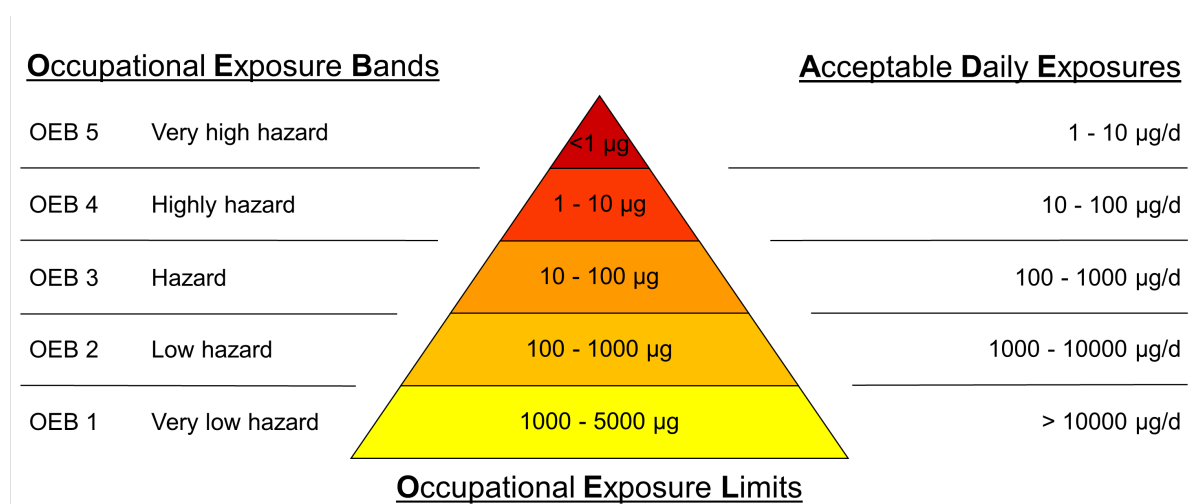


Figure 1: Overview of OEBs, OELs and ADEs and their relationship (modified from [59]).

1.3.3 Requirements for the design of containment systems

HPAPIs are accompanied by significant challenges to safety measures and quality assurance during production. Their low OELs resulting from their high potency require strict containment measures to minimise risks from inhalation, dermal contact or accidental ingestion [43,60–64]. Appropriate facility design includes measures such as negative pressure systems and advanced cleaning technologies [1,39,65].

Moreover, cross-contamination is a critical issue in multi-purpose facilities where shared equipment and processes increase the risk of exposure. Single-use technologies, such as single-use bioreactors and pipework systems, may significantly reduce this risk while simplifying cleaning and validation processes [5,39,43,44,66]. Additionally, robust ventilation systems need to be integrated in these facilities, as airborne particles are a primary concern when handling high-potency powders [39,66].

1.3.4 Regulatory and legal requirements for containment systems

Compliance with the EU GMP guidelines and international standards, such as the ILO recommendations, is essential for safe handling of HPAPIs [5,39]. These guidelines and standards emphasise a hierarchy of controls, prioritising technical containment measures over organisational interventions [1,39,51,65].

A detailed risk analysis based on toxicity data and exposure limits such as OELs and ADEs provides the basis for suitable protective measures (see Chapter 1.3.2). Closed systems such as isolators and glove boxes, which create effective physical barriers and prevent human contact with hazardous substances, are of high priority [39,43].

Validation and testing of these protective systems on a regular basis is crucial to guarantee their effectiveness [5,39,42]. Organisational measures, such as employee training and standardised work instructions as well as the provision of suitable protective equipment for the personnel and clearly defined responsibilities in

emergency plans are necessary to be prepared for potential incidents. Careful implementation and periodic review of these requirements are needed to ensure workplace safety and fulfil the high regulatory standards [5,19,39,43,57].

1.4 Mechanisms and influencing factors of dustiness

Dust generation is a crucial issue in terms of safety, particularly if handling HPAPIs. The dustiness (DTS) is the tendency of a powder to generate airborne particles and describes their quantity and distribution during handling or processing. As already mentioned, DTS poses a risk to the health of personnel, product quality, and the environment if the dust contains highly potent ingredients [21,67–69]. It is fundamental for the assessment of potential hazards during the manufacturing and development of solid dosage forms [69–71].

The factors that influence dust generation may be divided into material-related and external factors. Material-related factors include particle size and distribution, particle shape, cohesiveness, true density, sample mass, and residual moisture content [5,72–79]. External factors include mechanical stimuli or relative humidity [21,61,76,80,81]. An accurate assessment of the DTS is crucial to identify potential hazards during manufacturing at an early stage and to develop preventive measures [6]. This includes the selection of suitable production processes and manufacturing environments to ensure personnel safety and compliance with regulatory requirements [47,51].

1.4.1 Material-related factors in dustiness

The physicochemical properties of pharmaceutical powders are important determinants of their DTS. Factors such as particle size, particle size distribution, and particle shape significantly contribute to dust generation [67,74–78,80,82–86]. The particle size influences both the binding and separating forces that are decisive for the release and spread of dust. Binding forces such as capillary and van der Waals forces

depend on the particle size. Similarly, the forces required for separation are also influenced by the particle size. The particle size distribution is of particular interest as it directly affects the tendency to generate dust and to influence the DTS during manufacturing [32,61,77,80,87–89]. The shape and surface structure of particles also significantly influence DTS and the flowability of a powder. Spherical particles tend to generate less dust, while irregular and angular particles may generate more dust due to a higher abrasion tendency. At the same time, irregular particles reduce flowability and increase friction. Irregular particles often adhere more strongly to each other, releasing less dust, while angular particles generate more dust because of weaker binding points. Therefore, the combination of size, shape and surface characteristics determines the DTS and the flowability of a powder [61,82,84,86,87,90–94].

The bulk density of a powder also has a significant influence on DTS. Powders with a low bulk density have a higher tendency to disperse into the air, which leads to higher dust generation. Densified powders show different patterns of dustiness over time, which provide clues to the underlying mechanisms of dust generation and are relevant for assessing the exposure risk. The true powder density also influences how long particles remain airborne. Therefore, the bulk density should be considered as a fundamental factor in assessing dust generation [61,95,96].

The moisture content of a powder also significantly influences dust generation. Higher moisture levels promote the generation of a hydration layer and capillary bridges between the particles, which may increase coherence. These hydration layers and capillary bridges are much stronger than van der Waals or electrostatic binding forces and may thus significantly reduce dust generation. The moisture content is, therefore, a critical parameter that should be precisely adjusted to control dust generation [32,61,80,97].

Similar to the previously mentioned material-related properties, the sample mass also has a significant impact on the generation of dust from pharmaceutical powders. Larger sample quantities may initially lead to higher dust release as more particles are brought in motion. However, above a certain mass, dust generation often decreases again, which may be attributed to the increasing densification of the powder [98]. It has been shown that the relationship between sample mass and dust generation is not linear and depends on external influencing factors such as the relative humidity, the mechanical stimuli, and the material properties [61,99]. These should also be regarded as relevant parameters for controlling dust generation and have to be considered when assessing exposure risks.

The cohesiveness of a powder describes the strength of the bonds between particles, which are created by mechanisms such as capillary bridges, solid-state bridges, van der Waals forces or electrostatic interactions [100–102]. A pronounced cohesiveness often leads to less dust generation, as the particles are more strongly bound together and have a lower tendency to disperse into the air. This parameter is influenced by several material properties including moisture content, particle size, sample mass, and melting temperature. Therefore, cohesiveness should be considered as another factor influencing dust generation [61,88]. The cohesiveness of a powder is an important factor, as it defines the strength of the particle bonds and their stability against external influences and thus affects DTS.

The numerous material-related factors involved in dust generation demonstrate that this process is complex. A profound insight into these influencing factors is essential to evaluate the risks of dust generation when handling HPAPIs and to develop suitable measures for risk reduction [61]. Optimisation of material properties such as adjusting the particle size and/or the moisture content, may significantly influence DTS [33,80,87,88].

1.4.2 External factors affecting dustiness

The generation of dust during the handling of pharmaceutical powders is not only influenced by material-related factors but also by external factors [21,61,80,81,88].

The transfer of mechanical energy into powders significantly influences dust generation. Powders usually consist of primary particles that may aggregate or agglomerate [60,61]. The transferred mechanical energy, which exerts forces on the primary particles, causes their release from powders, and at higher energy, their separation from the powder aggregates and sometimes mechanically weak agglomerates, resulting in the generation of dust [61,103]. The separation forces must overcome the binding forces present within the powder. The higher the energy input, the more particles may be released. Even fragmentation of particles may occur if very high mechanical energies are transferred to the powder, potentially leading to the crushing of primary particles, which may subsequently result in an altered DTS [61,104,105].

As mentioned in Chapter 1.4.1, DTS is influenced by van der Waals forces, electrostatic interactions, and capillary forces [61]. Under conditions of high humidity, capillary forces may become more important as humidity reinforces the coherence between the particles [61,106]. Humidity changes may also influence the electrostatic charges between the particles by increasing or decreasing their charge, thus changing the mutual attraction between the particles [107–109]. The humidity of the environment also influences van der Waals forces and contributes to the binding forces within a powder and consequently to the DTS [100,110]. The strength of these binding forces is determined by properties such as particle size, surface structure and material composition. The interplay of mechanical stress and binding forces determines how much dust is released when a material is handled [67,94].

Technical measures such as the adjustment of humidity and temperature may also allow the management of dust generation in the event of exposure [76,97].

1.5 Methods for determination of powder dustiness

Different devices have been developed to measure the DTS of powders, thereby quantifying the dust particles released if powders are exposed to mechanical stress. Moreover, these devices allow a simulation of the particle release from powders under real conditions during their handling [61,111]. For this purpose, a defined quantity of powdery material is subjected to a mechanical force for a specified period [21]. The aim is to overcome the binding forces between the particles and to quantify the dust released into the air. Particular attention has to be paid to the capture of primary particles, even of those that are loosely bound to aggregates and agglomerates, while deagglomeration as well as the fragmentation of particles should be avoided [21,61,103,112]. For a representative dust measurement, it is important to ensure that the amount of transferred energy corresponds to typical industrial processes and that it is sufficient to aerosolise the primary particles of the powder [111]. At the same time, dustiness tests need to be carried out under controlled environmental conditions to minimise external interferences and to guarantee high reproducibility [61,81].

In Table 2, a variety of methods and devices for measuring dust emission are listed, which may be divided into the following four categories [61,113].

Table 2: Overview of methods and devices for measuring dust emission.

Method	Description	Examples
Mechanical dispersion [114–116]	Particle release occurs through mechanical effects (vibration, rotation)	Rotating drum, (e.g. Heubach Dustmeter), vortex shaker
Gravity dispersion [80,117–121]	Dust release through free fall of powder (gravity effects)	Continuous drop tester Palas Dustview
Gas dispersion [105,122,123]	Particle dispersion by rising air currents (suspension, distribution)	Venturi dustiness tester
Resuspension chamber [124]	Release of dust during continuous material flow	Special resuspension chambers

Versatile devices even allow a combination of the listed methods. The choice of the most suitable method depends on the material's properties and the type of powder processing [61,105].

1.5.1 Continuous Drop Test Apparatus

In the EN 15051 of European Standards, the Continuous Drop Test Apparatus is described as a standardised technique under Reference Test Method B [21,24,89,125].

In Figure 2, the apparatus is shown in which powder is continuously conveyed from a sample tank through a metering device into a vertically oriented drop tube.

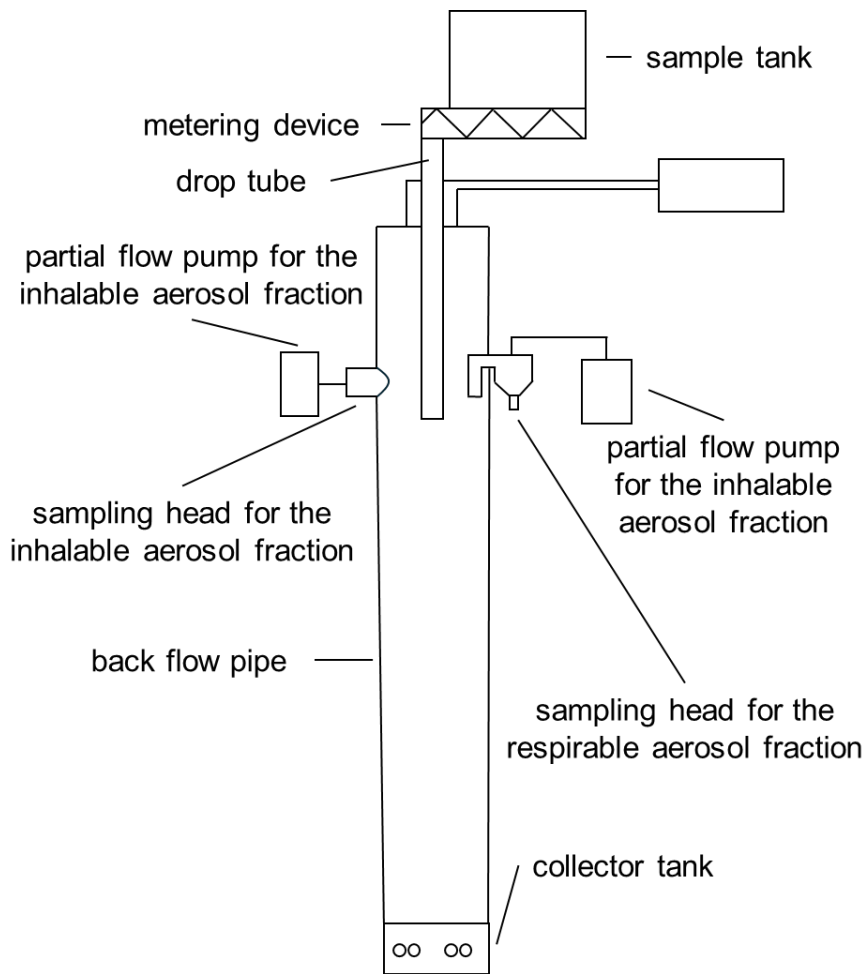


Figure 2: Schematic illustration of the Continuous Drop Test Apparatus [24].

Simultaneously, air is drawn from the bottom of a surrounding back flow pipe, creating an upward movement of the powder, thereby carrying the released dust into the sampling system. In this back flow pipe, a constant flow velocity of 0.05 m/s is preset [89,125]. As the powder falls, it is atomised by the air flow, thereby generating airborne particles, which are quantified by analytical methods [24,125]. The released dust is separated into two fractions, an inhalable fraction (airborne particles with a mean aerodynamic diameter $< 100 \mu\text{m}$) and a respirable fraction (mean aerodynamic particle diameter $< 4 \mu\text{m}$), each of which being collected by two calibrated pumps and subsequently quantified by analytical methods [125,126]. The sampling system consists of two different sampling heads, each equipped with a filter, one for the inhalable fraction and another one for the respirable fraction [24,89,125]. Each

measurement requires approximately 180 g of sample material to ensure a constant mass flow between 6 and 10 g/min [24,125]. The process is repeated five times to obtain a reliable result [125]. While the Continuous Drop Test offers high reproducibility, it requires a high sample quantity and has only limited ability to reflect the real conditions during powder processing [24,89].

1.5.2 Heubach Dustmeter

The Heubach Dustmeter is widely used for measuring DTS [24,80,127,128]. The Heubach Dustmeter consists of a rotating drum, a particle separator, a sampling unit, and a pump. In Figure 3, the Heubach Dustmeter is shown with its main components and setup.

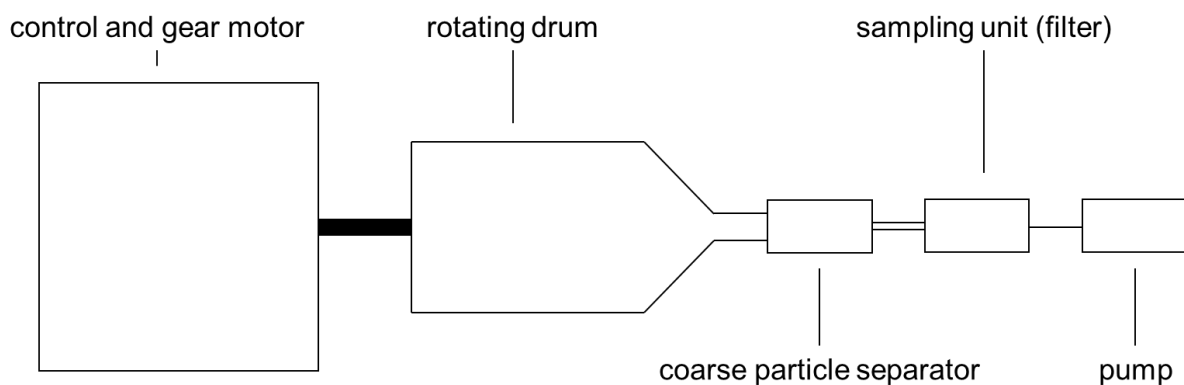


Figure 3: Simplified illustration of the Heubach Dustmeter, highlighting its main components (modified from [73,90,129]).

During the test, the drum constantly shakes the powder sample while three small hammers tap the outer wall of the drum to prevent possible caking. A 50 g sample is placed within the drum, which rotates at 30 rpm for a duration of 300 s [128]. These adjustments are controlled by the internal computer of the device [24]. An adjustable horizontal airflow transports the released dust through the particle separator into the sampling unit, where the inhalable and respirable fractions are collected depending on

the filter system used [128]. The Heubach Dustmeter allows precise and selective dust fraction measurements but requires substantial sample quantities [24].

1.5.3 Palas Dustview

The Palas Dustview is based on the so-called single-drop method, which is an optical method for measuring dust generation [24,85,130]. A small amount of powder (about 30 g) is filled into a funnel and released through an automatic valve into a measuring chamber [24]. In Figure 4, the Palas Dustview is illustrated, showing its design and the assembly used for dust measurements.

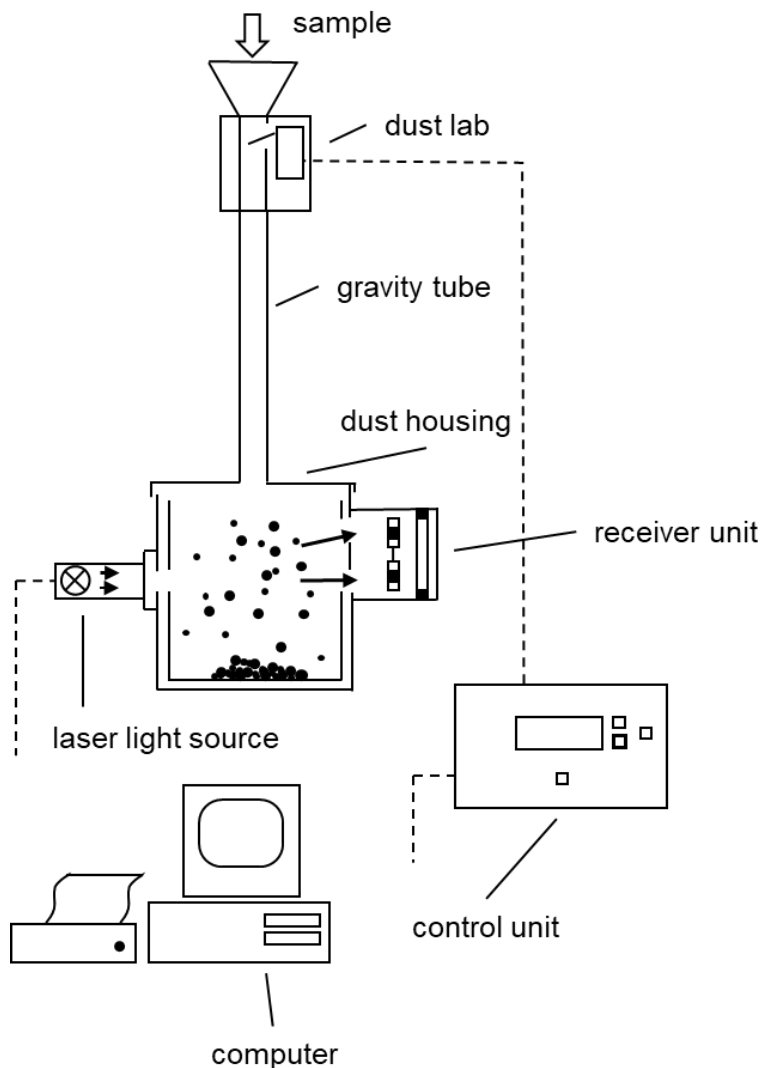


Figure 4: Illustration of the Palas Dustview with its setup and operational principle [24].

The shutter opens briefly, allowing the sample to drop through a falling tube into a cubic dust chamber. Dust generation is measured by the extinction of a laser beam, whereby the reduction in laser intensity is a measure of the amount of dust released. By positioning the laser beam beside the settling dust stream, only generated dust is registered [85]. The intensity of the laser beam may range from 0 % in the case of complete extinction to 100 % in the case of total transmission, with the laser attenuation being significantly influenced by the refractive index of the particles [24]. A reduction in laser light intensity for 40 s provides information on the fraction of inhalable and respirable particles [85]. Therefore, the DTS is calculated using two reference values: the value measured at 0.5 s reflects the total fraction of suspended and inhalable dust and at 30 s, the majority of the material has settled to the ground, making this time point suitable for analysing the respirable airborne fraction [24]. Compared to other methods, there is a tendency of the Palas Dustview to detect lower dust emissions depending on the particle properties and handling conditions [24].

1.5.4 UNC Dustiness Tester

The UNC Dustiness Tester was developed by the University of North Carolina for testing small sample quantities of 5 ± 0.1 mg under controlled conditions. The device consists of a glass container with a wide opening, an aluminium cover plate and a powder injector. In Figure 5, the UNC Dustiness Tester is shown with its components and main assembly.

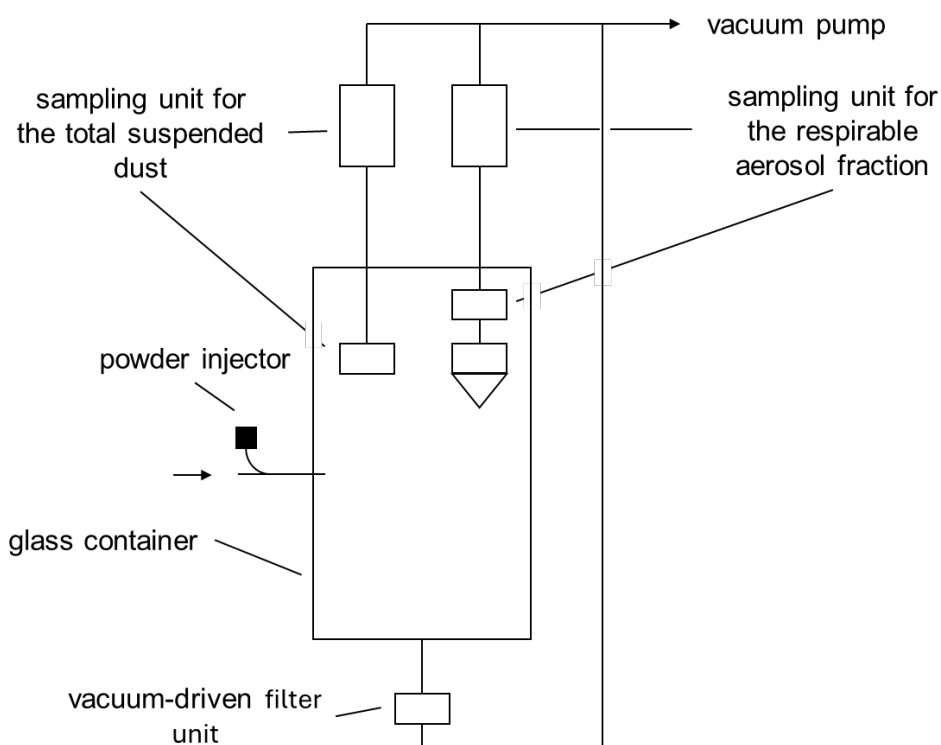


Figure 5: Schematic illustration of the UNC Dustiness Tester [86,98].

The powder is filled into the injector and dispersed by a short air stream for 1.5 s at a flow rate of 60 l/min [86,131]. After dispersion, the air with the airborne particles is drawn through two filter systems for further analysis. The total suspended particles, including the inhalable fraction, are collected in a filter at an air flow rate of 2 l/min, while the respirable fraction is collected in a cyclone at a flow rate of 4.2 l/min. This method is characterised by its low required sample amount and the controlled dispersion process [86,131,132].

1.5.5 Pros and cons of the methods for dustiness determination

Whereas the methods described in Chapters 1.5.1 to 1.5.4 represent significant progress in measuring DTS, all of them have limitations. Most methods require large sample quantities, are only suitable for the measurement of pharmaceutical powders to a limited extent, and only mimic dust generation without adequately representing the transport of the generated airborne particles within a closed system. Differences in

their operational principles and measurement conditions do not allow direct comparisons of dustiness measurements performed with presented devices [24,61,85,86,133,134].

1.6 Dustiness measurements in the pharmaceutical industry

In the pharmaceutical industry, the control of dust exposure while handling hazardous substances is essential, as even minimum quantities of these compounds may pose risks [5,17,64]. For this purpose, IOM (Institute of Occupational Medicine) samplers are used to ensure a precise measurement of the inhalable as well as respirable fraction of airborne particles in workplaces. They play a crucial role in monitoring dust emissions during critical operations, where the risk of exposure to hazardous substances is particularly high [5,17,33]. The IOM samplers bring along considerable benefits, including their conformity with inhalable dust standards and their robustness against changes in air flow direction and velocity [17,33,135]. Investigations have shown that the samplers deliver reproducible and reliable results in controlled environments and workplaces, enabling a precise exposure assessment by measuring dust concentrations in the breathing zone [33,135].

1.6.1 Principle of IOM samplers

The IOM samplers enable a precise detection of the inhalable dust fraction in workplaces. They have been designed to measure the concentration of dust that enters the respiratory tract, regardless of particle size, air flow direction or velocity [17,47,104,135–139]. The IOM samplers mimic the intake of particles by the human respiratory tract. The design of an IOM sampler is illustrated in Figure 6. A central component of the device is the 15 mm orifice through which air is drawn by a pump at a constant flow rate of usually 2 l/min [17,47]. The sampler is made of conductive plastic to reduce static charges and is equipped with a reusable filter holding cassette

connected to a pump by a flexible plastic tube. The construction of the samplers is such that particle collection corresponds to real inhalation conditions [47]. Particles that enter through the orifice are collected on a filter placed in the filter holding cassette which is positioned directly behind the sampler orifice. This integrated cassette minimises typical sources of error, such as particle loss through deposits on the inner walls or particles blown off the filter holding cassette [17,47]. The sampler enables a standardised collection of airborne particles, even under varying environmental conditions such as changing air velocities and particle sizes [5,17].

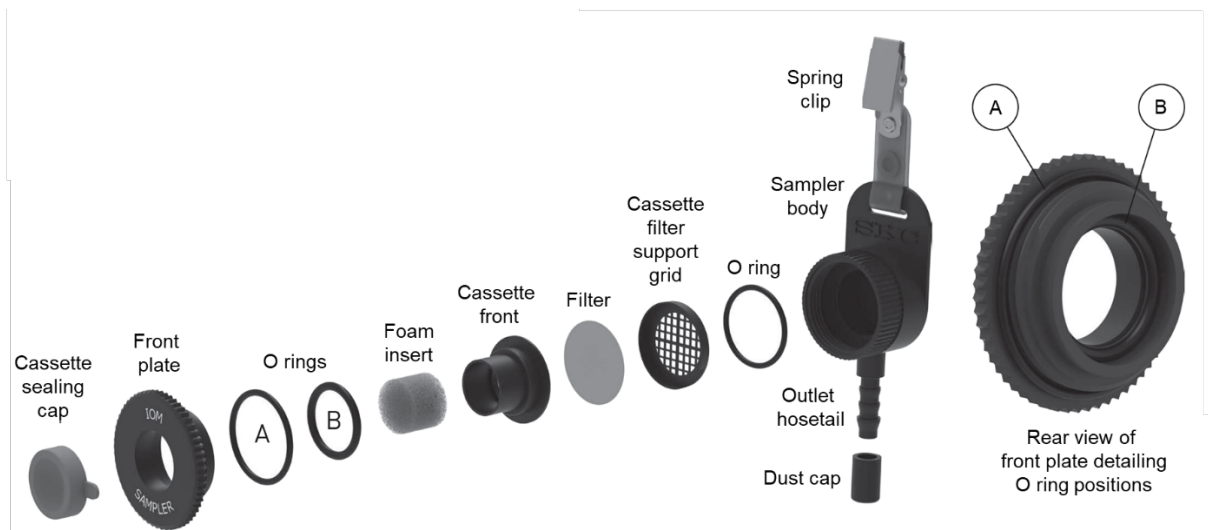


Figure 6: Design of an IOM sampler. With permission from SKC [140].

Compared to existing devices, the IOM sampler provides good precision in measuring dust exposure in the breathing zone and is less sensitive to external influences such as varying air flow conditions. These characteristics and its easy handling make the IOM sampler suitable for the determination of dust exposure in different workplaces [5,17,139].

1.6.2 IOM samplers in pharmaceutical settings

In pharmaceutical environments involving the handling of powders with a high potential for dust generation, the IOM samplers are essential instruments [5,47]. They accurately

monitor dust concentrations during powder processing such as filling, mixing, and transporting [78,141]. Especially in scenarios where HPAPIs are processed, IOM samplers provide a reliable way to measure the inhalable and respirable fraction and to assess potential exposure risks [5,47].

Measurements with the IOM samplers are performed by placing the device near the emission source, either directly near the breathing zone of the personnel or at the personnel's workplace [35,47]. During operation, all airborne particles are collected on a filter which is subsequently prepared for further analysis [5,17,47]. The amount of the collected particles may be quantified, for instance, by mass determination or by dissolution. The quantification is typically carried out by gravimetric or analytical methods such as high-performance liquid chromatography (HPLC) or/and mass spectrometry [5,47]. The concentration of airborne particles may be calculated according to the following equation (Eq. 3).

$$c = \frac{m \cdot 1000}{t \cdot PR} \quad (\text{Eq. 3})$$

where c is the concentration of airborne particles ($\mu\text{g}/\text{m}^3$); m is the mass of airborne particles (μg); t is the test duration (min); and PR is the sample pump rate (l/min) [47].

The calculated data allow an accurate assessment of the level of exposure and provides a basis for safety measures. It is important to make sure that the concentration of airborne particles is within the specified limits or that additional measures are required to minimise exposure [36,47].

The IOM samplers have been shown to serve as reliable instruments for dustiness investigations [47,141,142]. Their standardised design and ease of use make them a preferred choice for assessing the inhalable and respirable fraction of dust particles. The IOM samplers may be used in combination with other dust measurement methods

to perform comprehensive analyses and to characterise the specific properties of powders in terms of their dust release [5,47].

An accurate measurement of airborne particles allows risk assessment and the development of safe working methods. The data obtained with the IOM samplers serve as a basis for the optimisation of processes and technologies intended for the reduction of dust emissions and for an increase of safety in pharmaceutical manufacturing [5,47].

1.7 Surrogate substances for dust analysis and containment validation

1.7.1 Reasons for the application of surrogate substances

The direct application of HPAPIs for the validation and performance testing of containment systems is associated with considerable challenges and thus surrogate substances are commonly used for such purposes [5]. Surrogates are expected to mimic the physical properties of HPAPI-containing powders such as particle size, flow properties, dustiness, and adhesion [36]. Table 3 outlines the challenges associated with the use of HPAPIs for the mentioned purposes [5].

Table 3: Challenges during handling HPAPIs.

Challenge	Description
Extremely expensive	Economic costs of using these substances are enormous, especially if larger sample quantities are required.
Highly hazardous	Even smallest quantities may pose considerable health risks to personnel, necessitating the use of additional protective measures.
Analytically complex	There is often a lack of highly sensitive analytical methods to precisely quantify the concentration of released HPAPI.
Environmental harmful	Incorrect handling might lead to contamination of the environment.

These problems may be avoided by using suitable surrogate substances. They offer a practical and safe alternative for testing the performance of devices and systems under realistic conditions [5,143–145].

1.7.2 Selection criteria for surrogate substances

The selection of a suitable surrogate substance is essential for realistically mimicking the actual conditions during handling of HPAPIs without encountering the associated risks [5,143]. According to the International Society for Pharmaceutical Engineering (ISPE), the physicochemical properties of a surrogate substance are supposed to match those of the used API as closely as possible [5,36]. The main selection criteria are shown in Table 4 [5]:

Table 4: Criteria for selecting surrogate substances.

Criteria	Description
Particle size distribution and dustiness	Surrogate substances should have a dust behaviour similar to that of HPAPIs to provide a realistic challenge for the systems.
Analytical sensitivity	Surrogates must be easy and precise to analyse, ideally with a low limit of detection (LOD).
Pharmacological and environmental safety	The substance should not pose a risk to personnel or the environment.
Availability and cost	The substance should be inexpensive and available in sufficient quantity to allow repeated testing.
Disposal and cleaning	The substance must be easily disposed of and completely removed from the tested systems.

1.7.3 Examples for surrogate substances

In Table 5 various typical safe surrogate substances recommended by the ISPE and used in the pharmaceutical industry are listed [5].

Table 5: Summarised properties of potential surrogate substances [5].

Surrogate	Properties
Acetaminophen	<ul style="list-style-type: none"> • Relatively cost-effective • Wide range of detection limits (LOD: 0.1 - 40 ng) • Low toxicity • Highly soluble in water • Moderately dusty
Insulin	<ul style="list-style-type: none"> • Highly soluble in water • Sensitive analytical technique available • Very expensive, only available in small quantities • High skin and respiratory sensitisation
Lactose	<ul style="list-style-type: none"> • Available at various particle size distributions • Many suitable qualities available • No simple analytical method available • Very cost effective • Low toxicity • Highly soluble in water
Mannitol	<ul style="list-style-type: none"> • Available at various particle size distributions • Very cost effective • No simple analytical method available • Low toxicity • Highly soluble in water • Only few suitable qualities are available
Naproxen sodium	<ul style="list-style-type: none"> • Extremely dusty • Low toxicity • Simple analytical method with very low detection limit (LOD: ≤ 0.2 ng) • Highly soluble in water • Relatively expensive • Very useful for testing in systems with highly hazardous or dusty materials
Riboflavin	<ul style="list-style-type: none"> • Widely available and cost effective • Highly water-soluble as sodium phosphate salt • Real-time qualitative surface residue analysis with UV light • LOD: 5 ng • Widely used for qualitative surface residue analyses
Sucrose	<ul style="list-style-type: none"> • Very cost effective • Low toxicity • Highly soluble in water • Only available in small quantities • LOD: 5-10 ng • Useful if lactose or mannitol background noise is expected

1.7.4 Performance tests with surrogates

Testing with surrogate substances follows a standardised procedure to ensure reliable and meaningful results, as outlined in the ISPE Good Practice Guide: Assessing the Particulate Containment Performance of Pharmaceutical Equipment. The process begins with the preparation of the surrogate material in a qualified, controlled environment to avoid unintended contamination. Surrogate substances are stored under recommended conditions to maintain their integrity. In the next step, the surrogate substance is introduced into a containment system during the test and evaluated under defined conditions. Dust release and the airborne particle concentration is measured with devices such as the IOM sampler, thereby capturing the inhalable and respirable fraction of particles [47].

Testing may take place in the controlled environment of containment system-producing suppliers during a Factory Acceptance Test (FAT) or at the user's operational site as part of a Site Acceptance Test (SAT) or routine performance test [3,5,47,143]. Supplier environments are designed to minimise external influences by maintaining stable conditions, including temperature, humidity, and air exchange rates. In contrast, user-site testing is commonly conducted in less controlled environments, making thorough risk assessments essential to minimise potential contamination from surrounding processes or environmental factors [5,47].

The collected samples are then analysed gravimetrically and chemically to evaluate the dustiness and the performance of the tested containment system. This analysis not only assesses system effectiveness but also identifies potential weaknesses. To ensure valid, reproducible, and consistent results, additional measures may be implemented, such as pre-test cleaning of the area, air and surface sampling to establish baseline conditions, and adherence to strict gowning and degowning protocols [47].

By following the structured methodology provided in the ISPE Good Practice Guide, surrogate testing is conducted in a manner that ensures a controlled environment, enabling the collection of reliable and comparable data for performance evaluation [47].

1.7.5 Benefits and limitations of the surrogate substances

The application of surrogates in the pharmaceutical industry provides numerous advantages. Safe surrogate substances are characterised by low LODs [47]. They enable the safe and cost-efficient validation of containment systems and processes without directly using highly potent or expensive APIs. A safe validation reduces risks for personnel and the environment and facilitates the practical application of containment systems in early development or optimisation phases [5].

However, some limitations need to be taken into consideration. Surrogate substances may only approximate the physicochemical properties of HPAPIs, which limits their informative value [47]. Tests with the actual substances are often essential to verify the results and to ensure that the systems work just as reliably under real conditions [5]. In addition, the selection of a suitable surrogate requires extensive knowledge of the properties of the target substances to ensure the most accurate transmission and to obtain reliable results [47]. Despite the mentioned limitations, the application of surrogate substances as substitutes for target substances clearly demonstrates their relevance for safety assessment and process optimisations. Their importance for the pharmaceutical industry is particularly underlined by their versatile application potentials under safe conditions [5,47].

1.8 Computational Fluid Dynamics (CFD)

Computational Fluid Dynamics (CFD) is a numerical simulation method for analysing flows of fluids (liquids and gases) and their interrelation with physical variables such as particle concentration as well as heat and energy [146,147]. Moreover, fluid-surface interactions may be computed numerically by applying boundary conditions that define the physical behaviour at solid interfaces [148–150]. CFD is based on the fundamental principles of conservation of mass, energy and momentum, which are described by partial differential equations [146,147]. Within the pharmaceutical development and research, CFD has established itself as an indispensable tool for modelling and optimising complex processes to increase their efficiency [151,152].

CFD is also used in the field of containment and safe handling of pharmaceutical powders to analyse the distribution of airborne particles by simulations [127,152]. This method allows a safe and efficient process layout and product design.

1.8.1 General applications of CFD in the pharmaceutical context

CFD is used in a variety of manufacturing processes, such as mixing and drying as well as in the development of inhalers or nasal sprays [153–163]. In mixers or dryers, CFD allows optimal flow conditions to be determined, thereby increasing product quality and process efficiency [151,152,164]. In the development of inhalers or nasal sprays, CFD may be used to analyse fluid mechanics and spatial particle distribution, which enables an improvement of product design and an increase of product efficacy [151]. Thereby, CFD offers the possibility to test device variants virtually without having to create physical prototypes. This possibility not only saves costs but also significantly shortens the required development time [151,152].

Overall, the potential of CFD in the pharmaceutical industry is widespread. CFD simulations allow a detailed analysis of flows, heat and mass transport as well as

reaction mechanisms. Thus, they enable both the optimisation of individual processes and the development of new technical approaches [151,152,165].

The simulation of conditions that are difficult or impractical to implement experimentally is also possible by CFD, consequently reducing the need for expensive and time-consuming experiments [146,147,163].

In summary, CFD offers the possibility to improve efficiency and safety in pharmaceutical manufacturing in a targeted manner and, therefore, makes an important contribution to ensure high-quality standards [146,151,152].

1.8.2 Applications of CFD in the context of containment

CFD has become an important tool in pharmaceutical research and development, used in both the development of dosage forms and the planning of manufacturing equipment and production facilities. If dosage forms with HPAPIs are manufactured, which require special containment measures, CFD may be used for the simulation of the release and spread of dust [132,166–168]. For example, CFD is suitable for identifying risk zones with high particle concentrations within production facilities and manufacturing equipment, which simplifies the development and implementation of specific protective measures, such as air flow routing or pressure differentials. These measures not only contribute to the compliance with regulatory requirements but also reduce health risks for personnel [104,146,147,166,169].

2. Aim of the work

Highly potent active pharmaceutical ingredients (HPAPIs) are of increasing interest in medicine and pharmacy. Although HPAPIs play an important role in the treatment of serious diseases, their high pharmacological and toxicological potency poses challenges in terms of safe handling and minimisation of dust emissions during processing. Effective containment is not only essential to ensure the safety of personnel and products but also to protect against cross-contamination and environmental hazards by means of design optimisations.

The objective of this work was the development of a novel chamber setup to precisely and reproducibly analyse the transport of airborne particles released from pharmaceutical powders. This novel chamber setup consists of two chambers, an emission and a detection chamber. Acetaminophen (ACAM) was used as a surrogate substance, which is recommended as a substitute for powders with high toxic potential because of its low toxicity, good analytical detectability and high dustiness. So far, no device has been developed specifically for analysing airborne particle transport. The newly developed two-chamber setup (TCS) is designed to analyse small sample quantities of pharmaceutical powders with regard to dustiness and to simulate flow conditions as they occur during pharmaceutical processing to investigate their influence on dust emissions in detail.

In the first study, the focus was on the significant reduction of dust emission after a controlled atomisation of pharmaceutical powders by generating a convective flow from the detection to the emission chamber. In this context, the convective flow is induced by a pressure difference between the chambers and is directed against the diffusive transport. By this approach, a more precise control of the particle movement was possible and important insights into the influence of different flow conditions on the resulting dust emissions were provided. To investigate the transport of airborne

particles between the two chambers during plain diffusion and during diffusion with an oppositely directed convective flow, the pressure difference between the two chambers was adjusted suitably.

The aim of the second study was to further develop the TCS through design optimisations to achieve higher pressure differences and thus higher air flows. These adjustments allowed a further reduction of the dust emissions to such an extent that they are no longer measurable. Moreover, it was analysed whether the particle sizes of the surrogate substance ACAM influenced the emission rate, because only one uniform particle size was investigated in the first study.

The third study took into account the industrial practice by investigating powder blends. These blends consisted of the surrogate substance ACAM and lactose monohydrate, which is frequently used as an excipient in the manufacturing of pharmaceutical solid dosage forms. The aim was to analyse the influence of different mixing ratios and particle sizes on dust emission. Such powder blends are commonly used in industrial production. In terms of minimising dust emissions, the results of this study provided new insights into the role of the composition of powder blends and particle size distribution.

3. Cumulative part of the dissertation

3.1 A novel two-chamber setup for containment investigations with special focus on the dustiness of pharmaceutical powders depending on the airflow

The present work describes the development of a novel two-chamber system (TCS), which was especially designed for analysing the dust generation of pharmaceutical powders. This system enables the precise analysis of even small quantities of powder, as in the case of the surrogate substance acetaminophen (ACAM) [170]. The TCS consists of an emission and a detection chamber, which may be separated by a controllable flap. The focus of the study was on dust generation and the investigation of the transport of dust within the closed system under different air flow conditions, including plain diffusion and an oppositely directed convective flow, to significantly reduce dust emission.

The investigations using the TCS are divided into three phases: atomisation, transport and evacuation. After atomisation of the powder by overpressure, the resulting dust inside the TCS may either pass from the emission chamber to the detection chamber by plain diffusion or a flow may be generated from the detection chamber towards the emission chamber by generating a pressure difference of 1 - 4 Pa between the two chambers to counteract diffusive transport. The investigation of plain diffusive transport resulted in a linear correlation between the quantity of atomised ACAM and the measured dust emission up to an atomisation quantity of 400 mg. The results reveal that the dust emission measured in the detection chamber was significantly reduced by a convective air flow in the opposite direction of the diffusion.

A precise and reproducible detection of the particles that passed from the emission to the detection chamber was achievable. CFD simulations were carried out to simulate the evacuation of the detection chamber and to visualise the flow pattern and the resulting particle residence time. The simulations, supplemented by smoke and dust

tests, showed that an evacuation time of 9 minutes was sufficient to collect most of the dispersed ACAM particles.

In addition to the experimental investigations, the properties of the ACAM powder were analysed to characterise the factors that influence dust generation. From the results of this study, it may be concluded that the novel TCS enables the investigation of dustiness with small powder quantities and that dust emissions may be significantly reduced by adjusting the flow conditions. However, a complete elimination of dust emissions was not achieved. In Figure 7, an illustrative summary of the methodology and key aspects of this study is provided.

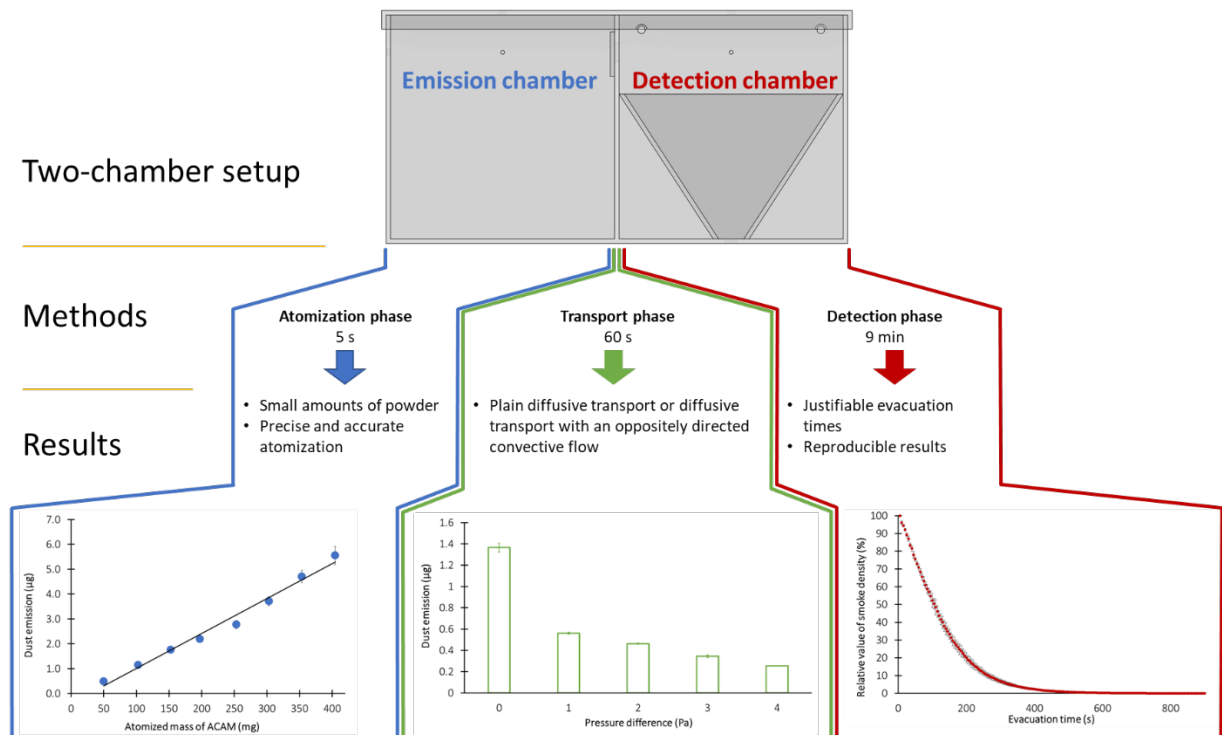


Figure 7: Illustrative summary of methodology and main outcomes of the study [170].

In a subsequent study, the influence of the particle size and of the increase of the pressure difference was investigated.

Article

A Novel Two-Chamber Setup for Containment Investigations with Special Focus on the Dustiness of Pharmaceutical Powders Depending on the Airflow

Steffen Wirth ¹, Martin Schöler ², Jonas Brüggmann ² and Claudia S. Leopold ^{1,*}

¹ Department of Pharmaceutical Technology, University of Hamburg, Bundesstr. 45, D-20146 Hamburg, Germany

² Fette Compacting GmbH, Grabauer Straße 24, D-21493 Schwarzenbek, Germany

* Correspondence: claudia.leopold@uni-hamburg.de; Tel.: +49-40-42838-3479

Abstract: In the present study, it was shown that a newly developed two-chamber setup (TCS) for containment investigations consisting of an emission and a detection chamber may serve to predict the dustiness of HPAPIs in a sealed system at different flow conditions. These flow conditions include the plain diffusive transport and the diffusive transport with the oppositely directed convective flow of airborne particles of the safe surrogate substance acetaminophen (ACAM). A linear correlation was found between an atomized amount of up to 400 mg of ACAM and the resulting dust emissions. The dust emission was reduced significantly by an oppositely directed convective flow. The results from the examinations, using either atomized ACAM or smoke for the determination of the evacuation time of the detection chamber, indicated that both methods are comparable. Furthermore, computational fluid dynamics (CFD) simulations were performed to determine the evacuation time. A time period of 9 min was sufficient for a reproducible evacuation and a reliable detection of most airborne ACAM particles within the detection chamber. CFD simulations were also carried out to simulate the air velocity resulting from various pressure differences and to visualize the flow of the airborne particles within the detection chamber.

Keywords: containment; two-chamber setup; HPAPI; dustiness; dust emission; dust transfer; evacuation time; smoke; computational fluid dynamics



Citation: Wirth, S.; Schöler, M.; Brüggmann, J.; Leopold, C.S. A Novel Two-Chamber Setup for Containment Investigations with Special Focus on the Dustiness of Pharmaceutical Powders Depending on the Airflow. *Pharmaceutics* **2022**, *14*, 2387. <https://doi.org/10.3390/pharmaceutics14112387>

Academic Editors: Rolf Daniels, Dagmar Fischer and Stephan Reichl

Received: 19 September 2022

Accepted: 3 November 2022

Published: 5 November 2022

Publisher's Note: MDPI stays neutral with regard to jurisdictional claims in published maps and institutional affiliations.



Copyright: © 2022 by the authors. Licensee MDPI, Basel, Switzerland. This article is an open access article distributed under the terms and conditions of the Creative Commons Attribution (CC BY) license (<https://creativecommons.org/licenses/by/4.0/>).

1. Introduction

In recent years, the number of highly active pharmaceutical ingredients (HPAPIs) has significantly increased, resulting in a high interest of pharmaceutical companies in the safe handling of these hazardous compounds [1–3]. For example, in oncological therapy, HPAPIs are commonly used as cytostatics or peptides. Hormones and antibiotics are other examples of high potency compounds with a high potential for hazard exposure to the personnel present in the intermediate environment. Therefore, measures must be taken regarding the technical design of the facilities and the equipment for handling HPAPIs [3–5].

The potential hazard exposures may lead to a health risk for the operators, as well as to a contamination of the outdoor environment and to cross-contaminations during manufacturing or other production processes within the facility. Therefore, the generation of dust, gases, or vapors is an important issue in the processing of dosage forms containing HPAPIs. The application of suitable containment equipment and, in some cases, additional personal protective equipment, is essential to ensure safe handling [6,7]. To guarantee the safe manufacture of dosage forms containing HPAPIs, special production setups are applied which are operated at a negative pressure to reduce the risk of potential airborne transfer to the immediate environment. In addition, barrier isolators, special transfer and valve systems, and high performance filters are further governance methods to reduce the risk of hazards [3,8].

Generally, the dustiness of formulations containing HPAPIs is a major problem concerning potential exposure. Thus, the minimization or elimination of any potential exposure is a common safety measure in the production of dosage forms containing HPAPIs [3,9,10].

Dustiness is defined as the propensity of a material to generate airborne particles during its handling [11]. Various processes in pharmaceutical manufacturing, such as processing, milling, grinding, and mixing, are associated with the generation of dust and, consequently, dustiness is a major risk of potential hazard exposure. Surprisingly, the number of studies on the dustiness of pharmaceutical powders is rather low, compared to that on the dustiness of non-pharmaceutical powders. The dustiness of a pharmaceutical powder is influenced by many factors, especially by the physicochemical and mechanical properties of the material and the method of dust determination. Therefore, the measurement of the dustiness of pharmaceutical powders is of particular importance for the assessment of the hazard exposure in pharmaceutical facilities [9,12–16]. For this reason, various systems and methods were developed to measure the dustiness of solid substances in a reproducible manner. Most of these systems are not designed for the measurements of pharmaceutical powders because the required substance quantities for these measurements are relatively high. Accordingly, because of the typically scarcely available quantities of HPAPIs, the measurements are limited and relatively expensive. The compounds used in the pharmaceutical production are exposed to a wide variety of stresses. Thus, no single test system may reproduce all conditions during handling [17–23].

The atomization of powders results in an airborne particle distribution and is achieved by the application of energy. Therefore, atomization may be obtained by using a mechanical stimulus or by the dispersion of the pharmaceutical powder in the air. The application of too much energy may result in a fragmentation of single particles and possibly, in a greater dustiness. Each method for the determination of the dustiness includes a different technique for atomization. Thus, a comparability of the different methods for determination of the dustiness is nearly unimaginable because of the complexity of the different measurement processes. Moreover, an accurate prediction of the dustiness based on material properties such as particle size and density is not possible. However, the particle size distribution, particle shape, bulk density, humidity, and the cohesive and adhesive forces of powder particles have a major influence on the resulting dustiness. A reproducible dust generation requires a standardized method, and thus detailed specifications, regarding test duration, type, intensity of the mechanical stimulus, and the amount of test material are necessary. Therefore, a high standardization with relation to industrial manufacturing processes is essential for suitable dustiness measurements [9,11,19,24–28].

The assessment of containment equipment and the evaluation of systems and devices for dustiness measurements should be performed using safe surrogate substances. These substances, such as lactose, naproxen sodium, mannitol, acetaminophen, insulin, riboflavin, and sucrose, along with additional information regarding such measurements, are listed in the Good Practice Guide of the International Society for Pharmaceutical Engineering (ISPE) [6]. The choice of the surrogates should not only depend on the physicochemical and mechanical substance properties, but also on the conditions of the analytical quantification [29].

The applications of computational fluid dynamics (CFD) are versatile, and it is currently used as an efficient tool in the pharmaceutical industry for various purposes, such as the characterization of dry powder inhalers, the Venturi dustiness tester, and the Heubach Dustmeter [30–33]. In addition, CFD is commonly applied to assess systems for the measurement of dustiness. In this context, CFD allows a modeling of the aerodynamics within the systems to assess the homogenous distribution of dust and to identify zones in which dust accumulates at the end of the sampling process. Furthermore, these simulations are also appropriate to investigate a possible inhomogeneous or delayed powder atomization [32]. Moreover, CFD is suitable to describe the atomization process of pharmaceutical powders and to assess their flow behavior within the systems [33,34].

The number of investigations regarding the dustiness of pharmaceutical powders is relatively low compared to the dustiness investigations of non-pharmaceutical powders [21,35]. In addition, in the literature, the description of the distribution of airborne particles in a defined environment as a function of various flows is rather vague.

Based on the above-mentioned remarks, further research is needed to expand the knowledge on the influence of the plain diffusive transport and the diffusive transport with an oppositely directed convective flow of pharmaceutical airborne particles on the dustiness of HPAPIs. Therefore, the objective of this work was to develop a novel TCS consisting of an emission and a detection chamber to investigate the dustiness depending on different flow conditions. A further aim of this study was to confirm that the newly developed TCS ensures a reproducible and precise dustiness investigation of pharmaceutical powders. The different parameters of the atomization phase, transport phase, and detection phase may influence the investigation of the TCS. In this context, both the reproducible and precise atomization of small amounts of the surrogate substance ACAM and the accurate determination of the dust emission by an IOM sampler (Institute of Occupational Medicine) are the crucial parameters that may significantly influence the dustiness investigations in terms of the reproducibility and precision of the results.

Modern equipment for the production of dosage forms containing HPAPIs is typically operated with negative pressure to reduce potential hazard exposure [1]. Consequentially, another objective of this study was the generation of an adjustable oppositely directed convective flow from the detection to the emission chamber within the TCS, simulating the negative pressure for reduction of the potential hazard exposure.

2. Materials and Methods

2.1. Materials

Acetaminophen (ACAM; Caelo, Hilden, Germany), as an industry-accepted safe surrogate substance, was used to measure dustiness [6]. Furthermore, a Dräger Air Flow Tester (Dräger, Lübeck, Germany) was used to generate smoke for flow visualization.

2.2. Two-Chamber Setup

2.2.1. Design of the Two-Chamber Setup

In Figure 1, a simplified illustration of the novel two-chamber setup (TCS) is shown. The setup consists of an emission chamber and a detection chamber, connected by an orifice with a diameter of 25.4 mm. A flap that is controllable via a double acting pneumatic cylinder is installed to separate the chambers, depending on the phase of the measurement course. The emission chamber shows dimensions of 300 mm × 300 mm × 300 mm, resulting in a volume of 27 L. The detection chamber has the same dimensions, but exhibits a smaller volume of approximately 15 L because of the pyramidal construction in the lower section of the chamber.

The emission chamber contains an orifice for pressure compensation during the first phase of the measurement course in which ACAM is atomized (Figure 2). The detection chamber comprises two orifices for pressure compensation during the second phase of the measurement course. An IOM sampler is fastened at the bottom of the detection chamber and is connected to the air sampling pump (AirChek ESSENTIAL Pump, SKC, Blendfort Forum, UK). The detachable lid allows for cleaning the TCS after each measurement. The lid contains two orifices for the fastening of two pneumatic ball valves and is attached to the TCS by toggle locks. In addition, a rubber seal is attached to the edges of the chambers to ensure tightness.

The TCS consists of acrylic glass with a wall thickness of 6 mm. Aluminum B type profiles were used to fasten measuring the instruments: a pneumatic cylinder, pneumatic valves and ball valves, as well as a programmable logic controller (PLC). Additionally, a ground cable was attached to the metal parts to minimize electrostatic charge.

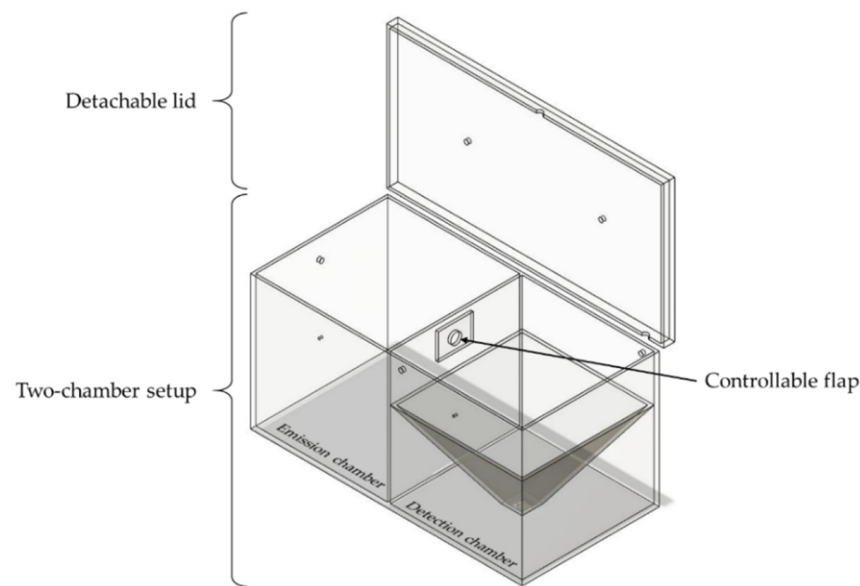


Figure 1. Simplified illustration of the TCS in the open state, consisting of a detachable lid, a controllable flap, and the two connected chambers.

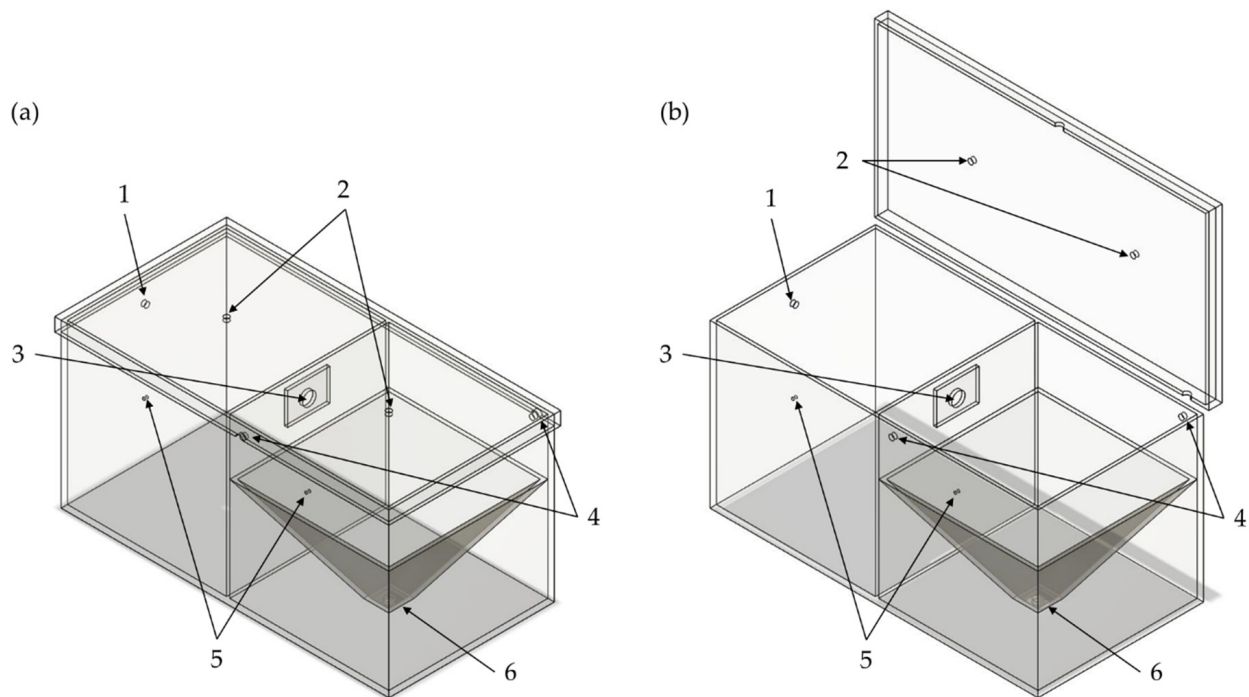


Figure 2. Schematic illustration of the TCS (a) in the closed state and (b) in the open state. 1: orifice for pressure compensation of the emission chamber; 2: orifices for the double-acting ball valves; 3: orifice for the connection between the emission and the detection chamber; 4: orifices for pressure compensation of the detection chamber; 5: orifices for the differential pressure gauge; 6: orifice for the IOM sampler.

The valve control of the TCS is executed by a PLC (Siemens LOGO! 12/24RC, Munich, Germany). The input signal for starting the program of the PLC was generated time-dependently by a single-board microcontroller (Arduino® Uno Rev3, Ivrea, Italy) and amplified with a DC-to-DC converter to a voltage of 12 V. Resulting from the ability of the single-board microcontroller to send a punctual input signal to the PLC, all phases of the measurement course may be controlled as a function of time. Therefore, the air sampling pump and the PLC were synchronized with the server time of a computer. The PLC allows

for the generation of various flow conditions within the TCS by controlling the pneumatic ball valves attached to the detachable lid.

In Figure 3, the pneumatic valves and devices are shown. The pneumatic ball valve (KH 14 P, PneumatikAtlas, Lübeck, Germany), located above the emission chamber, was used for the atomization of ACAM. Another identical pneumatic ball valve, positioned behind a throttle valve, is located above the detection chamber to generate a flow in the direction of the emission chamber. Both ball valves are controlled pneumatically by 5/2 solenoid valves (VUVS-L25-M52-AD-G14-F8, Festo, Esslingen, Germany). Two 3/2 solenoid valves (VUVS-LK25-M32C-14-B, Festo, Esslingen, Germany) were used to control 3/2 pneumatic valves (SFP4701, YPC, Jeongwang-Dong, South Korea) that manage the pressure compensations. All four solenoid valves are linked to the four outputs of the PLC. All pneumatic components and orifices for pressure compensation are attached to compressed-air tubes (PUN-10X, Festo, Esslingen, Germany). The air sampling pump is connected to the IOM sampler at the bottom of the detection chamber. A digital paddle wheel flow meter (35812, ANALYT-MTC Meßtechnik, Mülheim, Germany) was used to verify the flow rate of the air sampling pump. Additionally, the pressure and temperature difference between the emission and the detection chamber were measured by a differential pressure gauge (testo 400, Testo, Titisee Neustadt, Germany).

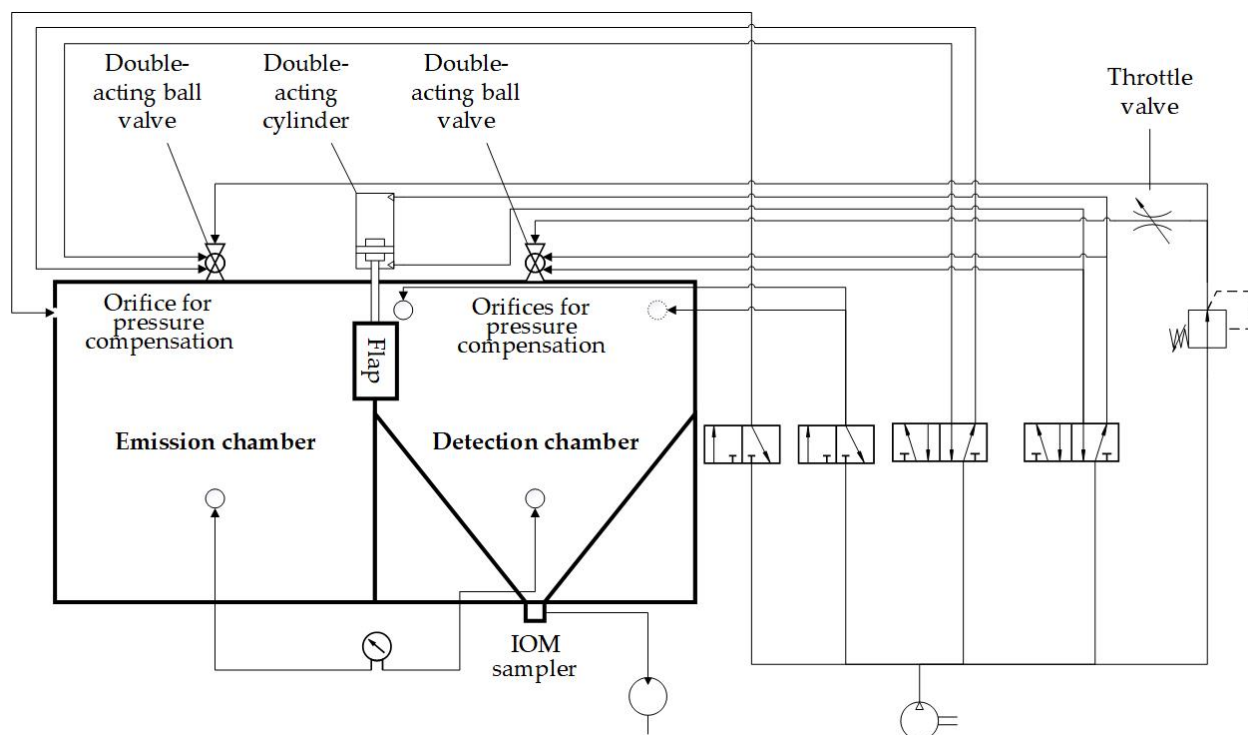


Figure 3. Piping and instrumentation diagram of the TCS.

2.2.2. Description of the Measurement Course

Three phases may be distinguished during the measurement course of the TCS. The first phase is defined as the atomization phase, in which 100 mg of ACAM were atomized through the ball valve above the emission chamber with an overpressure of 50,000 Pa for a time period of 5 s. The pressure was compensated for by opening the 3/2 pneumatic valve. The controllable flap was closed for the same time period to obtain a homogeneous dispersion of airborne particles and to prevent the transport of these particles from the emission to the detection chamber.

During the second phase, which is called the transport phase of the measurement course, the transport of airborne particles was investigated, depending on the flow conditions. This phase was intended to examine the plain diffusive and the oppositely directed

convective transport mechanism of airborne particles in the TCS. In this phase of the measurement course, the controllable flap was opened for 60 s to obtain either a diffusive or a convective flow between both chambers in order to investigate the transport of airborne particles. If there is no pressure difference between the chambers ($\Delta p = 0$ Pa), the plain diffusive transport of airborne particles may be investigated. In contrast, a flow from the emission to the detection chamber was generated by an adjustable pressure difference between these chambers to investigate the diffusive flow, reduced by an oppositely directed convective flow, in addition to the plain diffusive transport.

The third phase was defined as the detection phase of the measurement course, during which the dust emission of ACAM within the detection chamber was determined. The controllable flap was closed after 60 s to separate both chambers and to quantify the amount of ACAM transferred from the emission to the detection chamber. The detection chamber was evacuated using the air sampling pump, with a flow rate of 5.0 L/min for 9 min. The pump was connected to the IOM sampler located at the bottom of the detection chamber, which contained a glass microfiber filter (1820–025, Whatman, Little Chalfont, UK), as recommended by the ISPE [6]. In Figure 4, the three phases of the measurement course are shown schematically.

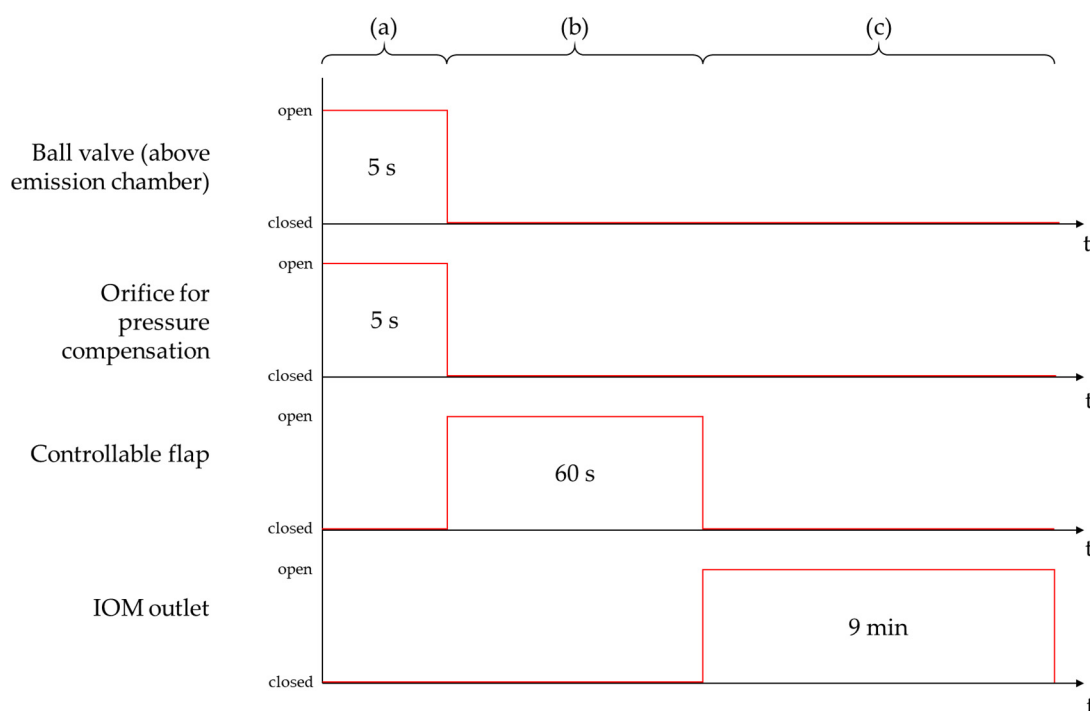


Figure 4. Schematic illustration of the three phases of the measurement course: atomization phase (a); transport phase (b); detection phase (c).

After 9 min, the filter containing the collected dust was transferred to an iodine flask. A moistened glass microfiber filter was used to swab the inner part of the IOM sampler and was then transferred to the same iodine flask. The total collected ACAM was extracted using the mobile phase of the HPLC assay and subsequently quantified (see Section 2.4.).

2.2.3. Investigation of the Atomization Process during the Atomization Phase

This investigation was performed to ensure that small amounts of pharmaceutical powders may be reproducibly atomized in the TCS. The atomization of the surrogate powder ACAM within the emission chamber of the TCS was caused by an overpressure of 50,000 Pa. To examine the influence of the amount of ACAM on the extent of dust emission, the amounts of atomized ACAM were predefined to cover a range between 50 mg and 500 mg, divided into 50 mg portions. The dust emission was measured by evacuating the

detection chamber through the filter-containing IOM sampler using the air sampling pump under the above-mentioned conditions. Thereafter, the glass microfiber filters containing the total collected ACAM were analyzed by HPLC. All measurements were performed in sextuplicate.

2.2.4. Investigation of the Dustiness during the Transport Phase in Dependence of the Airflow

In the second phase of the measurement course, the transport of the atomized ACAM between both chambers resulting from various pressure differences between 0 and 4 Pa was investigated. For this purpose, computational fluid dynamics (CFD) simulations and the atomization of ACAM were performed to assess the effect of plain diffusive transport and diffusive transport with an oppositely directed convective flow of airborne particles.

CFD was performed to simulate the air velocity at the orifice between the emission and the detection chamber for the determination of the average air velocity. The simulations were carried out with the SimScale CFD simulator (SimScale, Munich, Germany) using the k-omega shear stress transport turbulence model (k- ω -SST). The initial conditions of the CFD simulations are shown in Table 1.

Table 1. Initial conditions of the CFD simulations for the investigation of the transport phase of the measurement course.

Properties	Values
Density	1.196 (kg/m ³)
Kinematic viscosity	1.529×10^{-5} (m ² /s)

An overview of the airflow properties chosen for the simulations is presented in Table 2. The boundary conditions were set to a pressure difference of 1–4 Pa between the inlet and the outlet orifice to simulate the adjustable oppositely directed convective flow conditions of the TCS. The CFD simulation were performed to assess the flow conditions within the TCS at the orifice between the emission and the detection chamber. The average air velocities were also measured, depending on the pressure difference, using a thermal anemometer (testo 405 i, Testo, Titisee-Neustadt, Germany) at five positions.

Table 2. Airflow properties of the CFD simulations for the investigation of the transport phase of the measurement course.

Properties	Values
Gauge pressure	0 (Pa)
Δp between the inlet and outlet orifice	1, 2, 3, 4 (Pa)
Turbulence kinetic energy [k]	1.297×10^{-2} (m ² /s ²)
Specific dissipation rate [ω]	12.49 (s ⁻¹)

The simulated and measured average air velocities resulting from the applied pressure differences were used to investigate the effect of the air velocity on dustiness. For this purpose, the pressure difference between the two chambers was set to values of 0–4 Pa: At a pressure difference of 0 Pa, the plain diffusive transport of ACAM between the detection and the emission chamber was examined, whereas an increase in the pressure difference to 1–4 Pa allowed for the investigation of the diffusive transport of ACAM with an oppositely directed convective airflow. The pressure differences were set by the throttle valve positioned in front of the double-acting ball valve above the detection chamber. The highest achievable pressure difference was 4 Pa. At pressure differences greater than 4 Pa, there is a risk of the bursting of the chambers. The atomization of 100 mg of ACAM was performed as previously described. All measurements were carried out in triplicate.

2.2.5. Determination of the Evacuation Time of the Detection Chamber during the Detection Phase

The quantification of the emission of ACAM dust was enabled by evacuating the detection chamber with an air sampling pump via the IOM sampler equipped with a glass microfiber filter. The determination of the evacuation time is required to ensure a reproducible measurement of the ACAM dust emission within a justifiable time period. For this reason, three different methods were used to determine the evacuation time. One approach was the use of smoke to visualize the flow of airborne particles and their behavior during the evacuation of the detection chamber. Another approach for the determination of the evacuation time was the CFD simulation. A third approach was based on the number of evacuation cycles and thus, the resulting evacuation time necessary for the complete elimination of the dust from the detection chamber.

With the first approach to determine the evacuation time, smoke was generated in the detection chamber by using an airflow tester to visualize the flow. The tube end of the airflow tester was connected to the two orifices for 10 s for pressure compensation via the Y-connector to draw the smoke into the detection chamber. A black background was placed below the detection chamber to increase the contrast of the white smoke resulting from a chemical reaction of pyrosulfuric acid present in the filling layer of the airflow tube with the air humidity. The true flow conditions in the detection chamber during each measurement were simulated by using an IOM sampler with a glass microfiber filter. The smoke was evacuated by the air sampling pump, with a flow rate of 5.0 L/min for 15 min. The decrease in the smoke density during the evacuation was monitored using a digital camera (ZV-1, Sony, Tokyo, Japan) mounted centrally above the detection chamber to provide square-shaped pictures. A picture of the white smoke was taken automatically every 5 s. The focus, as well as the ISO value, were adjusted manually to minimize optical disturbances and remained constant during the measurement. In addition, a cold light source (CL 1500 ECO, Zeiss, Jena, Germany) was used to ensure a high level of visibility. The pictures were analyzed with the image processing software ImageJ (US National Institute of Health (NIH), Bethesda, MD, USA) [36] to determine the time point of complete removal of the smoke from the detection chamber. In Figure 5, the top view of the detection chamber is shown with three square fields (200 pixels \times 200 pixels) positioned around the center point of the chamber. The mean gray value of each picture, as well as of each resulting square field, was measured. All measurements for determination of the evacuation time were carried out in triplicate.

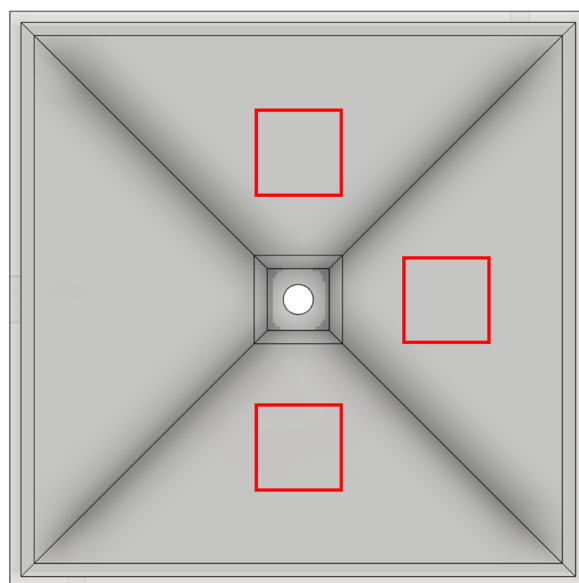


Figure 5. Detection chamber (top view) and the positions of the three square fields (highlighted in red) for the measurement of the mean gray value.

The second approach to investigate the evacuation time of the detection chamber was the CFD simulation. The same initial conditions were used as in the CFD simulation for the determination of the air velocity of airborne particles in the transport phase of the measurement course (Table 1). The boundary condition was set to a normal velocity (U_n) of 0.092 m/s at the outlet, which equals the volumetric flow of the evacuated airborne particles. The diffusion coefficient was set to $1 \times 10^{-8} \text{ m}^2/\text{s}$ in order to identify the zones of airborne particles with a high residence time. Data evaluation of the CFD results was performed with the data analysis and visualization application ParaView (version 5.10.1, Kitware, Clifton Park, NY, USA) [37].

For investigation of the evacuation time in the third approach, ACAM was again atomized in the emission chamber for 5 s, with an overpressure of 50,000 Pa, with the controllable flap closed. Subsequently, the controllable flap was opened for 60 s. Only the plain diffusive transport in the detection chamber was considered. The oppositely directed convective flow was excluded by closing the ball valve located above the detection chamber. Consequently, the pressure difference between both chambers was 0 Pa. To investigate the influence of various evacuation times on the measured dust emission of ACAM, evacuation times of 180, 360, 540, 720, and 900 s were predefined to evacuate the detection chamber up to five times at a flow rate of 5.0 L/min. Furthermore, dust emissions at an evacuation time of 3600 s were measured to investigate whether any significant differences existed in the collected ACAM amounts compared to those collected in the investigations with shorter evacuation times. A time period of 3600 s, corresponding to a 20-fold evacuation of the detection chamber, was assumed to be sufficient for the elimination of most airborne particles from the chamber. All measurements were again performed in triplicate. The amounts of ACAM collected in the glass microfiber filters were quantified by HPLC.

Finally, the three approaches for determination of the evacuation time of the detection chamber were compared (see Section 3.3) to ensure a comparability of the dustiness measurements within a justifiable time period.

2.3. Powder Characterization

2.3.1. Bulk Density and Tapped Density

The bulk density and tapped density of ACAM were measured using a jolting volumeter (STAV 2003, J. Engelsmann, Ludwigshafen, Germany) in accordance with the monograph 2.9.34, “Bulk Density and Tapped Density of Powders,” in the European Pharmacopoeia [38]. A 250 mL graduated measuring cylinder was filled with 100 g of ACAM. The V_{10} – V_{500} values, the compressibility index (Equation (1)), and the Hausner ratio (Equation (2)) were calculated using the powder density before (bulk density) and after 2500 taps (tapped density):

$$\text{Compressibility index} = 100 \times \left(\frac{\text{Tapped density} - \text{Bulk density}}{\text{Tapped density}} \right) \quad (1)$$

$$\text{Hausner factor} = \frac{\text{Tapped density}}{\text{Bulk density}} \quad (2)$$

The bulk density and tapped density of ACAM were measured in triplicate.

2.3.2. Particle Size Distribution

The particle size distribution of ACAM was investigated by laser diffractometry (Helos KR, Sympatec, Clausthal-Zellerfeld, Germany). A lens with an effective range of 0.5–875.0 μm was used for the measurements, which were performed in triplicate. The ACAM powder was dispersed by using compressed air with an air pressure of 150,000 Pa. The evaluation of the particle size distribution was performed with Paqxos software (Version 2.0.3, Sympatec, Clausthal-Zellerfeld, Germany).

2.3.3. True Density

The true density of ACAM was determined with a helium pycnometer (Pycnomatic ACT EVO, Porotec, Hofheim am Taunus, Germany). Approximately 8.0 g of ACAM were placed in the analysis chamber. The true density value was calculated as the mean of ten measurements. All determinations of true density were performed in triplicate.

2.3.4. Residual Moisture Content

The residual moisture content of ACAM was investigated using thermal gravimetric analysis (TG 209 F1 Libra[®], Netzsch-Gerätebau, Selb, Germany). The temperature was increased from 25 °C to 160 °C, with a heat rate of 10 K/min. These measurements were also performed in triplicate.

2.4. HPLC

The quantification of the collected ACAM in the glass microfiber filter was performed with a VWR-Hitachi Chromaster 5000 (Radnor, IN, USA), equipped with a 250 mm × 4 mm column (LiChroCART[®] 250-4, Merck, Darmstadt, Germany) containing an RP-18e phase (particle size 5 µm). HPLC measurements were carried out at 22 °C. A mobile phase consisting of a mixture of acetonitrile and water (75:25 *v/v*) was adjusted to a pH of 3.5 with phosphoric acid. The flow rate was set to 1 mL/min. A sample volume of 20 µL was injected, and a quantification of ACAM was performed spectrophotometrically at 245 nm. The total run time of one sample was 3.00 min. For elution of ACAM, 1.92 min were required.

The amount of ACAM in each glass microfiber filter was extracted with 2 mL of the mobile phase by shaking with a shaker (Unimax 1010, Heidolph Instruments, Kelheim, Germany) at 75 rpm for 20 min. The concentration of ACAM in the sample solutions was linear in the calibration range between 0.002 µg/mL and 2.212 µg/mL ($R^2 = 0.999$).

3. Results and Discussion

3.1. Validation of the Atomization Process

The two-chamber setup (TCS) was developed for the study of the dustiness of pharmaceutical powders by atomizing the powders with an overpressure of 50,000 Pa through the ball valve, centrally located above the emission chamber. The measurement process may be divided into three phases, the first of which is the atomization phase. Accordingly, the purpose of this study was to verify whether a reproducible and precise atomization of pharmaceutical powders is feasible using the TCS. For this purpose, various amounts of the surrogate substance acetaminophen (ACAM) were atomized in 50 mg portions. The dust emission was determined by the IOM sampler mounted in the detection chamber and by the subsequent quantification of ACAM with HPLC. In Figure 6, a linear correlation ($R^2 = 0.9842$) between the dust emission and the atomized amount of ACAM can be observed within the range of 50 and 400 mg of atomized ACAM. Within this range, the maximum relative SD is 6.58%. No significant increase in dust emission ($p > 0.05$) was observed within the range of 400 and 500 mg of atomized ACAM. Consequently, a reproducible atomization of ACAM is only possible within the range of 50 and 400 mg.

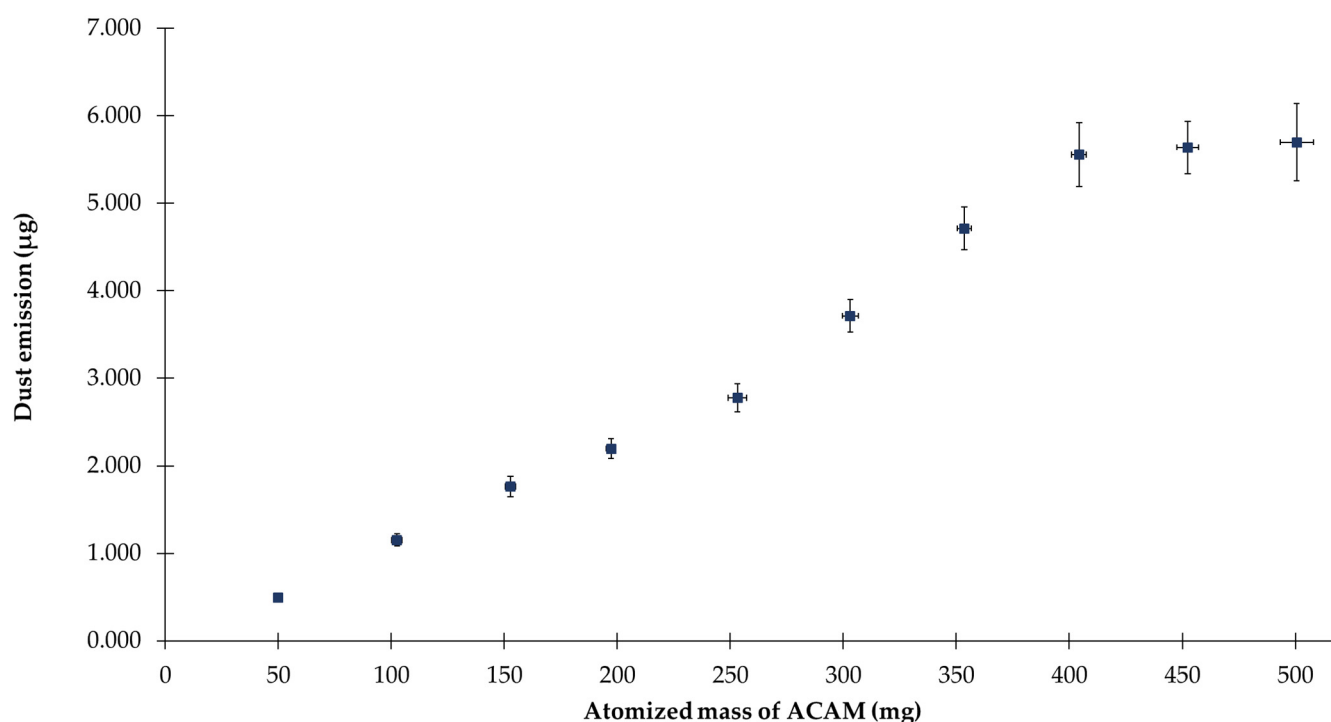


Figure 6. Dust emission versus the atomized mass of ACAM (means \pm SD, $n = 6$).

3.2. Results of the Dustiness Measurements during the Transport Phase

The TCS was constructed to study the dustiness of pharmaceutical powders affected by various flow conditions. In this study, four different pressure differences were generated between the emission and the detection chamber. The flows from the emission to the detection chamber resulting from the various pressure differences caused a reduction in the transport of airborne particles and were expected to lower the potential dust transfer from the emission to the detection chamber. The pressure differences between the chambers were obtained by compressed air flowing through the ball valve located above the detection chamber. The pressure difference was maintained for 60 s with the controllable flap open. By varying the pressure differences, resulting in corresponding flows, it was possible to determine whether a relationship exists between the air velocity and the decrease in the transfer of airborne particles from the emission to the detection chamber.

Currently, in the manufacturing of dosage forms containing HPAPIs, pharmaceutical production facilities commonly use negative pressure to reduce exposure due to potential leakage. Therefore, a convective flow from the outside to the inside occurs and prevents this leakage.

CFD was used in this study to simulate the resulting flows and flow velocities within the TCS. The air velocity within the setup is particularly crucial at the orifice (diameter 25.4 mm) between the emission and the detection chamber. In Figure 7, the CFD simulations are shown at pressure differences of 1–4 Pa. The four simulations showed that a high air velocity was observed at the position where the compressed air passes the ball valve. It is also apparent that the extent of the airflow affected the average air velocity at the orifice between both chambers, as a function of pressure difference.

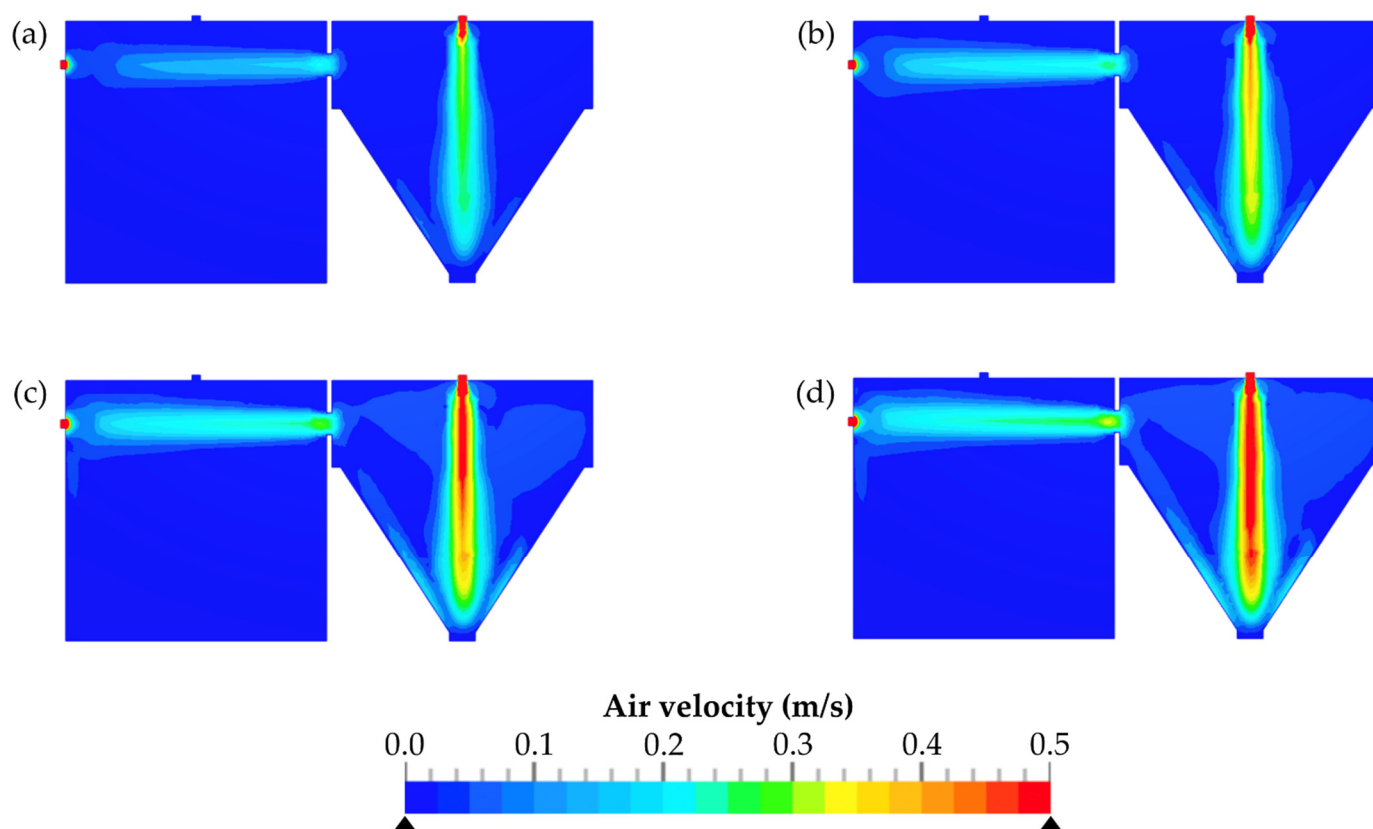


Figure 7. Resulting air velocities depending on the pressure difference between the emission and the detection chamber. Δp values: 1 Pa (a); 2 Pa (b); 3 Pa (c); 4 Pa (d).

The simulated and measured average air velocities are shown in Table 3. Accordingly, generating high pressure differences resulted in higher air velocities between both chambers.

Table 3. Simulated average velocity and measured average air velocities (means \pm SD, $n = 3$) at the orifice between the emission and the detection chamber.

Pressure Difference (Pa)	Simulated Average Air Velocity (m/s)	Measured Average Air Velocities (m/s)
1	0.081	0.08 ± 0.01
2	0.116	0.12 ± 0.01
3	0.144	0.15 ± 0.00
4	0.166	0.18 ± 0.01

The investigation of the effect of the air flow on dustiness was confirmed by atomizing ACAM, either with 0 Pa, for the examination of the plain diffusive transport of airborne particles, or with 1–4 Pa, for the examination of the diffusive transport with an oppositely directed convective flow. At 1–4 Pa, the oppositely directed convective air flow served as a measure to minimize dust emission. In Figure 8, the resulting dust emissions from various flow conditions are presented. The plain diffusive transport of airborne particles (0 Pa) resulted in the highest dust emission of $1.269 \pm 0.091 \mu\text{g}$ ACAM transported from the emission to the detection chamber for 60 s. A significant decrease in dust emission ($p < 0.05$) was observed during the examination of the diffusive transport of airborne particles with an oppositely directed convective flow. A pressure difference of 1 Pa between the emission and the detection chamber resulted in a significant decrease in the dust emission ($p < 0.05$) to a value of $0.557 \pm 0.042 \mu\text{g}$ ACAM. Furthermore, a significant reduction in dust emission ($p < 0.05$) was observed with increasing the pressure difference between both chambers. Compared to the examination at a pressure difference of 1 Pa, the dust emission was reduced

to 0.444 ± 0.029 μg ACAM at a pressure difference of 2 Pa. An increase in the pressure difference to 3 Pa resulted in a further reduction in the dust emission to 0.342 ± 0.027 μg ACAM. The maximum pressure difference of 4 Pa showed the highest reduction in the dust emission to a value of 0.256 ± 0.023 μg ACAM, compared to that of the plain diffusive transport of airborne particles.

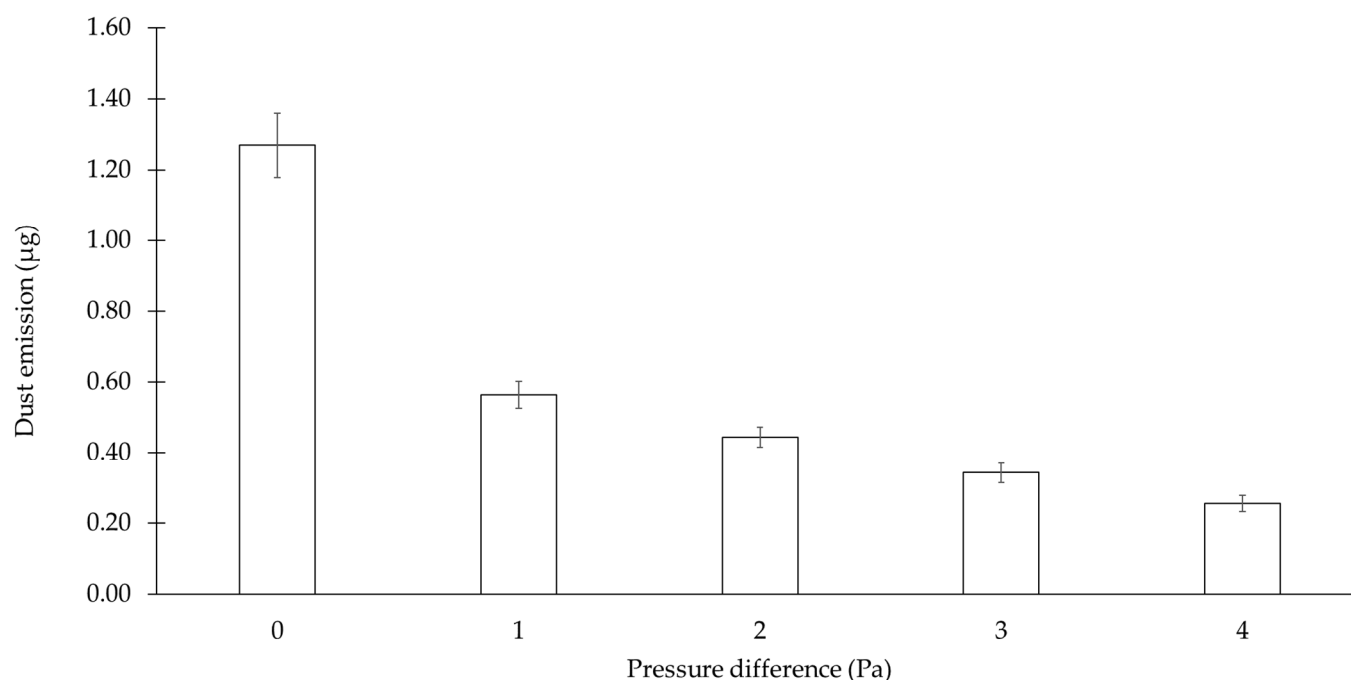


Figure 8. Dust emissions from the plain diffusive transport of ACAM (0 Pa) and from that of ACAM with the oppositely directed convective flow (means \pm SD, $n = 3$). For information on the simulated and measured average air velocity, refer to Table 3.

The results presented in Figure 8 show that the dust emissions of ACAM resulting from the plain diffusive transport within the TCS may be reduced by an oppositely directed convective flow. Furthermore, the results also indicate that an increase in the pressure difference led to a reduction in the dust emissions. Based on the CFD, the increase in the pressure difference enhanced the airflow velocities at the orifice between the emission and the detection chamber. Consequently, the higher airflow velocities resulted in a decrease in the dust emissions. The above-mentioned investigation showed that the pressure difference set within the TCS as a closed system exerted a substantial effect on the potential transfer of dust.

CFD enables the simulation of the average air velocity depending on the pressure difference between the emission and the detection chamber. These simulated average air velocities appear to be similar to the those found in the measured data, confirming the results of the CFD simulations (Table 3). However, the accuracy of the thermal anemometer is specified by the manufacturer with ± 0.1 m/s for air velocities between 0 and 2 m/s. This raises the question of how meaningful the measured values are. In this context, it must be considered that the accuracy increases with declining air velocities and decreases with rising air velocities (for example, the accuracy within an air velocity range of 2–15 m/s is specified with ± 0.3 m/s). As the measured average air velocities are very low, with about 0.1 m/s, it is therefore assumed that these values are trustworthy. A further argument for the relevance of the measured average air velocities is their low standard deviation, indicating a high reproducibility.

3.3. Determination of the Evacuation Time during the Detection Phase

The detection chamber is an essential part of the TCS, and it has a major impact on the detection phase of the measurement course. Because of the pyramidal design and the diagonal arrangement of the orifices for pressure compensation, most of the airborne ACAM particles should be detected within a reasonable time period. After the transport phase of the measuring course, which lasted for 1 min, the controllable flap was closed to detect the airborne ACAM particles that were transported by plain diffusive transport or by diffusive transport with oppositely directed convective flow from the emission to the detection chamber. For this purpose, the detection chamber containing the air with the airborne particles was evacuated, as previously described. The airborne ACAM particles were retained in the filter and were quantified by HPLC after extraction with the mobile phase.

To ensure that the airborne particles are collected in a reasonable time, CFD, flow visualization using smoke, and dustiness measurements with various evacuation times were performed. CFD was also used to evaluate the airflow within the detection chamber during evacuation.

A particle trace analysis was also performed with CFD, and the results are displayed in Figure 9. The negative pressure generated by the air sampling pump was compensated for by incoming air flowing through the diagonally arranged orifices (Figure 9a,b). Initially, the air flows were parallel to the walls of the detection chamber. Because of the diagonal arrangement of the orifices and the impingement of the airflow onto the walls opposite to the orifices, a rotation of the airflow occurred. The rotating airflow also shifted downwards within the detection chamber towards the IOM sampler attached to the bottom of the chamber (Figure 9c). The highest velocity of the airflow was measured directly at the orifices. After the incoming air passed the orifices, the velocity of the airflow within the chamber decreased.

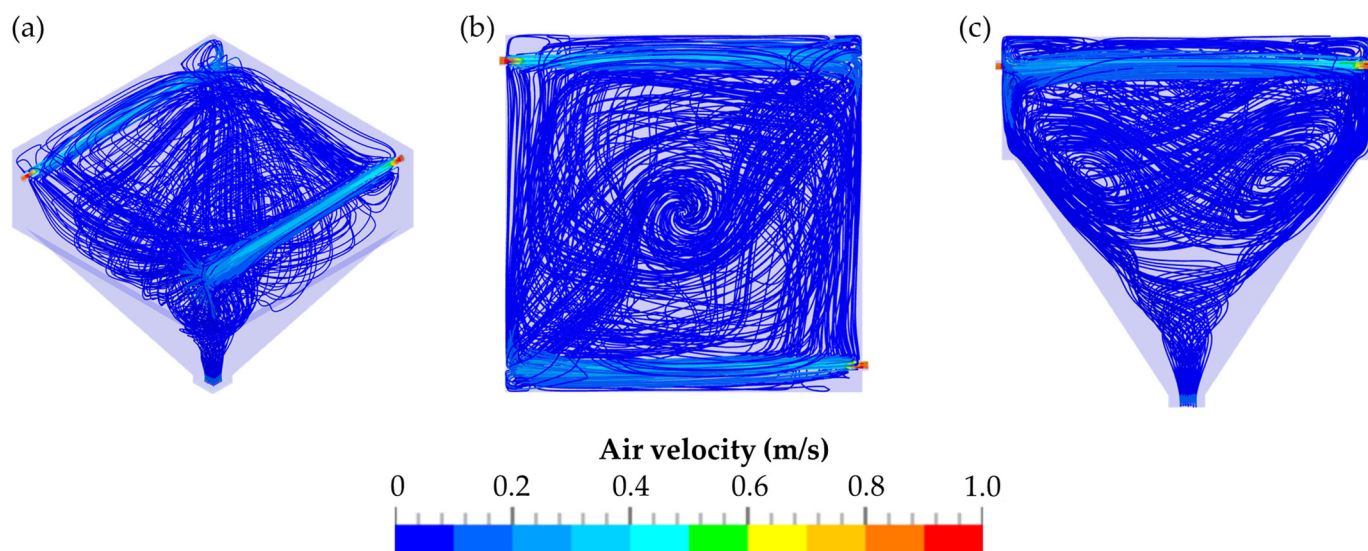


Figure 9. Particle trace analysis of the detection chamber during evacuation: overview of the TCS (a); top view of the TCS (b); lateral view of the TCS (c).

The residence time of the airborne particles within the detection chamber within different time periods is presented in Figure 10. The zones of the airborne particles, with a residence time between 540 and 900 s, are illustrated in Figure 10d. Compared to Figure 10a–c, which comprised three time periods of 180 s each up to the time point of 540 s, these zones are relatively small. These zones are located exclusively on the walls at the upper part of the detection chamber.

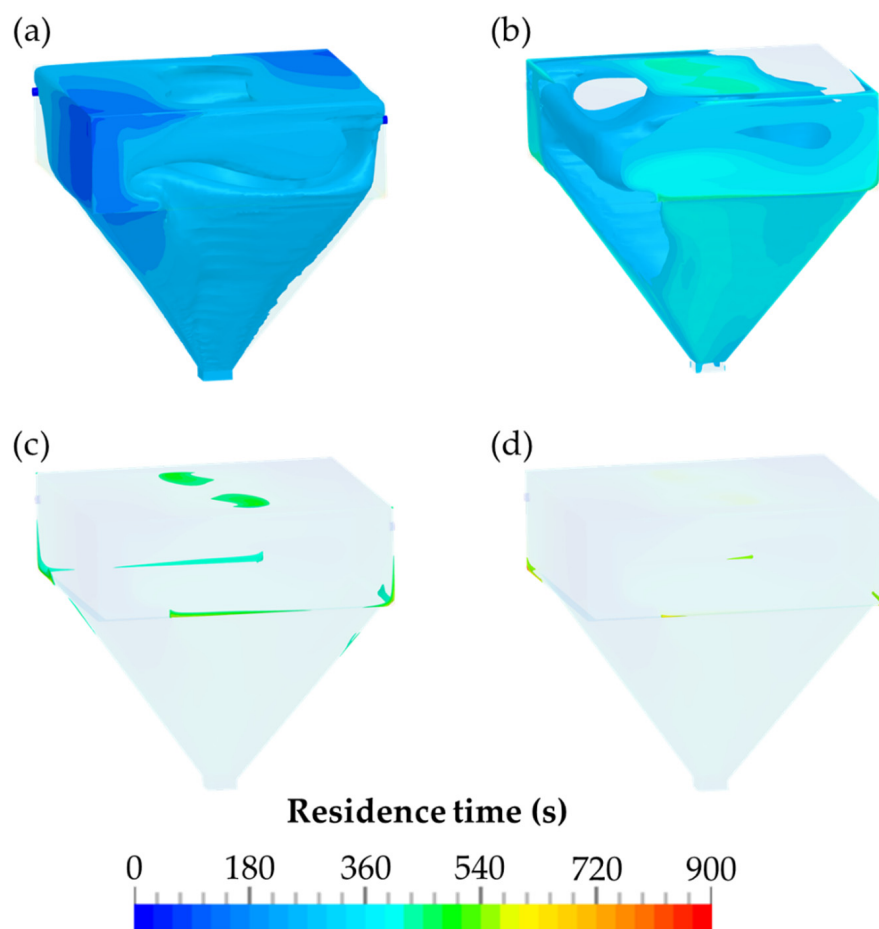


Figure 10. The residence time of the airborne particles within the detection chamber for various time periods: (a) 0–180 s; (b) 180–360 s; (c) 360–540 s; (d) 540–900 s.

In Figure 10a–c, the time course of the evacuation of the detection chamber is shown in time periods of 180 s. Every 180 s, a 15 L volume was evacuated through the glass microfiber filter of the detection chamber as a result of the flow rate of 5.0 L/min. Simultaneously, 15 L of particle-free air were introduced through the diagonally arranged orifices. The residence times of the airborne particles are shown in Figure 10. They indicate that after a three-fold evacuation of the detection chamber, which takes 540 s, the majority of the particles were already collected by the IOM sampler and could be quantified by HPLC.

The data obtained by CFD was analyzed by the ParaView application, and the total volume of the zones within the different time periods was determined. However, in the simulations, it should be considered that the diffusion coefficient was set to a low value of $1 \times 10^{-8} \text{ m}^2/\text{s}$ to accurately determine potential zones of airborne particles with a high residence time. These zones are especially perceptible at the transition from the upper part of the detection chamber to the pyramidal part of the chamber. The relative fraction of the zone within the time interval of 0–180 s was 61.92%. After an additional 180 s, 99.87% of the airborne particles within the TCS passed through the outlet of the detection chamber. As shown in Figure 10c, the zones for the time interval of 360–540 s are substantially smaller. After an evacuation time of 540 s, a volume of 99.99% was achieved.

An additional investigation was performed using smoke to visualize the flow within the detection chamber. For this purpose, smoke was passed through the two orifices for 10 s for pressure compensation to create a homogeneous smoke density. Subsequently, digital camera images were taken while the air sampling pump removed the smoke from the detection chamber at a flow rate of 5.0 L/min. The images were then analyzed for the gray value within the three square fields. The reason for this investigation was to

quantify the smoke density and thus, the amount of smoke removed based on the gray value. Therefore, the mean of the gray values of each square field was calculated. The evacuation time-dependent gray values were converted to relative values by defining the highest value as 100% and the lowest value of the resulting exponential decrease at the evacuation time of infinity as 0%. The removal of the smoke from the detection chamber resulted in a decrease in the relative values of the smoke density, as shown in Figure 11. Consequently, the obtained relative values of the exponential decrease in the smoke density were converted into the corresponding values defining the amount of removed smoke.

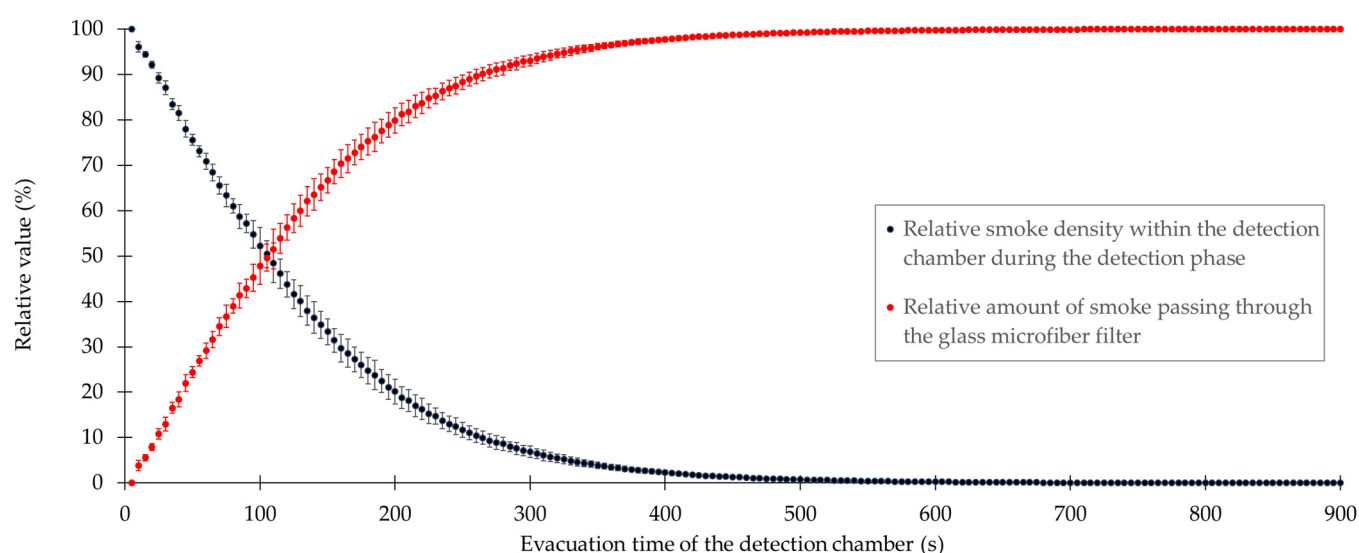


Figure 11. Relative values of the smoke density and the amount of removed smoke versus the evacuation time of the detection chamber.

After determination of the evacuation times of the detection chamber with both CFD simulations and smoke visualizations, additional experiments were performed with the surrogate substance ACAM to investigate whether a significant difference exists between the two evaluation methods. The results of the two evaluation methods revealed that within 900 s a large portion of the airborne particles has already passed through the glass microfiber filter, again in an exponential manner (Figure 11). An exponential decrease in the amount of tracer particles or surrogate substances over time was also observed using other devices for dustiness testing [29]. To ensure that most of the airborne particles were indeed collected within a reasonable time period, the detection chamber was evacuated for 3600 s. The ACAM dust emission measured at this time point was defined as the maximum achievable emission. The results obtained with this evacuation time were compared to those obtained with shorter evacuation times of 180, 360, 540, 720, and 900 s. With the data of the evacuation time-dependent CFD simulations and smoke visualizations, relative values were again calculated for comparative purposes. In Table 4, an overview of the evacuation times determined using CFD, smoke visualization, and dustiness measurements, using ACAM as a surrogate substance, is provided.

Table 4. Results of the three investigated methods for the determination of the evacuation time.

Evacuation Time (s)	Numbers of Evacuations	Relative Values \pm SD (%)		
		Smoke Visualization	CFD	Dustiness Investigation
180	1	75.24 \pm 2.93	61.92	74.00 \pm 5.40
360	2	96.50 \pm 0.62	99.87	92.14 \pm 7.35
540	3	99.51 \pm 0.13	99.99	99.18 \pm 5.13
720	4	99.93 \pm 0.02	100.00	99.47 \pm 5.97
900	5	100.00 \pm 0.00	100.00	99.56 \pm 6.36

For the evacuation time of 180 s, it was observed that the detection of airborne particles was insufficient using all three methods. Moreover, no significant difference ($p > 0.05$) between the relative values obtained by smoke visualization and dustiness measurements was found. However, a significant increase ($p < 0.05$) in the relative values obtained with all three methods was observed by extending the evacuation time to 360 s. The data obtained within the time period of 0–540 s showed that relative values over 99.00% were reached with all three methods. Prolonging the evacuation time to 720 or 900 s did not result in a significant increase ($p > 0.05$) in the relative values. The relatively large deviation of the relative values obtained with CFD from those obtained with the other two methods may likely be explained by the low diffusion coefficient of $1 \times 10^{-8} \text{ m}^2/\text{s}$. Therefore, increasing the evacuation time to 720 or 900 s did not result in the detection of higher amounts of dust.

3.4. Powder Characterization

As shown in previous studies, the dustiness of powders is influenced by various factors, such as true density, bulk density, and particle size [8,23]. Accordingly, the powder properties of the investigated ACAM were determined. The resulting values for the true density, the bulk density, the tapped density, the residual moisture content, and the particle size, with the respective standard deviations, are listed in Table 5. These values are comparable to other well-known and frequently used APIs.

Table 5. Physicochemical properties of the investigated ACAM (means \pm SD, $n = 3$).

Properties	Values
True density	$1.2886 \pm 0.0024 \text{ (g/cm}^3\text{)}$
Bulk density	$0.347 \pm 0.003 \text{ (g/cm}^3\text{)}$
Tapped density	$0.554 \pm 0.008 \text{ (g/cm}^3\text{)}$
Hausner ratio	1.60 ± 0.03
Compressibility index	$37.32 \pm 1.13 \text{ (%)}$
Residual moisture content	$0.138 \pm 0.053 \text{ (%)}$
Particle size	
\times_{10}	$1.67 \pm 0.08 \text{ (}\mu\text{m)}$
\times_{50}	$8.36 \pm 0.30 \text{ (}\mu\text{m)}$
\times_{90}	$24.33 \pm 0.90 \text{ (}\mu\text{m)}$

4. Conclusions

The two-chamber setup (TCS) presented in this study is a newly developed containment system created especially for the examination of the dustiness of pharmaceutical powders. A reproducible dustiness investigation of even small amounts of pharmaceutical powders is feasible with this setup, as was shown with the surrogate substance acetaminophen (ACAM). The ACAM used in the dustiness experiments exhibits powder properties comparable to other commonly used pharmaceutical powders. A high reproducibility of the dust emission was observed, as confirmed by low standard deviations and a linear correlation found between the atomized amount of up to 400 mg of ACAM and the resulting dust emissions. The deviation from the linearity for atomized amounts above 400 mg was possibly caused by a saturation effect within the system. Furthermore, the TCS was proven to be suitable for the investigation of the dust emission at different flow conditions (plain diffusive transport and diffusive transport with the oppositely directed convective flow of airborne particles). Particularly, the influence of the oppositely directed convective flow on the dust emissions was investigated, and the results indicate that an increase in the pressure difference between the emission and the detection chamber led to a major reduction in dust emissions. Moreover, a time period of 9 min for the evacuation of the detection chamber was sufficient for the detection of most airborne ACAM particles within the detection chamber. An extension of the evacuation time did not result in a significant increase in the detected particles. Computational fluid dynamics (CFD) simulations revealed that the air flowing through the orifices of the detection chamber for

pressure compensation caused a rotating and downward flow towards an IOM sampler. The relative values resulting from the examinations using either atomized ACAM or smoke for the determination of the evacuation time indicate that both methods are comparable. The deviation from the values simulated with CFD may be explained by the low diffusion coefficient of the simulation.

From the results of this study, it may be concluded that the presented TCS allowed for a containment investigation of small amounts of pharmaceutical powders, with regard to their dustiness, within a justifiable time. In future studies, other powder blends will be investigated in regards to their dustiness and their particle flow properties. Moreover, it is of interest to determine whether an additional increase in the pressure difference between the emission and the detection chamber may finally lead to a complete interruption of dust emission.

Author Contributions: Conceptualization, S.W, C.S.L. and M.S.; methodology, S.W.; software, J.B.; validation, S.W., C.S.L. and M.S.; formal analysis, S.W and C.S.L.; investigation, S.W.; data curation, S.W.; writing—original draft preparation, S.W.; writing—review and editing, S.W., C.S.L. and M.S.; visualization, S.W.; supervision, C.S.L.; All authors have read and agreed to the published version of the manuscript.

Funding: This research received no external funding.

Institutional Review Board Statement: Not applicable.

Informed Consent Statement: Not applicable.

Data Availability Statement: Not applicable.

Acknowledgments: The authors thank Petra Borbe and Kai Braunschweig for their technical support.

Conflicts of Interest: The authors declare no conflict of interest.

References

1. Mari, G.; Moccaldi, A.; Ludovisi, G. Handling of high potency drugs: Process and containment. *Trans. Ecol. Environ.* **1999**, *85*, 257–265. [CrossRef]
2. Wollowitz, S. Managing high-potency active pharmaceutical ingredients—A drug sponsor’s guide. *Drug Dev. Res.* **2010**, *71*, 420–428. [CrossRef]
3. Tiwari, P.; Chowdhury, S.R. Sustainable Production of Highly Active Pharmaceutical Ingredients (HAPIs). *Int. J. Sci. Res. Publ.* **2014**, *4*, 2250–3153.
4. Heron, R.J.L.; Pickering, F.C. Health effects of exposure to active pharmaceutical ingredients (APIs). *Occup. Med.* **2003**, *53*, 357–362. [CrossRef]
5. Michalson, E.T. High potency active pharmaceutical ingredients: An overview of safety and manufacturing concerns. *Chim. Oggi.* **2007**, *25*, 18–20.
6. International Society for Pharmaceutical Engineering (ISPE). *Good Practice Guide: Assessing the Particulate Containment Performance of Pharmaceutical Equipment*; ISPE: Tampa, FL, USA, 2012. Available online: <https://ispe.org/publications/guidance-documents/assessing-particulate-containment-performance> (accessed on 2 November 2022).
7. International Society for Pharmaceutical Engineering (ISPE D/A/CH Affiliate). *Containment Manual*. 2017. Available online: <https://ispe.org/publications/guidance-documents/dach-affiliate-containment-manual-english-translation> (accessed on 2 November 2022).
8. Liu, H.; Zhang, S.; Liu, L.; Yu, J.; Ding, B. High-performance filters from biomimetic wet-adhesive nanoarchitected networks. *J. Mater. Chem. A* **2020**, *8*, 18955–18962. [CrossRef]
9. Klippel, A.; Schmidt, M.; Krause, U. Dustiness in workplace safety and explosion protection—Review and outlook. *J. Loss Prev. Process Ind.* **2015**, *34*, 22–29. [CrossRef]
10. Van Nimmen, N.F.J.; Poels, K.L.C.; Veulemans, H.A.F. Identification of exposure pathways for opioid narcotic analgesics in pharmaceutical production workers. *Ann. Occup. Hyg.* **2006**, *50*, 665–677. [CrossRef]
11. Lidén, G. Dustiness testing of materials handled at workplaces. *Ann. Occup. Hyg.* **2006**, *50*, 437–439. [CrossRef]
12. Champmartin, C.; Clerc, F. Inhalable dust measurements as a first approach to assessing occupational exposure in the pharmaceutical industry. *J. Occup. Environ. Hyg.* **2014**, *11*, 85–92. [CrossRef]
13. Stein, J.; Fuchs, T.; Mattern, C. Advanced Milling and Containment Technologies for Superfine Active Pharmaceutical Ingredients. *Chem. Eng. Technol.* **2010**, *33*, 1464–1470. [CrossRef]
14. Levin, M.; Koponen, I.K.; Jensen, K.A. Exposure assessment of four pharmaceutical powders based on dustiness and evaluation of damaged HEPA filters. *J. Occup. Environ. Hyg.* **2014**, *11*, 165–177. [CrossRef] [PubMed]

15. Cherrie, J.W.; Gillies, A.T.; Smeuwenhoek, A.; van Tongeren, M.; McDonnell, P.; Coggins, M.; Bailey, S.R. Modelling exposure to pharmaceutical agents. *J. Phys. Conf. Ser.* **2009**, *151*, 012063. [CrossRef]
16. Hurychová, H.; Kuentz, M.; Šklubalová, Z. Fractal Aspects of Static and Dynamic Flow Properties of Pharmaceutical Excipients. *J. Pharm. Innov.* **2018**, *13*, 15–26. [CrossRef]
17. Bach, S.; Schmidt, E. Determining the dustiness of powders—A comparison of three measuring devices. *Ann. Occup. Hyg.* **2008**, *52*, 717–725. [CrossRef]
18. Hamelmann, F.; Schmidt, E. Methods for characterizing the dustiness estimation of powders. *Chem. Eng. Technol.* **2004**, *27*, 844–847. [CrossRef]
19. Bach, S.; Eickmann, U.; Schmidt, E. Comparison of established systems for measuring the dustiness of powders with the UNC dustiness tester developed especially for pharmaceutical substances. *Ann. Occup. Hyg.* **2013**, *57*, 1078–1086. [CrossRef]
20. Pensis, I.; Mareels, J.; Dahmann, D.; Mark, D. Comparative evaluation of the dustiness of industrial minerals according to European standard en 15051, 2006. *Ann. Occup. Hyg.* **2010**, *54*, 204–216. [CrossRef]
21. Boundy, M.; Leith, D.; Polton, T. Method to evaluate the dustiness of pharmaceutical powders. *Ann. Occup. Hyg.* **2006**, *50*, 453–458. [CrossRef]
22. Ohta, T.; Maeda, H.; Kubota, R.; Koga, A.; Terada, K. Establishment of powder dustiness evaluation method by dustmeter with small amount of pharmaceutical ingredients. *Int. J. Pharm.* **2014**, *472*, 251–256. [CrossRef]
23. Sethi, S.A. Generation of small particles by gas fluidization. *J. Aerosol. Sci.* **1997**, *28* (Suppl. S1), S539–S540. [CrossRef]
24. Plinke, M.A.E.; Maus, R.; Leith, D. Experimental examination of factors that affect dust generation by using heubach and mri testers. *Am. Ind. Hyg. Assoc. J.* **1992**, *53*, 325–330. [CrossRef] [PubMed]
25. Hjemsted, K.; Schneider, T. Dustiness from powder materials. *J. Aerosol. Sci.* **1996**, *27* (Suppl. S1), S485–S486. [CrossRef]
26. Lanning, J.; Boundy, M.A.G.; Leith, D. Validating a model for the prediction of dust generation. *Part. Sci. Technol.* **1995**, *13*, 105–116. [CrossRef]
27. Kenny, L. Scientific principles and pragmatic solutions for the measurement of exposure to inhalable dust. *Ann. Occup. Hyg.* **2003**, *47*, 437–440. [CrossRef] [PubMed]
28. Deng, T.; Paul, K.A.; Bradley, M.S.A.; Immins, L.; Preston, C.; Scott, J.F.; Welfare, E.H. Investigations on air induced segregation of pharmaceutical powders and effect of material flow functions. *Powder Technol.* **2010**, *203*, 354–358. [CrossRef]
29. Butler, O.; Forder, J.; Saunders, J. Analytical protocol for the sensitive determination of mannitol, sorbitol and glucose containing powders in pharmaceutical workplaces by ion chromatography using a pulsed amperometric detector. *J. Pharm. Biomed. Anal.* **2015**, *106*, 204–209. [CrossRef]
30. Lavanya, N.; Bhattacharyya, S. Computational fluid dynamics—the futuristic innovation in pharmaceutical industry. *Indian J. Pharm. Educ. Res.* **2021**, *55*, 930–938. [CrossRef]
31. Tong, Z.B.; Zheng, B.; Yang, R.Y.; Yu, A.B.; Chan, H.K. CFD-DEM investigation of the dispersion mechanisms in commercial dry powder inhalers. *Powder Technol.* **2013**, *240*, 19–24. [CrossRef]
32. Dubey, P.; Ghia, U.; Turkevich, L.A. Computational fluid dynamics analysis of the Venturi Dustiness Tester. *Powder Technol.* **2017**, *312*, 310–320. [CrossRef]
33. Chen, H.; Jog, M.A.; Turkevich, L.A. Computational fluid dynamics simulations of aerosol behavior in a high-speed (Heubach) rotating drum dustiness tester. *Particuology* **2023**, *72*, 68–80. [CrossRef]
34. Science, A.; Palakurthi, N.K. Aerodynamics of Particle Detachment from Surfaces—A Numerical Study. Master’s Thesis, University of Cincinnati, Cincinnati, OH, USA, 19 December 2016.
35. Pujara, C.P. Determination of Factors that Affect the Generation of Airborne Particles from Bulk Pharmaceutical Powders. Ph.D. Thesis, Purdue University, West Lafayette, IN, USA, 18 February 1997. Available online: <https://docs.lib.purdue.edu/dissertations/AAI9808505/> (accessed on 31 August 2022).
36. Schneider, C.A.; Rasband, W.S.; Eliceiri, K.W. NIH Image to ImageJ: 25 years of image analysis. *Nat. Methods* **2012**, *9*, 671–675. [CrossRef] [PubMed]
37. Geveci, B. *ParaView: An End-User Tool for Large Data Visualization ParaViewWeb View Project*; The Visualization Handbook 717(8); Elsevier: Amsterdam, Netherlands, 2005; Volume 836.
38. *European Pharmacopoeia 10.0*, 2.9.34. *Bulk Density and Tapped Density of Powders*; European Pharmacopoeia Commission: Strasbourg, France; European Directorate for the Quality of Medicines & Health Care: Strasbourg, France, 2019; pp. 384–387.

3.2 An Investigation on the relationship between dust emission and air flow as well as particle size with a novel containment two-chamber setup

In this study, the relationship of particle size, pressure difference, and air velocity with the resulting dust emissions were investigated.

Initially, increased pressure differences between the emission and detection chambers of 0 - 12 Pa, which could be achieved by design modifications of the TCS, resulting in increased air velocities were examined. For comparative purposes, a CFD was carried out to simulate the average air velocities between the two chambers. These simulated average air velocities within the TCS provided values between 0.09 and 0.37 m/s and matched the experimentally determined values of 0.09 - 0.41 m/s accurately. Furthermore, the results confirm that both simulated and experimentally determined air velocities increase with increasing pressure difference.

Subsequently, six different particle size fractions of ACAM were examined at pressure differences between 0 and 12 Pa to analyse their influence on the resulting dust emissions. In these experiments, fine particles led to higher overall dust emissions than coarse particles. An increase of the pressure difference between the two chambers, leading to an according increase in air velocity, caused a significant reduction in dust emission for all particle size fractions. Depending on the particle size of the surrogate substance ACAM, pressure differences of 5 - 8 Pa were sufficient to reduce emissions to non-quantifiable levels. With coarse particles, a lower pressure difference and, consequently, a lower air velocity is sufficient to decrease dustiness to undetectable ACAM quantities.

In summary, the results of this study show that, depending on the powder dustiness, pressure differences and the resulting air flows, which may form flow barriers, effectively prevent the leakage of dust particles from a containment system.

The overall concept and methodology of the presented study are visually summarised in Figure 8.

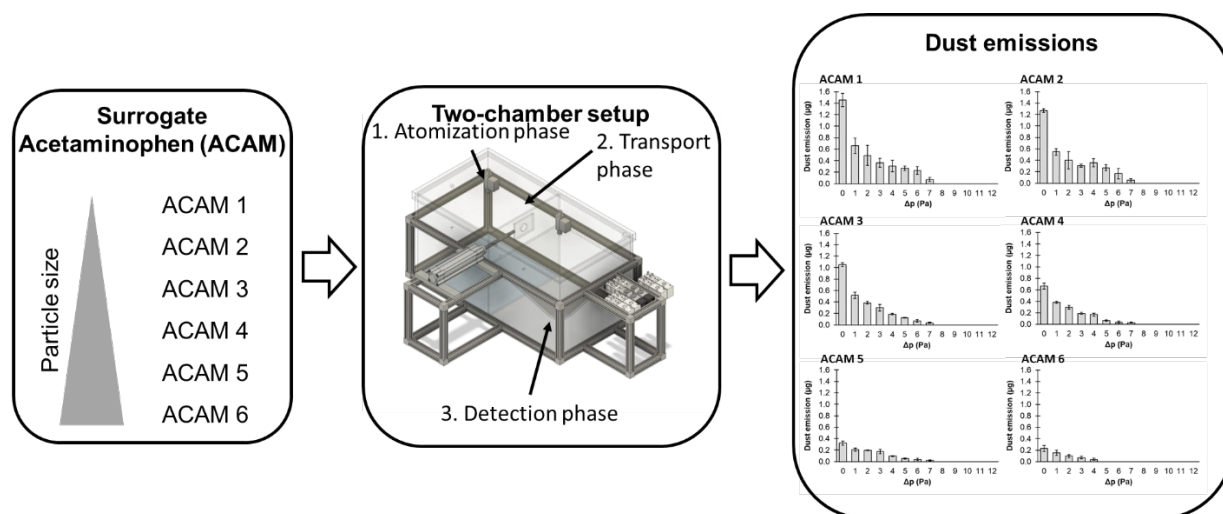


Figure 8: Comprehensive depiction of the study design and key results [171].

Dosage forms containing the plain active ingredient only play a minor role, because additional excipients are usually necessary for the manufacture of drug products. These excipients might not only affect the physicochemical properties of the APIs during processing but may also considerably alter the dust emissions of the active ingredients. Based on the results of this study, in which plain ACAM without excipients was investigated, in the next study, blends of an API and an excipient of varying particle sizes and their influence on DTS were examined. Such investigations of DTS may help to better understand and to take into consideration the interactions between active ingredients and excipients.

Article

An Investigation on the Relationship between Dust Emission and Air Flow as Well as Particle Size with a Novel Containment Two-Chamber Setup

Steffen Wirth ¹, Martin Schöler ², Jonas Brüggmann ² and Claudia S. Leopold ^{1,*}

¹ Department of Pharmaceutical Technology, University of Hamburg, Bundesstr. 45, 20146 Hamburg, Germany; steffen.wirth@uni-hamburg.de

² Fette Compacting GmbH, Grabauer Straße 24, 21493 Schwarzenbek, Germany; mschoeler@fette-compacting.com (M.S.)

* Correspondence: claudia.leopold@uni-hamburg.de; Tel.: +49-40-42838-3479

Abstract: In the present study with a novel two-chamber setup (TCS) for dustiness investigations, the relationship between pressure differences as well as air velocities and the resulting dust emissions is investigated. The dust emissions of six particle size fractions of acetaminophen at pressure differences between 0 and 12 Pa are examined. The results show that both simulated and measured air velocities increase with increasing pressure difference. Dust emissions decrease significantly with increasing pressure difference and air velocity. Fine particles cause higher dust emissions than coarse particles. A high goodness of fit is obtained with exponential and quadratic functions to describe the relationship between pressure difference and dust emission, indicating that even moderate increases in pressure may lead to a reduction in the emission. Average air velocities within the TCS simulated with Computational Fluid Dynamics are between 0.09 and 0.37 m/s, whereas those measured experimentally are between 0.09 and 0.41 m/s, both ranges corresponding to the recommended values for effective particle separation in containment systems. These results underline the ability of the novel TCS to control pressure and airflow, which is essential for reliable dust emission measurements and thus provide support for further scientific and industrial applications.

Keywords: containment; HPAPI; two-chamber setup; flow barrier; dustiness; dust emissions



Citation: Wirth, S.; Schöler, M.; Brüggmann, J.; Leopold, C.S. An Investigation on the Relationship between Dust Emission and Air Flow as Well as Particle Size with a Novel Containment Two-Chamber Setup. *Pharmaceutics* **2024**, *16*, 1088. <https://doi.org/10.3390/pharmaceutics16081088>

Academic Editor: Thierry Vandamme

Received: 23 July 2024

Revised: 13 August 2024

Accepted: 14 August 2024

Published: 20 August 2024



Copyright: © 2024 by the authors. Licensee MDPI, Basel, Switzerland. This article is an open access article distributed under the terms and conditions of the Creative Commons Attribution (CC BY) license (<https://creativecommons.org/licenses/by/4.0/>).

1. Introduction

In recent years, highly potent active pharmaceutical ingredients (HPAPIs) have become more prevalent, making the safe handling of these potentially hazardous substances increasingly important. HPAPIs not only cause pronounced pharmacological effects but may also compromise the environment even at very low concentrations [1–6]. They are used in various therapeutic areas, e.g., oncology, neurology, endocrinology, and in the treatment of autoimmune diseases. Examples for HPAPIs include cytostatics, hormones, antibody–drug conjugates, and immunomodulators [7–11]. Because of the high health risks associated with HPAPIs, appropriate safety measures, including specific plant and equipment designs, are required. These facilities have to be specifically designed to meet the unique requirements of HPAPI manufacturing, including complex filtration and ventilation systems with high efficiency regarding the removal of fine airborne particles and thus enhancing protection against hazardous airborne substances [12–16]. These precautions include establishing airlocks, maintaining pressure differentials, using high-efficiency filters, restricting access to areas where HPAPIs are handled, as well as the use of specialized personnel-protective equipment to reduce health risks [5,17]. Dust collection systems in milling plants, for example, may also help to minimize airborne exposure and ensure a safer working environment in pharmaceutical manufacturing [18].

A further important issue in this context is to avoid contamination of the environment as well as cross-contamination during production and its accompanying manufacturing processes [3,7,19,20]. As the processing of HPAPIs inevitably generates pharmaceutical dust, appropriate containment systems and special equipment designs are required to minimize potential hazard exposure [1,21–23]. In this regard, dustiness describes the tendency of powdery material to generate airborne particles during its handling [21,24,25]. Various processes in pharmaceutical manufacturing, such as material transfer, milling, blending, and granulation are associated with the generation of dust and therefore pose a risk for a potential hazard exposure if HPAPIs are used. Dust generation from pharmaceutical powders is influenced by numerous factors, particularly the physicochemical and mechanical properties of the powders [1,18,26–31].

The establishment of occupational exposure limits (OELs), detailed hazard and risk assessments, and a clear understanding and implementation of containment procedures are necessary for a careful approach to handling HPAPIs [3,8–10,32–34]. The measurement of dust formation is therefore of crucial importance for assessing the health hazards in pharmaceutical facilities. For this purpose, various systems and methods have been developed to reproducibly measure the dust generation of powdery solids. However, most of these systems and methods are not designed for pharmaceutical applications, as the material quantities required for these measurements are relatively high. HPAPIs, for example, are often available only in limited quantities and are relatively expensive [35–40]. In this study, therefore, a novel two-chamber model was used to investigate the dustiness of powders under different flow conditions.

The atomization of powders is achieved by applying energy to a powder bulk leading to the distribution of particles in the air. The use of excessive energy may even lead to fragmentation of single particles and therefore to a potentially higher dust generation. Each method for the detection of dust generation involves a different technique of atomization, making a comparison of the different dust detection methods difficult. An exact prediction of dust generation only based on material properties such as particle size and density is not yet possible. Nevertheless, particle size distribution, particle shape, bulk density, residual moisture, as well as cohesive and adhesive forces between powder particles have a significant influence on dust generation [36,38,41–44].

Reproducible dust generation requires a standardized atomization method with detailed specifications regarding test duration, type and intensity of the mechanical stimulus, and the amount of test material. A high degree of standardization is also essential for performing appropriate dust measurements to ensure reproducibility and a comparability of the results with the conditions during industrial manufacturing processes [38,41,45]. Powdery substances are frequently used to assess the containment performance of equipment by measuring their airborne particle concentration outside of the contained area. The ISPE (International Society for Pharmaceutical Engineering) recommends various surrogates in its Good Practice Guide, including acetaminophen, insulin, mannitol, naproxen sodium, riboflavin, sucrose, and lactose monohydrate [1,46].

Previous studies have shown that Computational Fluid Dynamics (CFD) simulations are suitable for analyzing the flow behavior during dustiness investigations [47,48]. CFD comprises the numerical simulation of fluid dynamics in liquids and gases including dust. By applying numerical models, CFD enables detailed analyses of flow patterns, temperature distributions, and other physical parameters in complex systems. It is an essential tool in various engineering disciplines as well as the pharmaceutical area as it provides profound insights into the behavior of fluids in general. CFD is used to model and optimize a variety of processes, including the characterization of devices and systems for the measurement of airborne particles. The numerical models allow a detailed visualization of the aerodynamics in these devices or systems for investigating the distribution of airborne particles and identify potential areas of particle accumulation [49]. In addition, CFD simulations may illustrate the particle flow in complex systems providing profound knowledge on the

atomization process of pharmaceutical powders and allowing the entire production chain to be optimized [25,39,50,51].

One strategy for preventing the unwanted emission of airborne substances is the implementation of a flow barrier, which is described as a displacement concept in EN ISO 14664-4, among others. In this concept, an air flow is directed from the surrounding region into the process zone through positive pressure, effectively preventing the reverse transport of particles. This principle is characterized by the use of a comparatively high air flow accompanied by relatively low pressure differences between the environment and the process zone. In the case of leakage, minimum flow velocities of 0.2 m/s are required for separation of the environment from the process zone. Therefore, flow velocities of 0.4–0.5 m/s are recommended [52,53]. Maintaining a high air flow is necessary to prevent the emission of harmful particles in the event of leakage.

The main objective of this study is to analyze pressure differences within a newly developed two-chamber setup (TCS) by applying these pressure differences to generate both plain diffusive and oppositely directed convective transport of air particles. The surrogate substance, acetaminophen, was atomized inside the TCS and subsequently quantified. In a previous study, it was already demonstrated that different flow conditions within the closed system may be investigated and even small amounts of pharmaceutical powders may be detected [47]. Based on these findings, the present study focuses on the influence of the particle size of the airborne particles and their transport at high air velocities on the resulting dust emissions.

2. Materials and Methods

2.1. Materials

Acetaminophen (ACAM; Caelo, Hilden, Germany and Fagron, Glinde, Germany) was used as an industry-accepted safe surrogate substance recommended by the ISPE for dustiness. ACAM from Caelo was micronized, whereas that from Fagron showed a particle size of about 20 to 500 μm .

2.2. Two-Chamber Setup (TCS)

2.2.1. Design of the TCS

In Figure 1, an illustration of the TCS which was recently described in the literature, is shown [47]. The TCS used in this study consists of 6 mm acrylic glass panes with external dimensions of $618 \times 312 \times 306$ mm. The TCS is divided into two chambers, which are separated by an acrylic glass wall of the same thickness. The two chambers, referred to as the emission and detection chambers, are connected to each other by an orifice with a diameter of 25.4 mm. Consequently, the dimensions of both the emission and detection chambers are $300 \times 300 \times 300$ mm.

The detection chamber has an additional pyramidal construction to improve the detection of airborne particles. By installing this construction, the volume of the detection chamber is reduced to about 15 L, while the volume of the emission chamber remains at 27 L. Both chambers are separated at the top by a removable lid, which is also made of acrylic glass and with dimensions of $630 \times 324 \times 30$ mm. To ensure that the removable lid is sealed, an adhesive elastic rubber seal is applied to the edges of the chambers. By means of toggle locks, which press the lid onto the seals of the chambers to hold them in position, the tightness of the TCS to the environment is ensured. The lid contains two orifices that are positioned centrally above both the emission and detection chambers and are required for atomization and the generation of oppositely directed convective flow. Additional orifices are provided in the lower part of the TCS, being mandatory over the course of the experiment process: In addition to the orifice that establishes a connection to the detection chamber in the emission chamber, in addition, there is another orifice that is necessary for pressure compensation during atomization. Furthermore, there is an orifice for the attachment of a TPE tube (PUN-10X, Festo, Esslingen, Germany), allowing a differential pressure gauge (testo 400, Testo, Titisee-Neustadt, Germany) to be directly

connected to the emission chamber. The differential pressure gauge is also connected to an orifice in the detection chamber via a TPE tube. Two type-K thermoelectric couples (thermoelectric couple type-K with TC plug, Testo, Titisee-Neustadt, Germany) are installed in both chambers to be able to monitor the temperature. In addition, the detection chamber contains two diagonally arranged orifices for pressure compensation during evacuation of the chamber. Previous studies have already shown that a diagonal arrangement of the orifices enables a reproducible collection of airborne particles within reasonable time [47,54]. A further orifice is located at the bottom of the detection chamber, towards which the pyramidal construction extends. An IOM sampler (Institute of Occupational Medicine; SKC, Blandford Forum, UK), which is required for the detection of airborne particles, is attached to this orifice. The IOM sampler is further connected to an air sampling pump (AirChek ESSENTIAL Pump, SKC, Blandford Forum, UK).

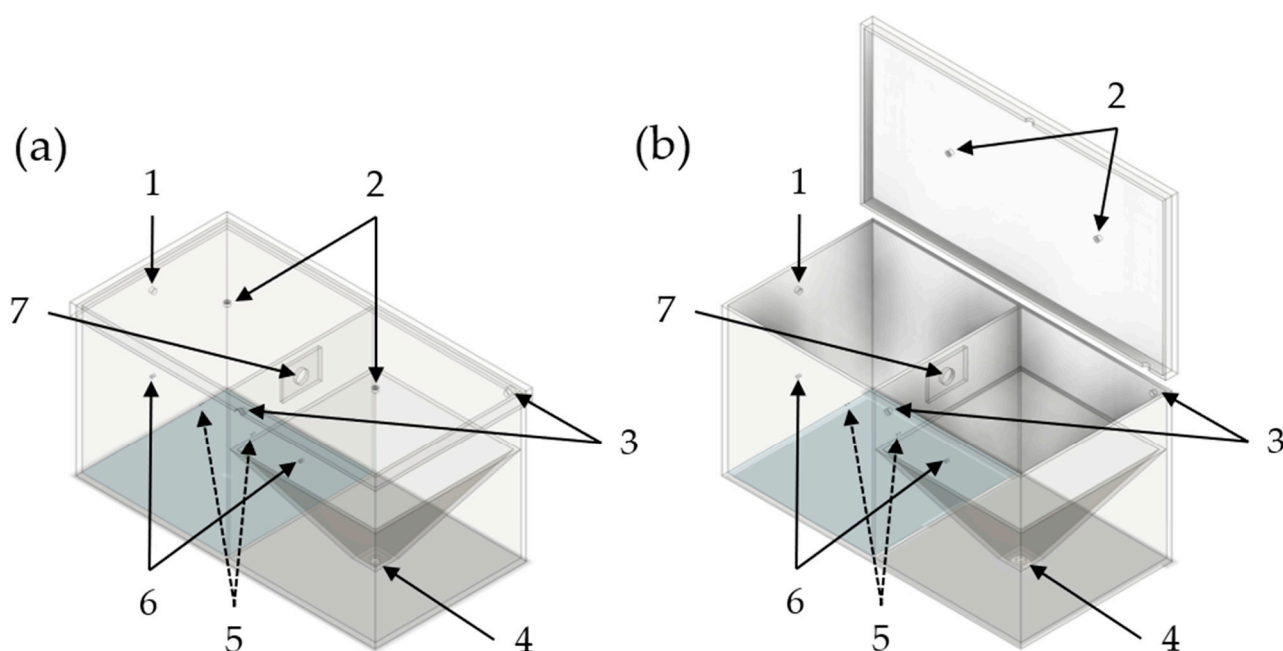


Figure 1. Simplified illustration of the TCS in a closed state (a) and an open state (b). 1: Orifice for pressure compensation of the emission chamber; 2: Orifices for the double-acting ball valves for atomization and oppositely directed convective flow; 3: Orifices for pressure compensation of the detection chamber during the detection phase; 4: Orifice for the IOM sampler; 5: Orifices for the attachment of thermal sensors of the differential pressure gauge; 6: Orifices for the measurement of the differential pressure with the differential pressure gauge; 7: Connection orifice between the emission and the detection chamber.

In Figure 2, a more detailed illustration of the TCS with further constructive parts is shown. The TCS is surrounded by a frame of B-type aluminum profiles to which measuring devices and electronic and pneumatic components for process control are mounted. To adjust predefined pressure differences and to control the pressure difference during the possible transport of airborne particles from the emission to the detection chamber, a differential pressure gauge is required, which is attached to the B-type aluminum profiles. A digital paddle wheel flow meter (35812, ANALYT-MTC Meßtechnik, Mülheim, Germany) is also fastened to the profiles to monitor the set flow rate during the evacuation of the detection chamber. The measurement process is centrally controlled via a programmable logic controller (PLC, Siemens LOGO! 12/24RC, Munich, Germany). The PLC is controlled by a single-board microcontroller (Arduino® Uno Rev3, Ivrea, Italy) and receives a signal from it, which is amplified by a DC/DC converter to provide a sufficiently high input

signal. The single-board microcontroller is necessary for synchronizing all devices with the server time and consequently with the measurement phases.

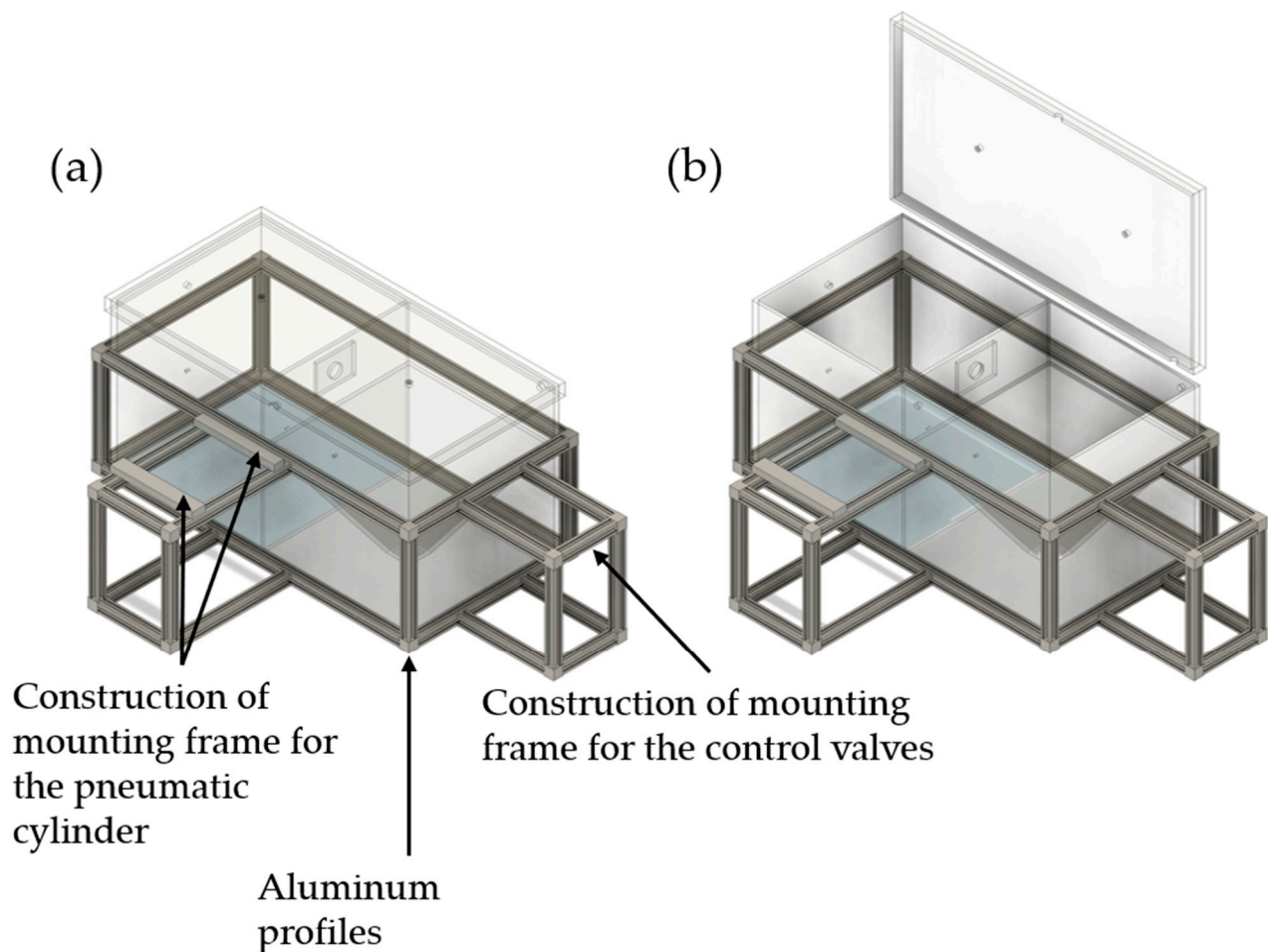


Figure 2. Illustration of the TCS and the constructive components for fastening the pneumatic components: (a) TCS in closed state; (b) TCS in open state.

In Figure 3, the system control of the individual pneumatic components by the PLC of the TCS is shown in a piping and instrumentation diagram. The different phases of a measurement are centrally controlled by two 5/2 and two 3/2 solenoid valves. These valves are connected to the corresponding pneumatic components and ensure that the signals sent by the PLC trigger the required operations. This configuration allows for precise control over all phases of the measurement.

In Figure 4, the pneumatic components of the TCS are illustrated. The four output slots of the PLC are connected to two 5/2 and two 3/2 solenoid valves, which are also attached to the aluminum profiles. One of the 5/2 solenoid valves is used for the pneumatic control of the first double-acting ball valve, which is responsible for atomizing the powder samples in the emission chamber. The other 5/2 solenoid valve is applied for the pneumatic control of the second double-acting ball valve (inlet orifice), required for the adjustment of plain diffusion or the generation of an oppositely directed convective flow. The 3/2 solenoid valves represent the outlet orifice and the opening for pressure control, respectively.

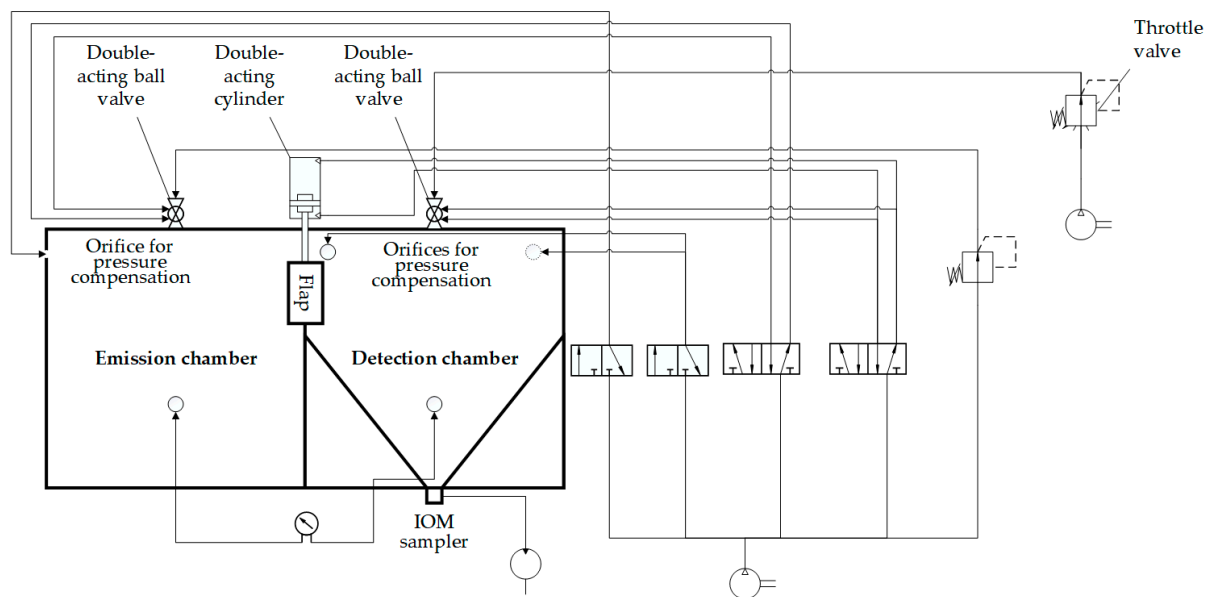


Figure 3. Piping and instrumentation diagram of the individual pneumatic components by the PLC of the TCS.

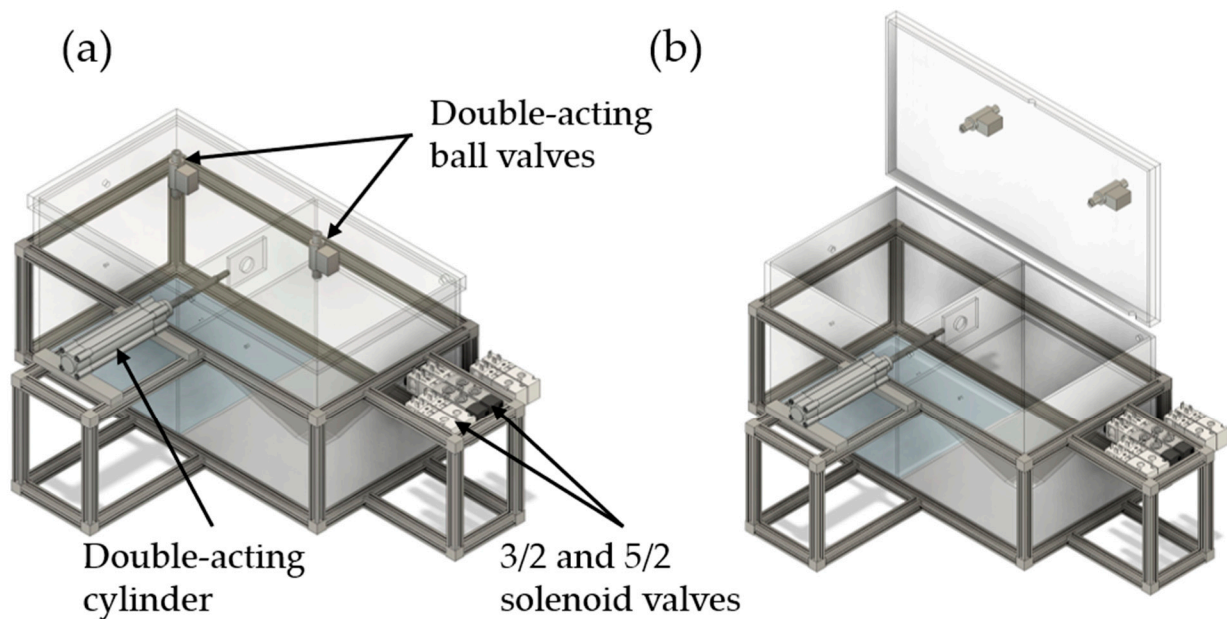


Figure 4. Detailed illustration of the TCS, its aluminum profiles, and pneumatic components: (a) TCS in closed state; (b) TCS in open state.

Two compressors are used in the design of the TCS. The first compressor (Mega 520-200 D Metabo, Nürtingen, Germany) is required to operate the pneumatic components. By adjusting the flow regulator of the second compressor (Mega 400–50 W; Metabo, Nürtingen, Germany), it is possible to choose between plain diffusive and oppositely directed convective transport. In addition, this 5/2 solenoid valve also pneumatically controls a double-acting cylinder which is connected to the flap required to control the opening or closing of the orifice between the emission and detection chambers.

2.2.2. TCS Measurement Phases

In general, the dustiness measurements with the TCS are divided into three phases, as shown in Figure 5. In the first phase, named the atomization phase, 100 mg of ACAM

with different particle sizes are atomized in the emission chamber with the double-acting ball valve at an overpressure of 50,000 Pa for 5 s. The pressure is compensated for the pneumatic control of the 3/2 valve, also for 5 s. During atomization, the double-acting cylinder is actuated so that the flap separates the emission from the detection chamber. This measure ensures that the ACAM particles are homogeneously distributed in the emission chamber without being transferred to the detection chamber.

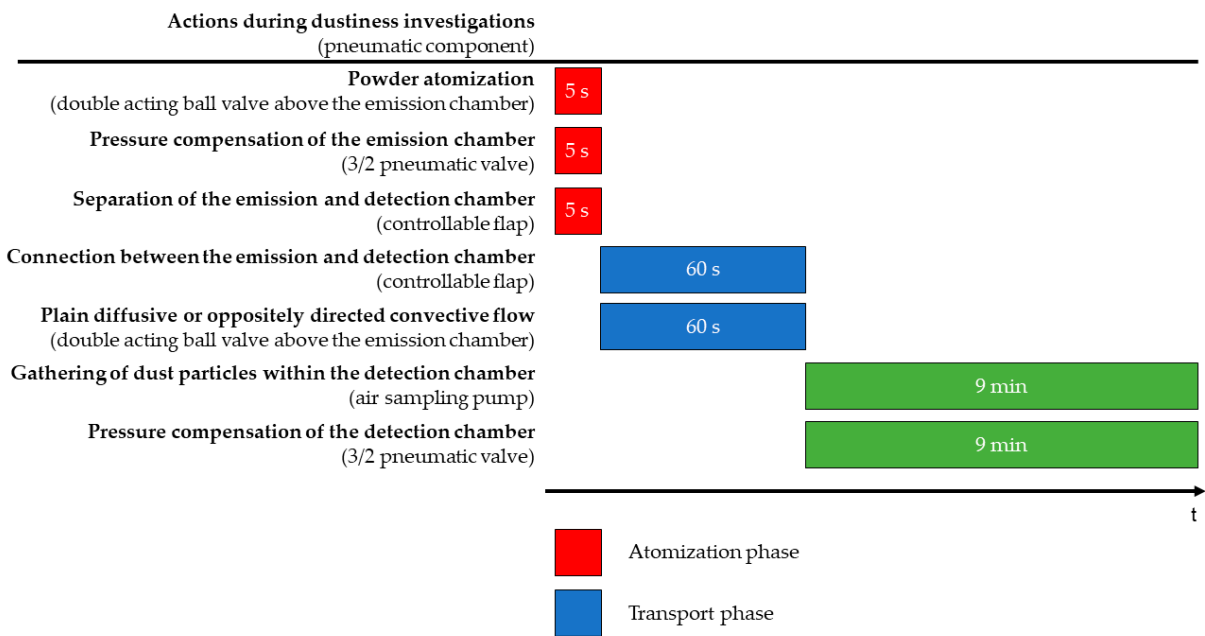


Figure 5. Simplified diagram of the three measurement phases of the TCS.

In the second phase of the measurement, also referred to as the transport phase, the transport of the airborne particles from the emission to the detection chamber is investigated. This phase is intended for analyzing the plain diffusive transport and the oppositely directed convective transport of the airborne particles within the TCS. By adjusting the pressure between the two chambers, it is either feasible to investigate a plain diffusive transport ($\Delta p = 0$ Pa) or a convective flow ($\Delta p > 0$ Pa). In this phase of the dustiness measurements, the controllable flap is opened for 60 s to allow either diffusive or convective flow between the two chambers and to observe the transport of airborne particles. At the same time, the double-acting ball valve above the detection chamber is opened and the double-acting cylinder is deactivated, thereby connecting the emission with the detection chambers. The pressure difference between the two chambers is verified by the differential pressure gauge.

The third phase, also known as the detection phase, involves the separation of the two chambers by closing the controllable flap after 60 s, thereby quantifying the amount of ACAM transferred from the emission to the detection chamber. Directly after the second measurement phase, the air sampling pump is activated, and the detection chamber is evacuated at a flow rate of 5.0 L/min for 9 min. Meanwhile, pressure compensation is ensured by opening the pneumatic 3/2 valve allowing the flow of filtered air through the diagonally arranged orifices.

2.2.3. Flow Velocities within the TCS

A thermal anemometer (testo 405i, Testo, Titisee-Neustadt, Germany) is used to measure the flow velocities during the transport phase of the dustiness measurements and to compare them with calculated values from CFD (Computational Fluid Dynamics) simulations. In Figure 6, the thermal anemometer is inserted through an acrylic glass plate

specifically designed for this purpose. Flow velocities are measured at five different points within the orifice.

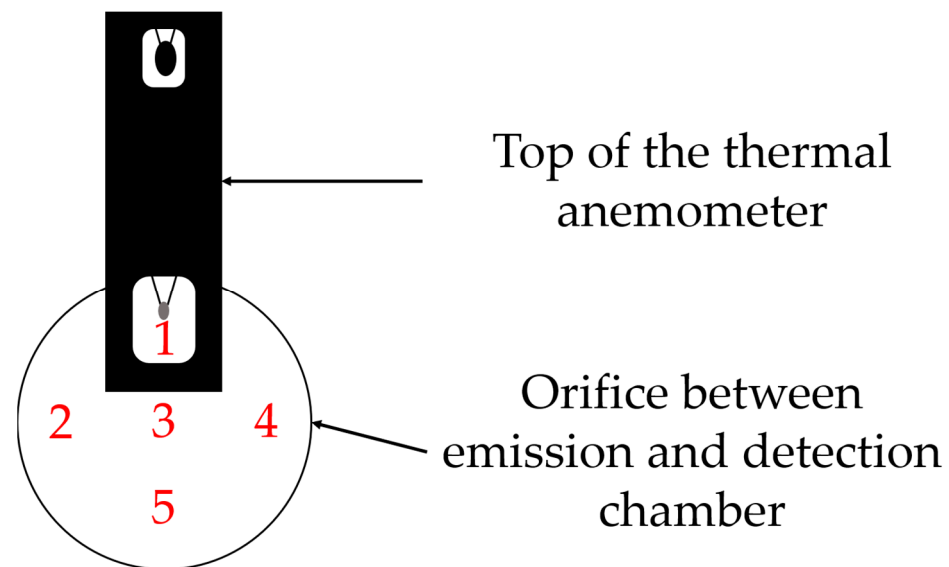


Figure 6. Simplified illustration of the thermal anemometer located within the orifice between the emission and detection chambers featuring five different measurement points.

In a previous study, pressure differences of 0–4 Pa were achieved by using one compressor and were compared with resulting dust emissions of ACAM with a defined particle size [47]. A second compressor, which is required for a separate pressure cycle, enables higher pressure differences of up to 12 Pa. In addition, ACAM fractions of different particle sizes are used to investigate the influence on dust generation. CFD is also used to investigate the flows resulting from the respective pressure differences within the TCS during the transport phase. Depending on the pressure difference (0–12 Pa), the resulting flow velocities within the TCS are measured. Subsequently, the mean flow velocities determined at the five measurement points in triplicate are calculated. The CFD simulations are carried out with the SimScale software (SimScale, Munich, Germany), applying the k- ω -SST turbulence model for shear stress transport (k- ω -SST) in a steady-state approach. The initial conditions of the CFD simulations are shown in Table 1.

Table 1. Initial conditions for CFD simulations.

Properties	Values
Kinematic viscosity	$1.529 \times 10^{-5} \text{ m}^2/\text{s}$
Density	$1.196 \text{ kg}/\text{m}^3$

The flow characteristics for the simulations are shown in Table 2. The boundary conditions are set to a pressure difference between the inlet and outlet in the range of 1–12 Pa in increments of 1 Pa to only take into account the convective flow.

Table 2. Boundary conditions for CFD simulations.

Properties	Values
Gauge pressure	0 Pa
Δp between inlet and outlet orifice	1–12 Pa in 1 Pa increments
Turbulence kinetic energy [k]	$1.297 \times 10^{-2} \text{ m}^2/\text{s}^2$
Specific dissipation rate [ω]	12.49 s^{-1}

The simulated and measured average air velocities resulting from the pressure differences are used to investigate the effect of air velocity on dust generation. For this purpose, the pressure difference between the two chambers is set to values between 0 and 12 Pa: At a pressure difference of 0 Pa, the plain diffusive transport of ACAM between the detection and emission chambers is investigated, while increasing the pressure difference from 1 to 12 Pa allows the investigation of the diffusive transport of ACAM with an oppositely directed convective flow.

2.3. Investigated Powder Fractions

Sieving of the untreated ACAM powders through sieves with mesh sizes of 500, 355, 250, 150, and 63 μm (RETSCH, Haan, Germany) is performed to obtain five different powder fractions, designated as ACAM 2-6. As the ACAM from Caelo was micronized, the sieving procedure was not necessary.

2.4. Powder Characterization

2.4.1. True Density

The true density of ACAM is determined with a helium pycnometer (Pycnomatic ACT EVO, Porotec, Hofheim am Taunus, Germany). Between 6 and 8 g of the powder fractions are added to the sample chamber. The true density is determined as the constant value achieved after the samples have reached an equilibrium state. All measurements are carried out in triplicate to minimize the weighing error.

2.4.2. Bulk and Tapped Density

Following monograph 2.9.34 “Bulk and tapped density of powders” of the European Pharmacopoeia [55], the bulk and tapped densities of the different ACAM fractions as well as the micronized ACAM are measured using a vibrating volumeter (STAV 2003, J. Engelsmann, Ludwigshafen, Germany). The 250 mL measuring cylinder is filled with 100 g of ACAM and subjected to tapping. All bulk and tapped densities are measured in triplicate.

2.4.3. Laser Diffraction

The particle size distribution of ACAM is analyzed by laser diffraction (Helos KR, Sympatec, Clausthal-Zellerfeld, Germany). A lens with an effective measuring range from 0.5 to 875 μm is used. Compressed air at a pressure of 150,000 Pa is used to disperse the powder samples. The particle size distribution is analyzed using PaqXos software (version 2.0.3, Sympatec, Clausthal-Zellerfeld, Germany). All measurements are carried out in triplicate.

2.4.4. Residual Moisture Content

The residual moisture content of ACAM fraction as well as the micronized ACAM is analyzed by thermogravimetric analysis (TGA; TG 209 F1 Libra[®], Netzsch-Gerätebau, Selb, Germany). The samples are heated up from room temperature to 105 °C at a heating rate of 10 K/min and are kept at this temperature for 30 min. Measurements are carried out in triplicate.

2.5. HPLC Analysis

The quantification of ACAM collected in the glass microfiber filters is performed with a VWR-Hitachi Chromaster 5000 (VWR International, Radnor, PA, USA), equipped with a 250 \times 4 mm column (LiChroCART[®] 250-4, Merck, Darmstadt, Germany) containing an RP-18e phase (particle size 5 μm), as described in a previous study [47]. Briefly, the amount of ACAM in each glass microfiber filter is extracted with 2 mL of the mobile phase (acetonitrile:water (75:25 v/v)) by shaking with a shaker (Unimax 1010, Heidolph Instruments, Kelheim, Germany). A sample volume of 20 μL is injected into the chromatograph and ACAM content is determined at 245 nm (Chromaster 5430 Diode Array Detector, Hitachi,

Chiyoda, Japan). The concentration of ACAM in the sample solutions is linear in the calibration range between 0.002 µg/mL and 2.212 µg/mL ($R^2 = 0.999$). The high-performance liquid chromatography (HPLC) assay exhibited reliable analytical performance, with the limit of detection (LOD) determined to be 0.0064 µg/L, and the limit of quantification (LOQ) was at 0.0214 µg/L.

3. Results and Discussion

3.1. Air Flow Conditions within the TCS

For investigating the air flow conditions within the TCS, it is essential to obtain information about the pressure differences during the individual measurement phases. As already mentioned in Section 2.2.2, the measurement of dust emissions is conducted in three phases, illustrated in Figure 7: the atomization phase, the transport phase, and the detection phase.

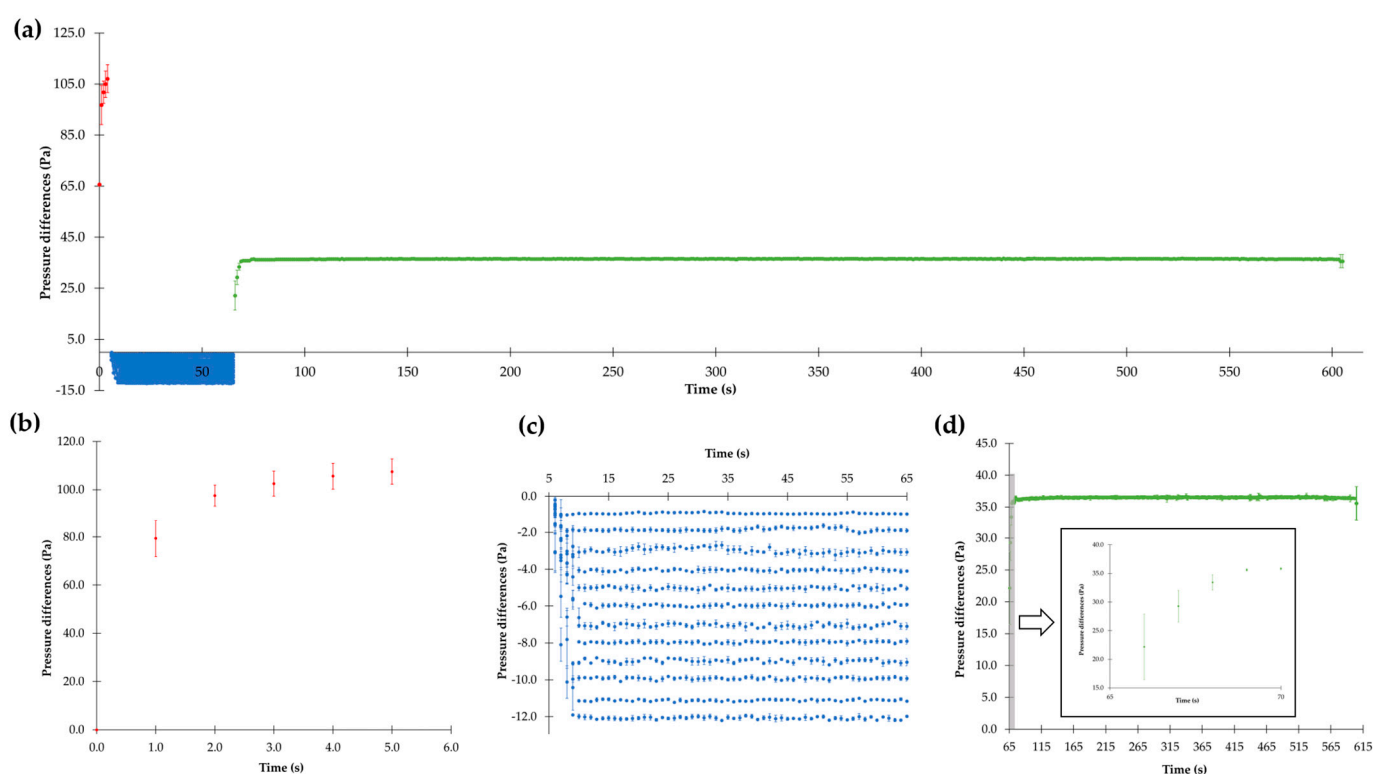


Figure 7. (a) Overview of the three measurement phases (red: atomization phase, blue: transport phase, green: detection phase); (b) pressure differences during the atomization phase; (c) pressure differences of 0–12 Pa during the transport phase; (d) pressure differences during the detection phase (means \pm SD, $n = 3$).

In Figure 7a, an overview of all three phases, shown in more detail in Figure 7b–d, is given. This figure clearly illustrates that the TCS operates satisfactorily. In the atomization phase (first phase), the powder in the ball valve is atomized by overpressure. For a time period of 5 s, the pressure in the emission chamber is higher than that in the detection chamber. During this phase, both chambers are separated from each other by the controllable flap. After this time period, the pressure differences decrease to values between 0 and 12 Pa. During this transport phase (second phase), preset pressure differences are reached by opening the ball valve above the detection chamber. After 60 s, the detection phase (third phase) starts. The increase in the pressure differences in this phase is caused by activation of the air sampling pump for 540 s.

The mean values of the pressure differences between the emission and detection chambers during the atomization phase are shown in more detail in Figure 7b. To ensure

reproducible and comparable results, the pre-adjusted overpressure is identical for all measurements. With regard to the results, it is important to consider that the atomization phase lasts only for 5 s, and the sampling rate of the differential pressure device is 1/s. The pressure required for atomizing the powder within the emission chamber increases quickly during the 5 s to reach a constant overpressure.

The mean values of the pressure differences between the two chambers during the transport phase in Figure 7c are shown. It is noticeable that the pressure differences, preset between 0 and 12 Pa in clearly distinguished 1 Pa increments, remain constant over the entire duration of this measurement phase because of the second compressor (see Section 2.2.1), despite the permanent opening of the controllable flap during this phase.

In Figure 7d, the detection phase is shown, which is designated by reaching constant pressure difference in a range between 36.1 and 36.7 Pa after a few seconds. This phase ends after exactly 540 s completing the dust analysis. All dustiness measurements last for 605 s.

Overall, the presented results confirm that the TCS enables precise and reproducible control of the pressure differences providing reliable information on the air flow conditions. This is crucial for the consistent measurement of dust emissions and provides a reliable base for further dustiness investigations in the context of containment.

3.2. Air Velocities Resulting from Different Pressure Differences

The Computational Fluid Dynamics (CFD) simulations were already carried out in a previous study within a pressure difference range between 1 and 4 Pa [47]. By constructive changes in the TCS and the addition of a second compressor, pressure differences of up to 12 Pa may be reached. The simulations of the resulting average air velocities at pressure differences between 1 and 12 Pa are shown in Figure 8. In this context, it has to be mentioned that pressure difference and air velocity are related to each other.

In Figure 9, a comparison between the simulated and measured average air velocities is presented as a function of the pressure difference. The simulated average air velocities range from 0.09 to 0.37 m/s, while the measured average air velocities are between 0.09 and 0.41 m/s. Again, with increasing pressure difference, both the simulated and measured air velocities increase. However, the measured values are generally slightly higher than the simulated values, especially at higher pressure differences. Despite the slight differences between the simulated and measured data, the curved profiles of both are similar.

3.3. Dust Emission Depending on the Pressure Difference/Air Velocity and ACAM Particle Size

In Figure 10, the measured dust emissions at different pressure differences between 0 and 12 Pa are shown. Six different ACAM powder fractions (ACAM 1–ACAM 6) differing in their particle size are examined. The results show that the dust emissions vary depending on the particle size: a significant decrease ($p < 0.05$) in the measured dust emissions is observed with increasing the particle size of ACAM. As expected, the dust emissions also decrease with increasing pressure difference between the emission and detection chambers of the TCS and consequently with higher air velocities. Except for ACAM 6, dust emissions are no longer quantifiable above a pressure difference of 7 Pa (about 0.2 m/s). With the coarsest powder fraction (ACAM 6), dust emissions are measurable only up to a pressure difference of about 4 Pa.

To describe the obtained data series, suitable mathematical functions are used, and their goodness of fit is evaluated. Three different models are examined for this purpose: a linear function, an exponential function, and a quadratic function. The results of the calculations are summarized in Table 3 for the ACAM 1–ACAM 6 samples. The goodness of fit is evaluated by the coefficient of determination R^2 . The first model, a linear function in the form of

$$y = m \cdot x + b, \quad (1)$$

leads to R^2 values between 0.674 and 0.882 for the six ACAM fractions, indicating a low goodness of fit. Thus, the linear function does not describe the data appropriately. The second model, an exponential function in the form of

$$y = a \cdot e^{-b \cdot x}, \quad (2)$$

results in an R^2 values in the range of 0.926 and 0.987 for the investigated ACAM fractions, providing a considerable goodness of fit. The third model, a quadratic function in the form of

$$y = a \cdot x^2 + b \cdot x + c, \quad (3)$$

leads to R^2 values of 0.863–0.977, which also represents a good-fitting model, especially for ACAM 5. Overall, the data are best described by the exponential function, followed by the quadratic function, and the linear function shows the lowest goodness of fit.

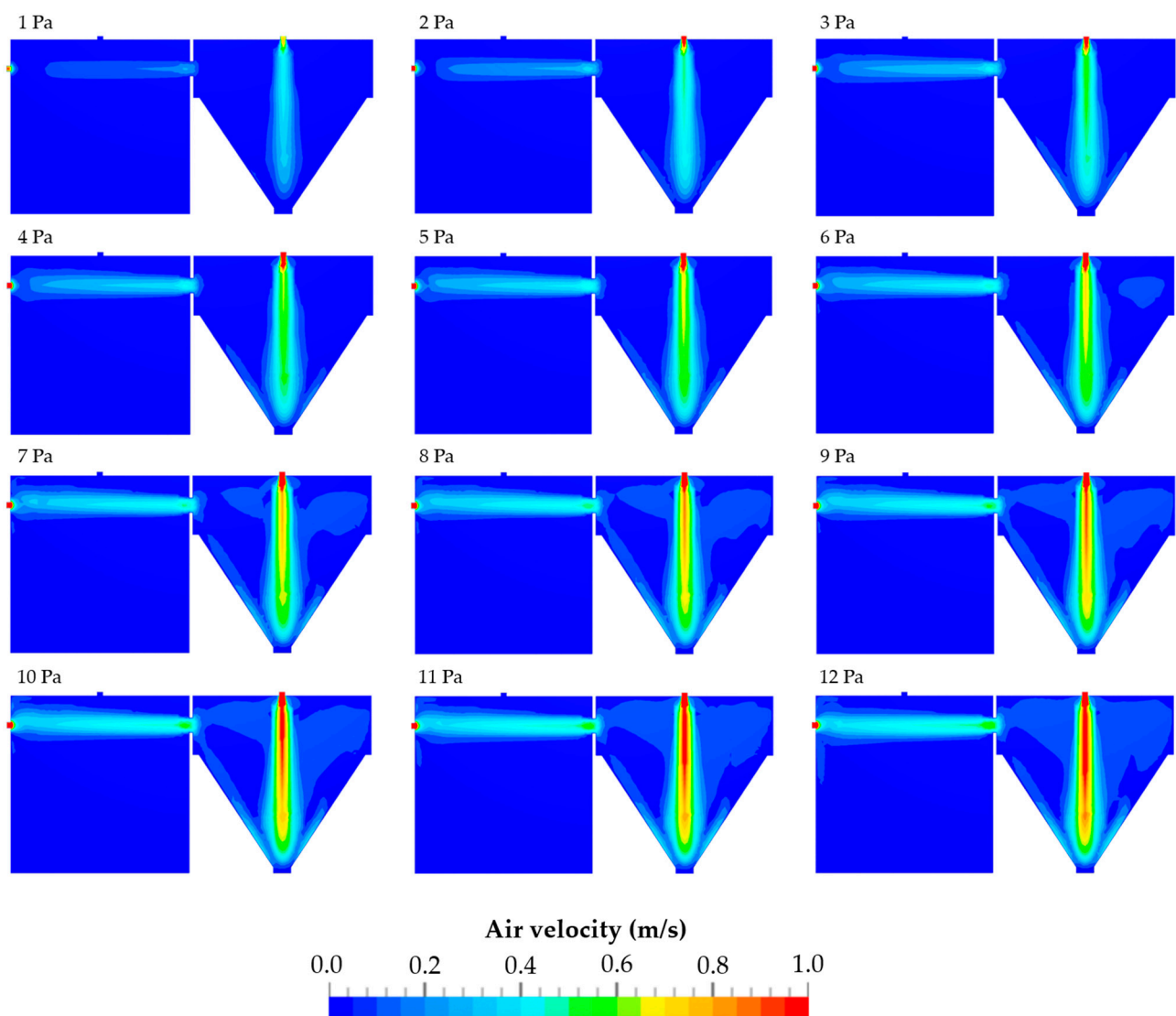


Figure 8. Air velocities at pressure differences of 1–12 Pa between the emission chamber (left) and the detection chambers (right).

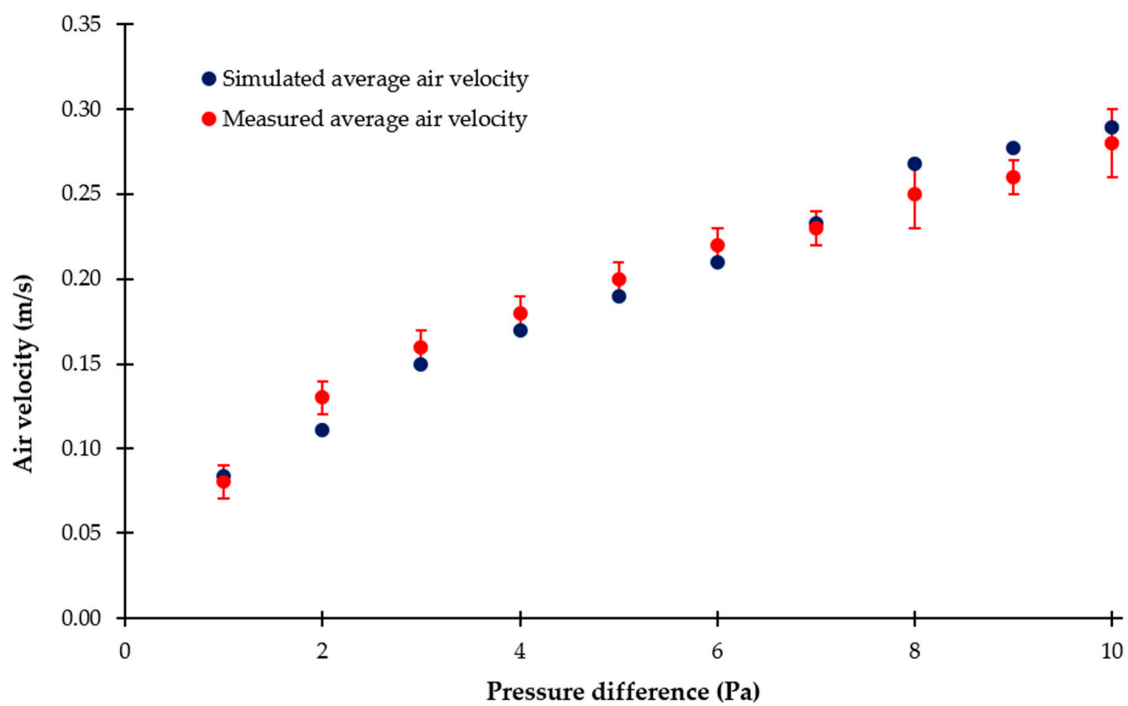


Figure 9. Air velocity versus pressure difference (means \pm SD, $n = 3$).

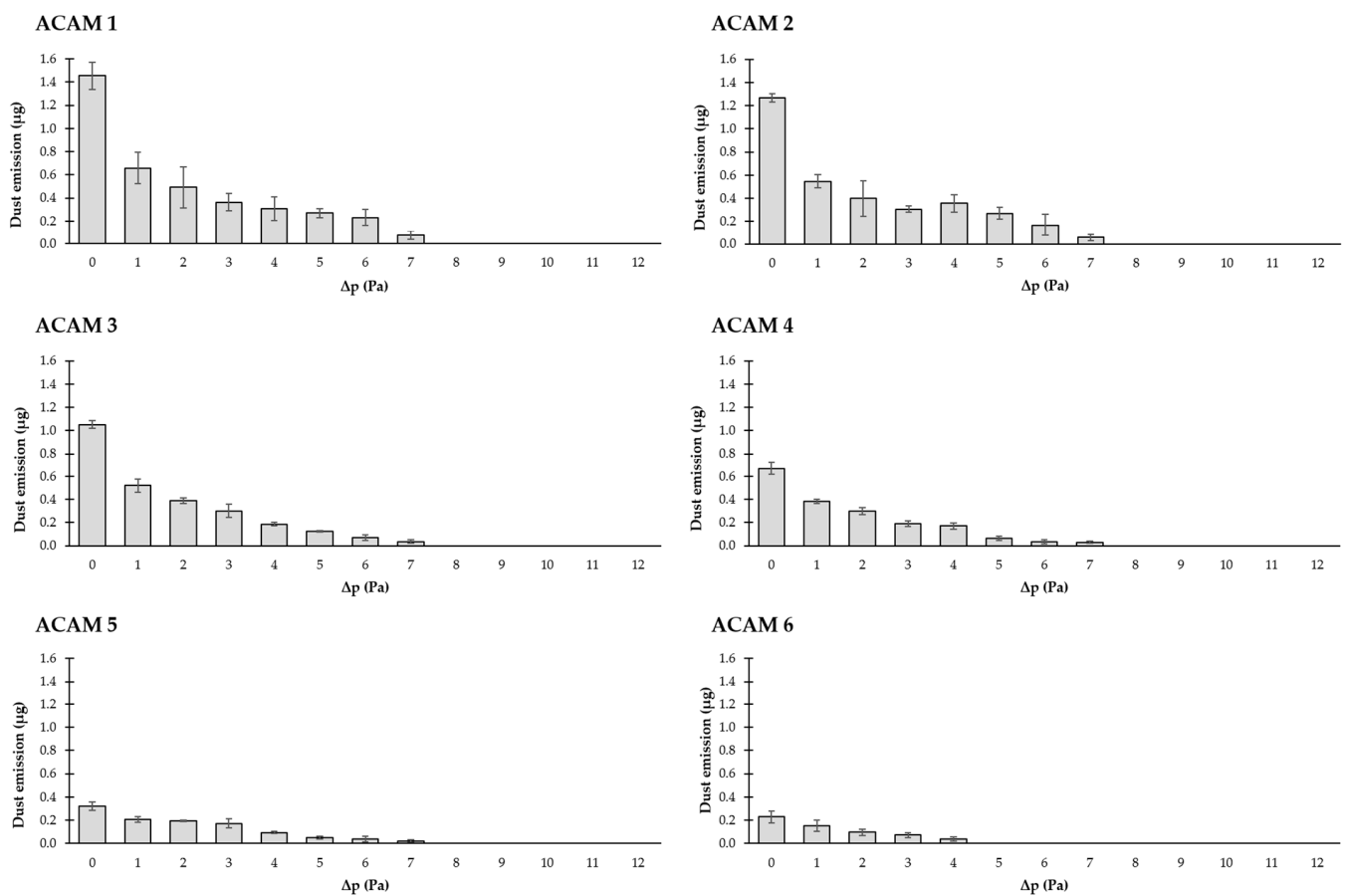


Figure 10. Dust emissions of ACAM 1–ACAM 6 at pressure differences between 0 and 12 Pa (means \pm SD, $n = 3$).

Table 3. Results of the linear, exponential, and quadratic functions for mathematical modeling for the dust emissions depending on the pressure difference (ACAM 1–ACAM 6).

Sample	Linear Parameters	Linear R ²	Exponential Parameters	Exponential R ²	Quadratic Parameters	Quadratic R ²
ACAM 1	m = −0.087 Pa ^{−1} b = 0.820 µg	0.691	a = 1.34 µg b = 0.444 Pa ^{−1}	0.950	a = 0.014 µg Pa ^{−2} b = −0.253 µg Pa ^{−1} c = 1.124 µg	0.8804
ACAM 2	m = −0.076 Pa ^{−1} b = 0.714 µg	0.689	a = 1.15 µg b = 0.431 Pa ^{−1}	0.926	a = 0.012 µg Pa ^{−2} b = −0.214 µg Pa ^{−1} c = 0.967 µg	0.8630
ACAM 3	m = −0.065 Pa ^{−1} b = 0.595 µg	0.683	a = 1.00 µg b = 0.472 Pa ^{−1}	0.982	a = 0.012 µg Pa ^{−2} b = −0.204 µg Pa ^{−1} c = 0.850 µg	0.923
ACAM 4	m = −0.044 Pa ^{−1} b = 0.406 µg	0.724	a = 0.65 µg b = 0.423 Pa ^{−1}	0.987	a = 0.008 µg Pa ^{−2} b = −0.135 µg Pa ^{−1} c = 0.573 µg	0.957
ACAM 5	m = −0.025 Pa ^{−1} b = 0.233 µg	0.822	a = 0.324 µg b = 0.321 Pa ^{−1}	0.958	a = 0.003 µg Pa ^{−2} b = −0.0633 µg Pa ^{−1} c = 0.304 µg	0.977
ACAM 6	m = −0.016 Pa ^{−1} b = 0.138 µg	0.673	a = 0.234 µg b = 0.465 Pa ^{−1}	0.982	a = 0.003 µg Pa ^{−2} b = −0.052 µg Pa ^{−1} c = 0.206 µg	0.963

It should be noted that these findings are transferable to an only limited extent to the conditions in pharmaceutical manufacturing, as some factors such as the method of atomization, the energy transfer to the powder, the flow conditions, and the composition of the investigated powders have a significant influence on the expected dust emission. These factors may cause a considerable variation in the data, which makes the direct transfer of the experimental results to industrial processes difficult. In addition, the exact configuration and specifications of the TCS play a crucial role in the interpretation of the data and the transferability to other systems and conditions. Overall, the present results illustrate the versatile interactions between particle size, pressure difference, and dust emission.

3.4. ACAM Powder Characterization

In the present study, six different ACAM particle size fractions are examined, with ACAM 1 showing the finest and ACAM 6 the coarsest particles. The results of the powder characterization are summarized in Table 4.

Table 4. Overview of the ACAM powder properties.

Properties	ACAM 1	ACAM 2	ACAM 3	ACAM 4	ACAM 5	ACAM 6
x ₁₀ (µm)	2.00 ± 0.03	4.87 ± 0.59	11.70 ± 0.02	20.10 ± 1.27	27.98 ± 1.00	58.80 ± 5.49
x ₅₀ (µm)	9.91 ± 0.21	21.99 ± 1.82	70.28 ± 0.07	126.85 ± 6.83	218.32 ± 4.02	346.16 ± 7.13
x ₉₀ (µm)	29.98 ± 1.78	61.39 ± 3.62	139.24 ± 0.20	250.43 ± 1.64	366.13 ± 2.77	574.84 ± 1.75
True density (g/cm ³)	1.300 ± 0.009	1.295 ± 0.002	1.299 ± 0.002	1.289 ± 0.006	1.288 ± 0.005	1.288 ± 0.006
Bulk density (g/cm ³)	0.35 ± 0.02	0.46 ± 0.00	0.53 ± 0.00	0.65 ± 0.00	0.67 ± 0.01	0.70 ± 0.00
Tapped density (g/cm ³)	0.57 ± 0.01	0.69 ± 0.00	0.76 ± 0.01	0.78 ± 0.00	0.78 ± 0.01	0.82 ± 0.01
Hausner ratio	1.61 ± 0.08	1.52 ± 0.01	1.43 ± 0.00	1.20 ± 0.00	1.16 ± 0.00	1.16 ± 0.01
Compressibility index (%)	37.62 ± 3.20	34.09 ± 0.27	29.88 ± 0.21	16.57 ± 0.17	13.95 ± 0.00	13.84 ± 1.09
Residual moisture content (%)	0.14 ± 0.02	0.14 ± 0.01	0.15 ± 0.02	0.14 ± 0.02	0.14 ± 0.03	0.15 ± 0.04

The particle size distributions of the ACAM fractions show a distinct difference. The finest ACAM particles (x₁₀) show a size of 2.00 µm, while the coarsest particles reach a size

of 58.80 μm . The mean particle sizes (x_{50}) increase from 9.91 μm for ACAM 1 to 346.16 μm for ACAM 6. The x_{90} values are the lowest for ACAM 1 with 29.98 μm and the highest for ACAM 6 with 574.84 μm .

The true densities of the particle fractions show only slight differences and are similar (about 1.29 g/cm^3). The bulk and tapped densities of the particle fractions increase from ACAM 1 to ACAM 6. ACAM 1 shows a bulk density of 0.35 g/cm^3 and a tapped density of 0.57 g/cm^3 , while with ACAM 6, a bulk density of 0.70 g/cm^3 and a tapped density of 0.82 g/cm^3 are observed.

The Hausner index, which describes the flow behavior of the powders, decreases from 1.61 for ACAM 1 to 1.16 for ACAM 6. This shows an improvement in flow behavior with increasing particle size. At the same time, the compressibility index decreases from 37.62% for ACAM 1 to 13.84% for ACAM 6.

The residual moisture content is similar in all the samples and ranges between 0.14% and 0.15%.

In summary, the results show that with increasing particle size of the ACAM fractions, the bulk and tapped densities increase, and the flowability improves (decreased Hausner index and compressibility index), whereas the true density and the residual moisture content remain steady.

4. Conclusions

To investigate the dustiness of the surrogate substance acetaminophen at six particle size fractions, a novel two-chamber setup is employed. The dust emissions show a significant dependence on the particle size: Fine particles cause higher dust emissions because of their better dispersion within the TCS. Where the correlation between dust emissions and pressure difference or air velocity is concerned, model fitting indicates either an exponential or quadratic relationship. Even moderate increases in pressure difference lead to significant reductions in dust emission. Moreover, there is a significant decrease in dust emission with increasing pressure difference and air velocity.

According to EN ISO 14664-4, one strategy to prevent the undesirable transport of airborne substances is the implementation of a flow barrier. The simulated as well as measured air velocities within the TCS are similar in their range of 0.2–0.5 m/s , recommended in the literature to ensure effective particle separation and control. In fact, depending on the particle size of ACAM, air flow velocities of around 0.2 m/s within the TCS are sufficient to ensure that no quantifiable amounts of ACAM are detected. In summary, the results demonstrate that the investigated TCS enables precise and reliable control of the pressure conditions, which is crucial for reproducible measurements of dust emissions.

In a future study, a more detailed investigation of the flow conditions within the TCS should be performed. The change in the diameter of the orifice between the emission and detection chamber and the resulting change in the cross-section area of the orifice might also influence the flow conditions within the TCS and thus the potential transportation of particles.

Author Contributions: Conceptualization, S.W., M.S. and C.S.L.; Methodology, S.W.; Software, S.W. and J.B.; Validation, S.W., M.S. and C.S.L.; Formal analysis, S.W. and C.S.L.; Investigation, S.W.; Data curation, S.W.; Writing—original draft, S.W.; Writing—review & editing, S.W., M.S. and C.S.L.; Visualization, S.W.; Supervision, C.S.L. All authors have read and agreed to the published version of the manuscript.

Funding: This research received no external funding.

Institutional Review Board Statement: Not applicable.

Informed Consent Statement: Not applicable.

Data Availability Statement: Data is contained within the article.

Acknowledgments: The authors express their gratitude to Petra Borbe and Kai Braunschweig for their help with the technical aspects.

Conflicts of Interest: Authors Martin Schöler and Jonas Brüggmann were employed by the company Fett Compacting GmbH. The remaining authors declare that the research was conducted in the absence of any commercial or financial relationships that could be construed as a potential conflict of interest.

References

1. International Society for Pharmaceutical Engineering (ISPE). *ISPE D/A/CH Affiliate: Containment Manual*; ISPE D/A/CH: Offenbach, Germany, 2017.
2. Hristozov, D.; Gottardo, S.; Semenzin, E.; Oomen, A.; Bos, P.; Peijnenburg, W.; van Tongeren, M.; Nowack, B.; Hunt, N.; Brunelli, A.; et al. Frameworks and Tools for Risk Assessment of Manufactured Nanomaterials. *Environ. Int.* **2016**, *95*, 36–53. [\[CrossRef\]](#)
3. Becker, J.; Pohlmann, T. Development and Implementation of a Large-Scale HPAPI Manufacturing Process. *Chim. Oggi-Chem. Today* **2019**, *35*, 20–24.
4. Franco, G. Ramazzini and Workers' Health. *Lancet* **1999**, *354*, 858–861. [\[CrossRef\]](#)
5. Wollowitz, S. Managing High-Potency Active Pharmaceutical Ingredients—A Drug Sponsor's Guide. *Drug Dev. Res.* **2010**, *71*, 420–428. [\[CrossRef\]](#)
6. Mari, G.; Moccaldi, A.; Ludovisi, G. Handling of High Potency Drugs: Process and Containment. *Trans. Ecol. Environ.* **1999**, *85*, 257–265. [\[CrossRef\]](#)
7. Dunny, E.; O'Connor, I.; Bones, J. Containment Challenges in HPAPI Manufacture for ADC Generation. *Drug Discov. Today* **2017**, *22*, 947–951. [\[CrossRef\]](#) [\[PubMed\]](#)
8. Barle, E.L.; Winkler, G.C.; Glowienke, S.; Elhajouji, A.; Nunic, J.; Martus, H.J. Setting Occupational Exposure Limits for Genotoxic Substances in the Pharmaceutical Industry. *Toxicol. Sci.* **2016**, *151*, 2–9. [\[CrossRef\]](#) [\[PubMed\]](#)
9. Glogovac, M.; Paulson, C.; Lambert, A.; Winkler, G.C.; Lovsin Barle, E. Disease Area and Mode of Action as Criteria to Assign a Default Occupational Exposure Limit. *Regul. Toxicol. Pharmacol.* **2021**, *122*, 104891. [\[CrossRef\]](#) [\[PubMed\]](#)
10. Blum, K.; FitzGerald, R.; Wilks, M.F.; Barle, E.L.; Hopf, N.B. Use of the Benchmark-Dose (BMD) Approach to Derive Occupational Exposure Limits (OELs) for Genotoxic Carcinogens: N-Nitrosamines. *J. Appl. Toxicol.* **2023**, *43*, 1183–1200. [\[CrossRef\]](#)
11. Haigney, S. HPAPI Capacity Challenges. *Pharm. Technol.* **2019**, *2019*, 6–10.
12. Heron, R.J.L.; Pickering, F.C. Health Effects of Exposure to Active Pharmaceutical Ingredients (APIs). *Occup. Med.* **2003**, *53*, 357–362. [\[CrossRef\]](#) [\[PubMed\]](#)
13. Stahl, H. How to Make Tablets from Potent APIs. *Pharm. Technol.* **2010**, *3*, 34–39.
14. Levin, M.; Koponen, I.K.; Jensen, K.A. Exposure Assessment of Four Pharmaceutical Powders Based on Dustiness and Evaluation of Damaged HEPA Filters. *J. Occup. Environ. Hyg.* **2014**, *11*, 165–177. [\[CrossRef\]](#)
15. Abueva, C.; Ryu, H.S.; Bae, J.S.; Kim, J.; Padalhin, A.; Lee, H.Y.; Park, S.Y.; Mo, J.H.; Chung, P.S.; Woo, S.H. Bioaerosol and Fine Dust Protection with Quaternary Trimethyl Chitosan Integration in Polypropylene Filters. *Mater. Des.* **2024**, *238*, 112615. [\[CrossRef\]](#)
16. Zhang, S.; Liu, H.; Tang, N.; Zhou, S.; Yu, J.; Ding, B. Spider-Web-Inspired PM_{0.3} Filters Based on Self-Sustained Electrostatic Nanostructured Networks. *Adv. Mater.* **2020**, *32*, 2002361. [\[CrossRef\]](#) [\[PubMed\]](#)
17. Adams, N.J.; Johnson, D.L.; Lynch, R.A. The Effect of Pressure Differential and Care Provider Movement on Airborne Infectious Isolation Room Containment Effectiveness. *Am. J. Infect. Control* **2011**, *39*, 91–97. [\[CrossRef\]](#) [\[PubMed\]](#)
18. Kanjiyangat, V.; Hareendran, M. Engineering Intervention to Reduce API Dust Exposure during Milling Operation. *J. Chem. Health Saf.* **2018**, *25*, 36–39. [\[CrossRef\]](#)
19. Denk, R.; Ag, S.; Flueckinger, A.; Kisaka, H.; Maeck, R.; Restetzki, L.; Schreiner, A.; Schulze, R.; Sachsen, L. Isolators Key to Preventing Cross-Contamination. *PDA Lett.* **2017**, *LIII*, 34–40.
20. Tiwari, P.; Chowdhury, S.R. Sustainable Production of Highly Active Pharmaceutical Ingredients (HAPIs). *Int. J. Sci. Res. Publ.* **2014**, *4*, 2250–3153.
21. Lanning, J.; Boundy, M.A.G.; Leith, D. Validating a Model for the Prediction of Dust Generation. *Part. Sci. Technol.* **1995**, *13*, 105–116. [\[CrossRef\]](#)
22. Sethi, S.A. Generation of Small Particles by Gas Fluidization. *J. Aerosol Sci.* **1997**, *28*, 539–540. [\[CrossRef\]](#)
23. Champmartin, C.; Clerc, F. Inhalable Dust Measurements as a First Approach to Assessing Occupational Exposure in the Pharmaceutical Industry. *J. Occup. Environ. Hyg.* **2014**, *11*, 85–92. [\[CrossRef\]](#)
24. Lidén, G. Dustiness Testing of Materials Handled at Workplaces. *Ann. Occup. Hyg.* **2006**, *50*, 437–439. [\[CrossRef\]](#) [\[PubMed\]](#)
25. Chen, H.; Jog, M.A.; Turkevich, L.A. Computational Fluid Dynamics Simulations of Aerosol Behavior in a High-Speed (Heubach) Rotating Drum Dustiness Tester. *Particuology* **2023**, *72*, 68–80. [\[CrossRef\]](#) [\[PubMed\]](#)
26. Stein, J.; Fuchs, T.; Mattern, C. Advanced Milling and Containment Technologies for Superfine Active Pharmaceutical Ingredients. *Chem. Eng. Technol.* **2010**, *33*, 1464–1470. [\[CrossRef\]](#)
27. Setty, P. *Optimal Handling of Highly Active Pharmaceutical Ingredients during Milling and Blending Operations*; Massachusetts Institute of Technology (Department of Chemical Engineering): Cambridge, MA, USA, 2013.
28. Phalen, R.F.; Hinds, W.C.; Angeles, L.; John, W.; Researcher, I.; Liou, P.J. Particle Size-Selective Sampling in the Workplace: Rationale and Recommended Techniques. *Ann. Occup. Hyg.* **1988**, *32*, 403–411. [\[CrossRef\]](#)

29. Armenta, S.; Blanco, M. Ion Mobility Spectrometry: A Comprehensive and Versatile Tool for Occupational Pharmaceutical Exposure Assessment. *Anal. Chem.* **2012**, *84*, 4560–4568. [\[CrossRef\]](#)
30. Calhoun, D.M.; Coler, A.B.; Nieusma, J.L. Strategies for Preventing Occupational Exposure to Potent Compounds. *Toxicol. Mech. Methods* **2011**, *21*, 93–96. [\[CrossRef\]](#) [\[PubMed\]](#)
31. Palakurthi, N.K.; Ghia, U.; Turkevich, L.A. Numerical Investigation of Aerosolization in the Venturi Dustiness Tester: Aerodynamics of a Particle on a Hill. *J. Fluids Eng. Trans. ASME* **2022**, *144*, 061113. [\[CrossRef\]](#)
32. Vincent, J.H.; Mark, D. The Basis of Dust Sampling in Occupational Hygiene: A Critical Review. *Ann. Occup. Hyg.* **1981**, *24*, 375–390. [\[CrossRef\]](#)
33. Ku, R.H. An Overview of Setting Occupational Exposure Limits (OELs) for Pharmaceuticals. *Chem. Health Saf.* **2000**, *7*, 34–37. [\[CrossRef\]](#)
34. Ahuja, V.; Krishnappa, M. Approaches for Setting Occupational Exposure Limits in the Pharmaceutical Industry. *J. Appl. Toxicol.* **2022**, *42*, 154–167. [\[CrossRef\]](#) [\[PubMed\]](#)
35. Carlson, K.H.; Herman, D.R.; Markey, T.F.; Wolff, R.K.; Dorato, M.A. A Comparison of Two Dustiness Evaluation Methods. *Am. Ind. Hyg. Assoc. J.* **1992**, *53*, 448–454. [\[CrossRef\]](#)
36. Ohta, T.; Maeda, H.; Kubota, R.; Koga, A.; Terada, K. Establishment of Powder Dustiness Evaluation Method by Dustmeter with Small Amount of Pharmaceutical Ingredients. *Int. J. Pharm.* **2014**, *472*, 251–256. [\[CrossRef\]](#) [\[PubMed\]](#)
37. Bach, S.; Schmidt, E. Determining the Dustiness of Powders—A Comparison of Three Measuring Devices. *Ann. Occup. Hyg.* **2008**, *52*, 717–725. [\[CrossRef\]](#) [\[PubMed\]](#)
38. Hamelmann, F.; Schmidt, E. Methods for Characterizing the Dustiness Estimation of Powders. *Chem. Eng. Technol.* **2004**, *27*, 844–847. [\[CrossRef\]](#)
39. Dubey, P.; Ghia, U.; Turkevich, L.A. Computational Fluid Dynamics Analysis of the Venturi Dustiness Tester. *Powder Technol.* **2017**, *312*, 310–320. [\[CrossRef\]](#) [\[PubMed\]](#)
40. Klippel, A.; Schmidt, M.; Krause, U. Dustiness in Workplace Safety and Explosion Protection—Review and Outlook. *J. Loss Prev. Process Ind.* **2015**, *34*, 22–29. [\[CrossRef\]](#)
41. Boundy, M.; Leith, D.; Polton, T. Method to Evaluate the Dustiness of Pharmaceutical Powders. *Ann. Occup. Hyg.* **2006**, *50*, 453–458. [\[CrossRef\]](#) [\[PubMed\]](#)
42. Bach, S.; Eickmann, U.; Schmidt, E. Comparison of Established Systems for Measuring the Dustiness of Powders with the UNC Dustiness Tester Developed Especially for Pharmaceutical Substances. *Ann. Occup. Hyg.* **2013**, *57*, 1078–1086. [\[CrossRef\]](#)
43. Deng, T.; Paul, K.A.; Bradley, M.S.A.; Immins, L.; Preston, C.; Scott, J.F.; Welfare, E.H. Investigations on Air Induced Segregation of Pharmaceutical Powders and Effect of Material Flow Functions. *Powder Technol.* **2010**, *203*, 354–358. [\[CrossRef\]](#)
44. Plinke, M.A.E.; Leith, D.; Boundy, M.G.; Löffler, F. Dust Generation from Handling Powders in Industry. *Am. Ind. Hyg. Assoc. J.* **1995**, *56*, 251–257. [\[CrossRef\]](#)
45. Vincent, J.H. *Aerosol Sampling: Science, Standards, Instrumentation and Applications*; John Wiley & Sons: Hoboken, NJ, USA, 2007.
46. International Society for Pharmaceutical Engineering (ISPE). *Good Practice Guide: Assessing the Particulate Containment Performance of Pharmaceutical Equipment*; ISPE: North Bethesda, MD, USA, 2012.
47. Wirth, S.; Schöler, M.; Brüggmann, J.; Leopold, C.S. A Novel Two-Chamber Setup for Containment Investigations with Special Focus on the Dustiness of Pharmaceutical Powders Depending on the Airflow. *Pharmaceutics* **2022**, *14*, 2387. [\[CrossRef\]](#) [\[PubMed\]](#)
48. Wirth, S.; Schöler, M.; Leopold, C.S. Investigation on the Dustiness of a Binary Powder Mixture with a Newly Developed Two-Chamber Setup. In Proceedings of the 12th PBP World Meeting 2021, Online, 11–14 May 2021; Volume 320.
49. Wendt, J. *Computational Fluid Dynamics*; McGraw-Hill: New York, NY, USA, 1995.
50. Lavanya, N.; Bhattacharyya, S. Computational Fluid Dynamics—the Futuristic Innovation in Pharmaceutical Industry. *Indian J. Pharm. Educ. Res.* **2021**, *55*, 930–938. [\[CrossRef\]](#)
51. Tong, Z.B.; Zheng, B.; Yang, R.Y.; Yu, A.B.; Chan, H.K. CFD-DEM Investigation of the Dispersion Mechanisms in Commercial Dry Powder Inhalers. *Powder Technol.* **2013**, *240*, 19–24. [\[CrossRef\]](#)
52. European Committee for Standardization (CEN). *EN ISO 14664-4: Cleanrooms and Associated Controlled Environments—Part 4: Design, Construction and Start-Up*; CEN: Brussels, Belgium, 2001.
53. American Industrial Hygiene Association; American National Standards Institute. *N.S. American National Standard for Laboratory Ventilation*; American Industrial Hygiene Association (AIHA): Fairfax, VA, USA, 2003.
54. Wirth, S.; Schöler, M.; Leopold, C.S. Dust Emissions of Surrogates Substances Resulting from Diffusive and Convective Transport for Containment Investigations with a Newly Developed Two-Chamber Setup. In Proceedings of the PharmSci 360 Annual Meeting 2022, Boston, MA, USA, 16–19 October 2022.
55. *European Pharmacopoeia 10.0*; European Directorate for the Quality of Medicines & Health Care (EDQM): Strasbourg, France, 2019.

Disclaimer/Publisher’s Note: The statements, opinions and data contained in all publications are solely those of the individual author(s) and contributor(s) and not of MDPI and/or the editor(s). MDPI and/or the editor(s) disclaim responsibility for any injury to people or property resulting from any ideas, methods, instructions or products referred to in the content.

3.3 Investigations on the dustiness of binary acetaminophen - lactose monohydrate powder blends

In this third study, the TCS was used to analyse the dust generation of ACAM and binary blends of ACAM and lactose monohydrate (LM) at different particle sizes [172]. The two previous studies focused on the investigation of plain ACAM. The objective of this study was to specifically vary both the particle size and the mixing ratio to analyse their influence on dust emission.

Three different particle size fractions were prepared by sieving: fine, medium-size and coarse particles. Subsequently, powder blends with mixing ratios of 20:80, 40:60, 60:40 and 80:20 (ACAM:LM) were produced. With the TCS, these powder blends were examined in comparison to plain ACAM in terms of dust emissions.

The results show that the dust generation of ACAM and its binary blends with LM strongly depends on the particle size. Fine particles of ACAM generate significantly higher dust emissions than medium-size and coarse particles. In contrast, blends of ACAM and LM show reduced dust emissions, this effect being most pronounced with fine and medium-size LM particles, depending on the ACAM particle size. However, in the case of coarse LM particles, this reduction in dust emission is less pronounced: blends of coarse LM particles with fine ACAM particles led to the comparably lowest reduction in dust emission. These results emphasise the importance of particle size and mixing ratio for dust generation.

Thus, this study significantly contributes to the knowledge of dust generation during processing of powder blends. It provides information on the influence of excipients and their particle sizes on dust emission. The obtained data may be used to optimise containment strategies, being particularly important for safely manufacturing dosage forms with highly potent active ingredients.

In Figure 9, the operational framework and essential features of the presented study are highlighted.

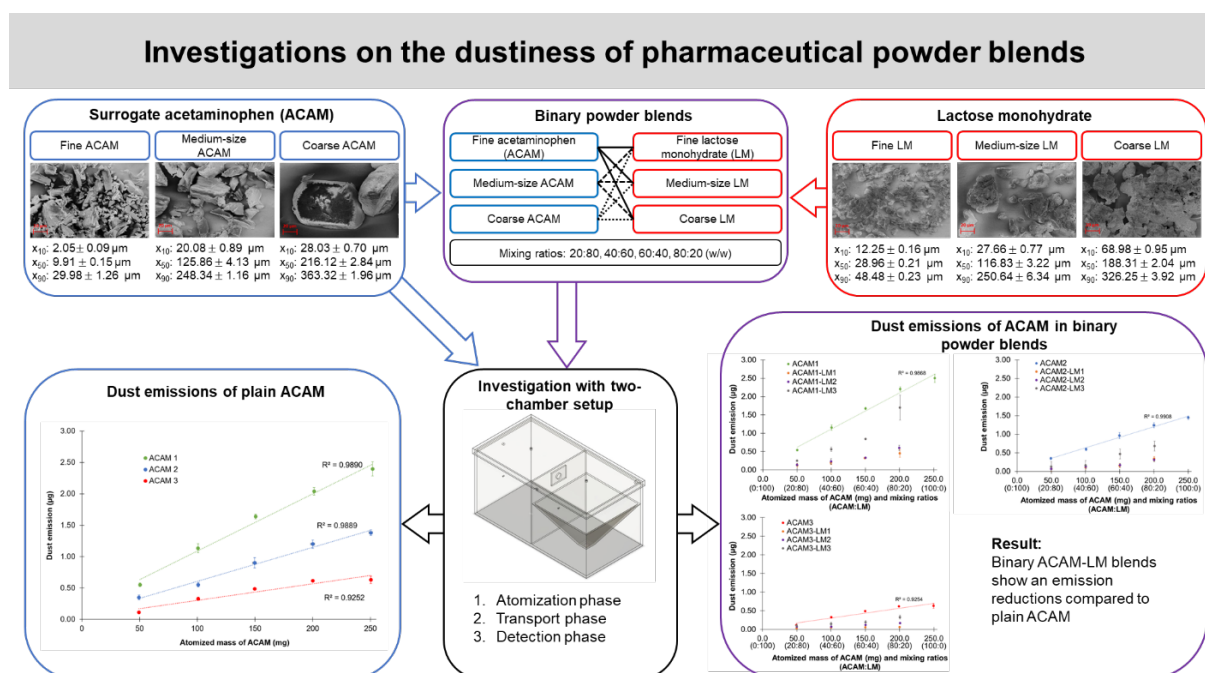


Figure 9: Visual representation of the essential features and outcome of the study [172].



Investigations on the dustiness of binary acetaminophen - lactose monohydrate powder blends

Steffen Wirth^a, Martin Schöler^b, Claudia S. Leopold^{a,*}

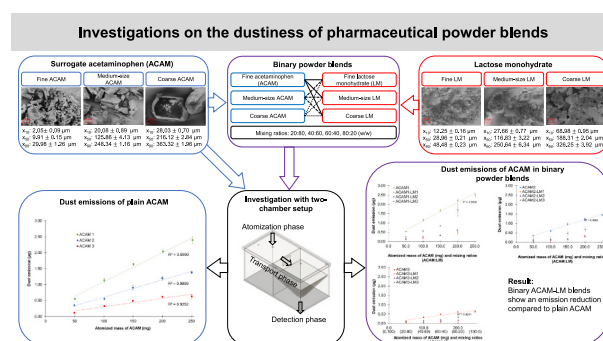
^a University of Hamburg, Dept. of Pharmaceutical Technology, Bundesstr. 45, D-20146 Hamburg, Germany

^b Fette Compacting GmbH, Grabauer Straße 24, D-21493 Schwarzenbek, Germany

HIGHLIGHTS

- Two-chamber setup for investigating dust emissions with minimal amount of substance.
- ACAM (9.91–216.12 μm) and LM (28.96–188.31 μm) particle sizes affect dust emissions.
- Mixing of ACAM with LM significantly reduces dust emissions.
- Blend of fine ACAM and coarse LM shows the highest dust emission, while the blend of coarse ACAM and fine LM reveals the lowest emissions.

GRAPHICAL ABSTRACT



ARTICLE INFO

Keywords:

Containment
Dustiness
Dust emission
ISPE surrogate
Dust measuring device

ABSTRACT

In this study, binary powder blends of acetaminophen (ACAM) and α -lactose monohydrate (LM) at different mixing ratios, with fine, medium-size, and coarse particles are investigated with a new two-chamber setup (TCS) to assess dustiness. The TCS consists of an emission and a detection chamber, allowing plain diffusive or convective particle transport. The aim is to compare the diffusive transport of ACAM with binary blends of ACAM and LM at different particle sizes and similar apparent density. Fine ACAM exhibits significantly higher dust emissions compared to medium and coarse ACAM. With increasing LM portion in the blends, ACAM dust emissions decrease. The blend of fine ACAM and coarse LM shows the highest dust emission, while the blend of coarse ACAM and fine LM reveals the lowest emissions. The TCS offers precise, reproducible measurements with good repeatability, making it beneficial for laboratory and industrial applications, even with small powder quantities.

1. Introduction

The use of so-called highly potent active pharmaceutical ingredients (HPAPIs) has substantially increased in recent years. HPAPIs are

characterized by their ability to exert a significant pharmacological effect or environmental exposure even at very low amounts. These HPAPIs are increasingly being used in various therapeutic areas including oncology, neurology, endocrinology, and the treatment of autoimmune

* Corresponding author.

E-mail addresses: steffen.wirth@uni-hamburg.de (S. Wirth), mschoeler@fette-compacting.com (M. Schöler), claudia.leopold@uni-hamburg.de (C.S. Leopold).

<https://doi.org/10.1016/j.powtec.2024.120317>

Received 5 July 2024; Received in revised form 18 September 2024; Accepted 22 September 2024

Available online 24 September 2024

0032-5910/© 2024 The Authors. Published by Elsevier B.V. This is an open access article under the CC BY-NC license (<http://creativecommons.org/licenses/by-nc/4.0/>).

diseases [1]. Common examples of HPAPIs include cytostatics, hormones, antibody-drug conjugates, and immunomodulators [2–6]. Consequently, among other considerations, the importance of managing HPAPIs properly has also come up in the context of safe handling, protection of personnel, avoidance of cross-contamination during pharmaceutical manufacture, and safeguard of the environment [5,7–11]. Therefore, containment systems have been developed to increase safety and are of crucial importance with regard to the transfer of technologies from laboratory to industrial use. There are high demands on both technical and measuring equipment to prevent risks concerning the health of personnel during manufacturing as well as the patients taking medication containing HPAPIs, and the environment [12–14]. As the manufacture and handling of HPAPIs inevitably lead to the generation of pharmaceutical dust, suitable containment equipment and containment strategies as well as specialized facility designs are necessary to minimize potential exposure to HPAPIs [15,16]. These containment measures involve the use of airlocks, pressure differentials, high performance filters, and restricted access to HPAPI-handling areas. Furthermore, special personal protective equipment may be required to minimize health hazards [2,5,17,18]. The establishment of occupational exposure limits (OELs), detailed hazard and risk assessments, and a clear understanding and implementation of containment procedures emphasize the importance of a careful approach to handling HPAPIs [2,5,13,19–22].

The dustiness of a powder is described as the tendency of a substance to generate airborne particles during handling [14,16]. Processes important to the manufacture of dosage forms consistently comprise the generation of dust [23]. For instance, operations such as grinding, pulverizing, mixing, transferring, or transporting, and drying of powders invariably lead to the generation of dust, which represents a potential hazard exposure, especially if inhaled [7,24–26]. Inhalable dust includes all airborne particles with an aerodynamic diameter of less than 100 μm that may be inhaled through the mouth and nose. Thoracic dust refers to particles with an aerodynamic diameter of less than 10 μm that pass through the larynx into the bronchi. Alveolar dust includes particles with an aerodynamic diameter of less than 4 μm that penetrate into the non-ciliated respiratory tract and reach the alveoli [27].

The tendency of an HPAPI to generate dust is basically influenced by its physicochemical and mechanical characteristics. These properties, which have an influence on dustiness, include true density, bulk density, particle size and distribution, particle shape, residual moisture content as well as cohesiveness and adhesiveness [14,28–34]. Particle motion is significantly influenced by parameters such as powder mass and particle size, which may provide valuable data for the prediction of dust emissions. Particularly, the particle size distribution at the level of the raw materials plays a crucial role, as it directly influences the tendency for dust generation and may strongly affect dustiness during the manufacturing process [35,36]. In addition, dust emission is not constant and may vary over time, making long-term tests essential to fully understand emission behavior, particularly in industrial applications [37,38]. However, exclusive analysis of these pharmaceutical powder attributes is not sufficient for precise prediction of dust propensity. Interestingly, research dedicated to dustiness of non-pharmaceutical powders is more extensive than that devoted to pharmaceutical powders, underscoring a significant gap in the literature and emphasizing the urgency for more research and development of standardized testing methods in pharmaceutical area [39,40].

Various devices, systems, and methods have already been developed for testing the dustiness of powders [41]. Such systems, which investigate dust generation on a laboratory scale, include the Heubach rotating method, single drop method, continuous drop method, or the Venturi Dustiness Tester. Despite the increasing preference for computer simulations in various fields, it is still essential to perform experimental studies on powder characterization to ensure accuracy and reliability that simulations alone cannot provide [19,34,42–49]. However, due to the usually scarcely available quantities of HPAPIs, measurements are

limited and relatively expensive, emphasizing the challenges and costs associated with dustiness testing in the pharmaceutical industry [12]. Furthermore, the energy required for atomization of powders may result in high mechanical stress on the powder particles, which may lead to a decrease in particle size. The energy required for atomization during dustiness tests should therefore be adjusted in such a way that the particles are separated from each other without being further fragmented by mechanical stress. Nevertheless, an influence of atomization on the dustiness resulting from a decrease in particle size in these systems cannot be ruled out. Other types of particle separation, such as fluidization or vibration, may also influence dust generation [50–52]. To ensure comparability of dustiness between laboratory and industrial scale, the energy transferred to the investigated powder samples during atomization should be similar. For this reason, standardized procedures are imperative for the evaluation of powder dustiness. It is essential that these procedures allow a correlation between dustiness measurements and the actual conditions encountered during manufacture of pharmaceutical dosage forms. The atomization method, duration, and intensity as well as the selected quantity of the powder samples play an important role in this process [16,30,41,47]. A high level of standardization guarantees reproducibility, which is necessary for the evaluation of the obtained results and the potential transferability of these results to real situations [12,19,40]. The experimental conditions, such as temperature, humidity, and air flow, are crucial for this reproducibility, as they may influence significantly the results.

To ensure that the investigations for equipment testing or the evaluation of containment systems are as safe as possible, surrogates are used to measure the exposure of airborne particles in containment equipment. The ISPE (International Society for Pharmaceutical Engineering) recommends various safe surrogates in the Good Practice Guide, including acetaminophen, insulin, mannitol, naproxen sodium, riboflavin, sucrose, and lactose monohydrate. The selection of surrogates depends on their physicochemical and mechanical properties as well as on the possibility of their quantification. Lactose monohydrate (LM), for example, is a surrogate that is available in various particle size distributions, has distinctive microscopic properties and is frequently used in pharmaceutical dosage forms. However, other surrogates such as riboflavin and acetaminophen are analytically easier to quantify. The high transferability of the surrogate properties to those of HPAPIs and their resulting dustiness may also be selection criteria [2,12,32,45,53–55].

Previous studies have already shown that a novel two-chamber setup (TCS) is suitable for investigating small amounts of pharmaceutical powders [53,56,57]. The safe surrogate acetaminophen (ACAM), recommended by the ISPE, was used in this study. A linear correlation of the atomized mass of ACAM with the resulting dust emission at a comparatively low standard deviation was found in a range of up to 400 mg of atomized powder. A plateau effect was observed with this system if more than 400 mg of ACAM were used. By adjusting the pressure difference between the emission/atomization chamber and detection chamber, it was possible to generate an oppositely directed convective flow. If the pressure difference between the two chambers is set to 0 Pa, the investigation of plain diffusive transport is also possible with the TCS.

Powder blends containing one or more excipients in addition to the active ingredient are frequently used in the manufacture of pharmaceutical dosage forms. This study therefore investigates the influence of the composition of binary powder blends containing ACAM and LM as well as of their particle size distribution on the resulting ACAM emissions. ACAM emissions of the binary powder blends were measured in comparison to those of plain ACAM at the same amounts. LM was selected as a potential filler material, which is commonly used in pharmaceutical dosage forms. Fine, medium-size, and coarse particles of both ACAM and LM were prepared and blends at the different mixing ratios were formulated. In addition, the influence of the particle size on the measured dust emission was investigated.

2. Materials and methods

2.1. Materials

Acetaminophen (ACAM; Caelo, Hilden, Germany and Fagron, Glinde, Germany) was used as an industry-accepted safe surrogate substance for the measurement of dust emission. α -Lactose monohydrate (LM; Tablettose® 70 and Tablettose® 100, Meggle, Wasserburg am Inn, Germany) was used as an excipient for the preparation of binary powder blends consisting ACAM and LM.

2.2. Methods

2.2.1. Sieving

For sieving, sieves with a mesh size of 355, 250, and 63 μm (RETSCH, Haan, Germany) were used. The unprocessed powders were passed through the sieves in decreasing order to obtain different sieve fractions. In this manner, a total of three fractions with fine particles (ACAM1, LM1), medium-size particles (ACAM2, LM2), and coarse particles (ACAM3, LM3) were obtained.

2.2.2. Blending

Binary powder blends (100 g) were prepared by addition of ACAM and LM to the blender (Turbula T2, Muttenz, Switzerland) at the ratios of 20:80, 40:60, 60:40, and 80:20 ACAM:LM (w/w) and mixed for 5 min at a blending speed of 96 min^{-1} . After the blending process, the powders were stored in 200 ml screw-top containers.

In Table 1 the compositions of the investigated binary powders are shown.

2.2.3. Two-chamber setup (TCS)

In Fig. 1, a simplified version of the TCS already used in previous studies [53] for dustiness investigations is shown. The setup consists of an emission chamber and a detection chamber. Both chambers are connected to each other by an orifice with a diameter of 25.4 mm, which may be closed by a flap controllable by a pneumatic cylinder and consequently allowing a separation of the two chambers. The dimensions of each chamber are of 300 \times 300 \times 300 mm. Thus, the volume of each chamber amounts to 27 l. However, the volume of the detection chamber is reduced to approximately 15 l caused by the pyramidal construction of the lower part of the chamber (see Fig. 1). The edges of the chamber are equipped with adhesive tape for sealing purposes and may be closed by a lid which may be fastened by toggle locks.

The TCS is made of acrylic glass with a wall thickness of 6 mm and is surrounded by 20 mm aluminum B-type profiles to mount four solenoid valves (two 3/2 and two 5/2 valves), a pneumatic cylinder, a programmable logic controller (PLC; Siemens LOGO! 12/24RC, Munich, Germany), and the measuring instruments (e.g. differential pressure gauge). Furthermore, a ground wire is attached to the aluminum profile, which has a direct connection to all electronic and metallic components as well as to the acrylic glass.

Table 1

Sieve fractions and mixing ratios of the investigated ACAM:LM powder blends (fine particles: ACAM1 and LM2; medium-size particles: ACAM2 and LM2; coarse particles: ACAM3 and LM3).

Sieve fraction of powder blends	Mixing ratios of ACAM:LM (w/w)
ACAM1:LM1	20:80, 40:60, 60:40, 80:20
ACAM1:LM2	20:80, 40:60, 60:40, 80:20
ACAM1:LM3	20:80, 40:60, 60:40, 80:20
ACAM2:LM1	20:80, 40:60, 60:40, 80:20
ACAM2:LM2	20:80, 40:60, 60:40, 80:20
ACAM2:LM3	20:80, 40:60, 60:40, 80:20
ACAM3:LM1	20:80, 40:60, 60:40, 80:20
ACAM3:LM2	20:80, 40:60, 60:40, 80:20
ACAM3:LM3	20:80, 40:60, 60:40, 80:20

The PLC, which controls the solenoid valves, first receives the input signal to start the measurement from a single-board microcontroller (Arduino® Uno Rev3, Ivrea, Italy). Amplification of the voltage by a DC-to-DC converter is required to generate a sufficiently high input signal. The use of the single-board microcontroller allows the generation of an input signal that can be synchronized with the server time. An air sampling pump (AirChek ESSENTIAL Pump, SKC, Blandford Forum, UK) connected to an IOM sampler (Institute of Occupational Medicine; SKC, Blandford Forum, UK), which is attached to the bottom of the detection chamber, can also be synchronized with the server time. This enables all phases of a dustiness measurements to be controlled over the time course of the experiments. The four output slots of the PLC are connected to the four solenoid valves, which are used to control the TCS. In Fig. 2, the pneumatic system of the TCS is shown. The two 3/2 solenoid valves are used to control 3/2 pneumatic valves to reach a pressure compensation either during atomization by overpressure in the emission chamber or during detection of the airborne particles in the detection chamber. The two 5/2 solenoid valves are used to control the ball valve for atomization of the powder samples and the controllable flap. The second ball valve above the detection chamber may serve to generate an oppositely directed convective flow. Attachment of a differential pressure gauge (testo 400, Testo, Titisee-Neustadt, Germany) to the orifices of the emission and the detection chamber (Fig. 1, digit 4) enables the measurement of the pressure and temperature differences between the two chambers.

2.2.4. Measurement with the TCS

The measurements with the TCS are characterized by three phases. In the first phase (atomization phase), an amount of approximately 250 mg of each powder sample, accurately weighed, is atomized under specified conditions. For this purpose, the powder samples are first introduced into the ball valve above the emission chamber and atomized in this chamber by opening the ball valve, using an overpressure of 50,000 Pa for 5 s. While the resulting overpressure is compensated for by a 3/2 pneumatic valve, connected to the emission chamber via a TPE tube (PUN-10 \times , Festo, Esslingen, Germany). The controllable flap is closed during atomization.

In the second phase (transport phase) of the measurement sequence, the controllable flap is opened for 60 s to allow for diffusive transport from the emission to the detection chamber. To ensure that there is no flow between the two chambers caused by pressure differences, the pressure difference is measured by the differential pressure gauge during the entire measurement sequence.

In the third phase (detection phase), the amount of surrogate that diffuses from the emission to the detection chamber during the transport phase is determined. For this purpose, the controllable flap is closed and a negative pressure is generated by the air sampling pump via an IOM sampler. The pressure is compensated for by two orifices arranged diagonally to each other. Because of the diagonal arrangement, a downward rotating flow is generated in the direction of the IOM sampler. A glass microfiber filter (1820–025, Whatman, Little Chalfont, UK) with a pore size of 1.6 μm is inserted into the IOM sampler to collect the airborne particles. To also capture the particles trapped within the IOM sampler, the inner parts of the sampler are swabbed with a further moistened glass microfiber filter. Both filters are transferred to an iodine flask. The total amount of collected ACAM is quantified by dissolving it in 2 ml of the mobile phase of the HPLC assay. In a previous study, it was already shown that an evacuation of the detection chamber for 9 min is sufficient to detect most of the ACAM particles in the detection chamber [53]. The described method in the present TCS is used to characterize plain ACAM with fine, medium, and coarse sizes. Similarly, all binary powder blends of ACAM and LM, also with fine, medium, and coarse particles are measured in the TCS at mixing ratios of 20:80, 40:60, 60:40, and 80:20 (w/w) to investigate the variations in dust emission dependent on particle size and mixing ratio. All measurements are conducted in triplicate.

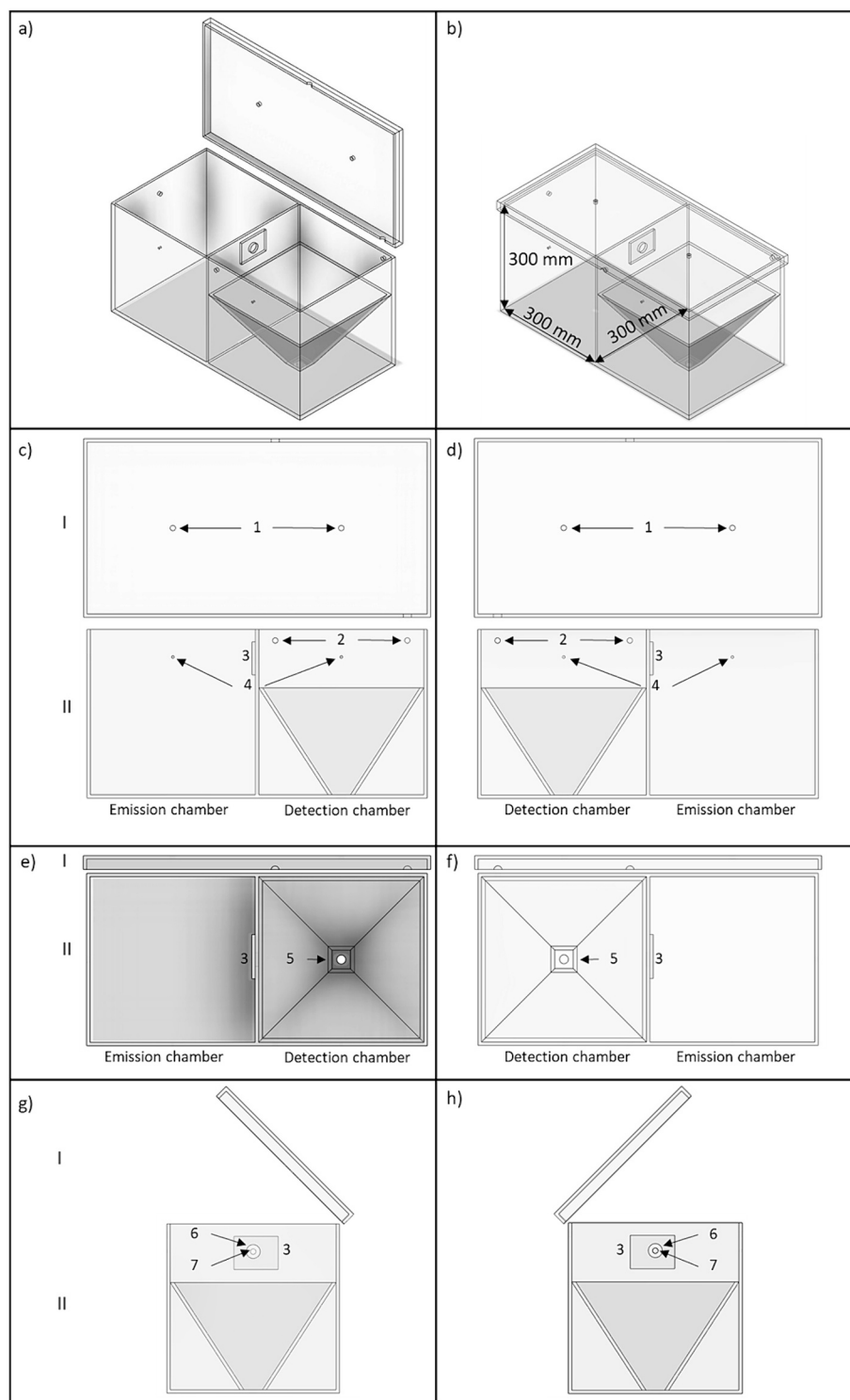


Fig. 1. Simplified design of the two-chamber setup: a) overview of the TCS in open state b) overview of the TCS in closed state [53] c) front view, d) back view, e) top view, f) bottom view, g) right lateral view, h) left lateral view; I: detachable lid, II: lower part of the setup; 1: orifices for the double-acting ball valves, 2: orifices for pressure compensation of the detection chamber, 3: controllable flap, 4: orifices for the differential pressure gauge, 5: orifice for the IOM sampler, 6: orifice for the connection between the emission and the detection chamber, 7: orifice for pressure compensation of the emission chamber.

An important aspect is the proper cleaning of the TCS. Generally, it is cleaned with low-lint, chemically inert wipes (Kimtech Science, Dallas, USA) by first moistening them with demineralized water and then wiping them along the acrylic glass walls of the TCS. This process is performed at least three times during each cleaning cycle to ensure that all ACAM particles are removed without leaving any residue.

2.2.5. HPLC assay for ACAM

The mobile phase (2 ml) consisting of acetonitrile and water (75:25 v/v) is added to the glass microfiber filters and shaken for 20 min at 75 rpm on a shaker (Unimax 1010, Heidolph Instruments, Kelheim, Germany) to retrieve the collected ACAM. The pH of the mobile phase is adjusted to 3.5. After ACAM is completely dissolved in the mobile phase,

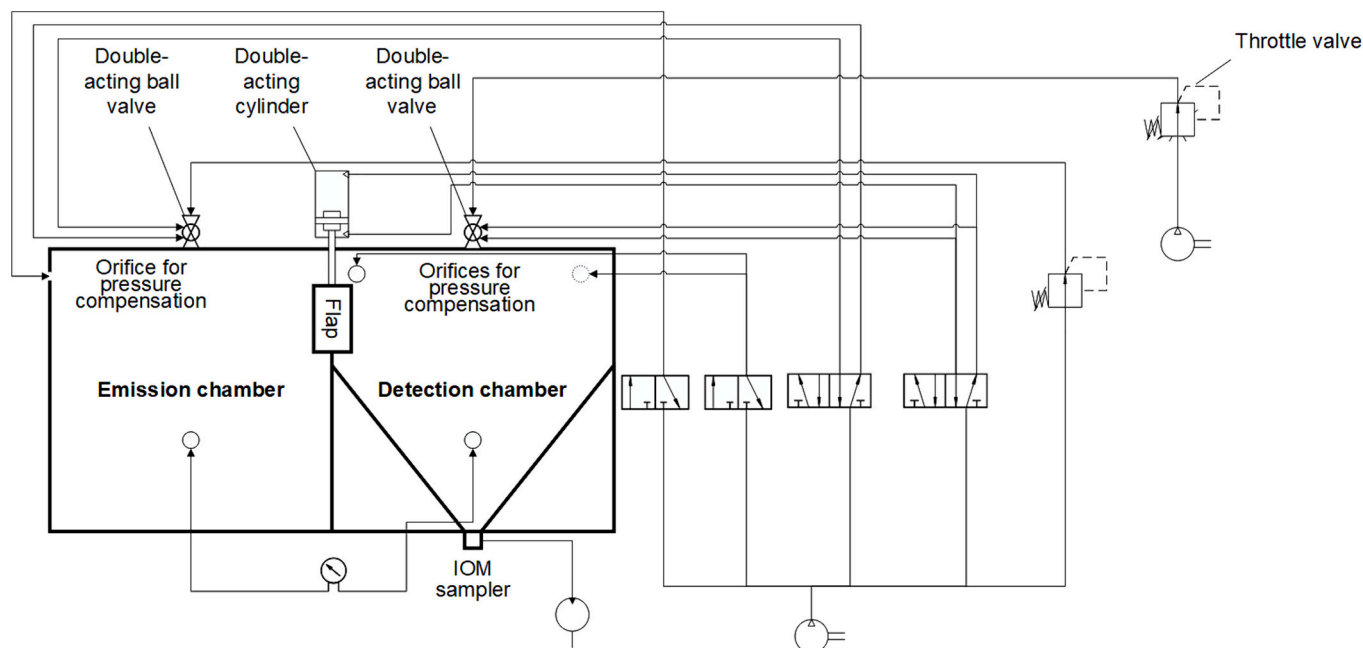


Fig. 2. Piping and instrumentation diagram of the TCS [58].

the solution is filtered (PTFE 13 mm, 0.45 μm , VWR, Radnor, USA) and transferred to vials for the HPLC analysis. HPLC is performed with a VWR-Hitachi Chromaster 5000 (Radnor, USA) equipped with a 250×4 mm column (LiChroCART® 250–4, Merck, Darmstadt, Germany) with an RP-18e phase (particle size 5 μm). The ACAM samples (20 μl) are injected into chromatograph and quantified spectrophotometrically at a wavelength of 245 nm (Chromaster 5430 Diode Array Detector, Hitachi, Chiyoda, Japan). The flow rate is 1 ml/min and the temperature out is 22 °C. ACAM is eluted at 1.92 min, while the total run time for the measurement of each sample is 3 min. A calibration curve is created to detect ACAM concentrations in the range between 0.002 and 2.212 $\mu\text{g}/\text{ml}$ ($R^2 = 0.9999$).

2.2.6. Angle of repose

To determine the angle of repose for ACAM1–3 and LM1–3 according to the monograph 2.9.36 “Powder flow”, powder sample quantities ranging from 50 to 100 g are dispensed through a conical funnel onto a plate of specified diameter. The funnel is aligned to ensure a minimal gap between the pike of the resulting pile and the funnel’s outlet. The angles of repose for the powder samples are determined by gauging the pile’s heights [59]. All measurements were performed in triplicate.

2.2.7. Bulk density and tapped density

In accordance with the monograph 2.9.34 “Bulk and tapped density of powders” in the European Pharmacopoeia [59], the bulk and tapped densities of the powder samples are measured by using a jolting volumeter (Stav 3000; J. Engelsmann AG, Ludwigshafen, Germany). 100 g of each powder sample is transferred into a 250 ml graduated measuring cylinder and subjected to the corresponding tapped movements. The measured values are then used to calculate both the Hausner ratios and the compressibility indices.

2.2.8. True density

The true densities of the powder samples are measured with a helium pycnometer (Pycnomatic ACT EVO, Porotec, Hofheim am Taunus, Germany). For this purpose, between 6 and 8 g of the powders are transferred into the analysis chamber of the helium pycnometer. The true density is calculated as the mean value of ten measurements. All measurements for determination of the true density are carried out in

triplicate.

2.2.9. Particle size distribution

The particle size distributions of the sieved ACAM and LM powder samples are measured with laser diffractometry (Helos KR, Sympatec, Clausthal-Zellerfeld, Germany) using a lens with an effective measuring range between 0.5 and 875 μm . The dry dispersion method (RODOS, Sympatec, Clausthal-Zellerfeld, Germany) is used to introduce the sample into the system for particle size measurement. An overpressure of 150,000 Pa is used to atomize the powder samples. The Paqxos software (version 2.0.3, Sympatec, Clausthal-Zellerfeld, Germany) is used to determine the particle size distribution. All measurements are performed in triplicate.

2.2.10. Scanning electron microscopy (SEM)

SEM images are taken to determine the exact particle shape. For this purpose, the samples are imaged with a scanning electron microscope (SEM; LEO 1525; Carl Zeiss, Oberkochen, Germany) at a magnification of 250 after coating with a thin carbon layer. The measurements are carried out in a high vacuum at an acceleration voltage of 2 kV with a 7.5 μm aperture.

2.2.11. Loss on drying

All ACAM and LM powder samples are subjected to loss on drying by thermal gravimetric analysis (TGA; TG 209 F1 Libra®, Netzsch-Gerätebau, Selb, Germany). The samples are heated up with a heat rate of 10 K/min from room temperature to 105 °C and kept at that temperature for 30 min.

3. Results and discussion

3.1. Powder characterization

In the present study, ACAM and LM are used as surrogate substances recommended by the International Society for Pharmaceutical Engineering (ISPE) to evaluate the impact of binary powder blends on dustiness by application of the TCS methodology. As noted in the introduction, the physical characteristics of powders may affect dustiness. In this study, binary powder blends were selected to evaluate the

impact of LM on the dustiness of ACAM using the TCS, considering that active ingredients are typically combined with other excipients during dosage form manufacture. Consequently, it is necessary to characterize HPAPIs either as plain powders or powder blends regarding to their dustiness.

In Fig. 3 the different particle shapes of ACAM1–3 and LM1–3, with a noticeable increase in particle size from ACAM1 to ACAM3 and from LM1 to LM3 are shown as SEM images.

Particularly, the particles in ACAM1 exhibit distinct variations in particle size. Their shapes range from elongated irregular to angular. In contrast, the ACAM2 particles are much more angular, while the particles of ACAM3 are as significantly more rounded. The particles of LM1 are characterized by a distinct angular shape and a rough surface texture. Interestingly, the sphericity of these particles varies considerably; some show an approximation to a round shape, while others deviate significantly from this ideal shape and have a very low sphericity. In comparison, the particles of LM2 are characterized by larger dimensions and share the rough surface features and prominent angularity with LM1, making them similar in shape but different in size. On the other hand, LM3 particles stand out resulting from their large size and again confirm a strong angularity, a characteristic feature that proceeds through the entire series of observations.

The observations regarding the particle sizes of ACAM1, 2, and 3 as well as LM1, 2, and 3 are further confirmed by the results obtained through laser diffractometry, as presented in Table 2.

ACAM1 shows the smallest particle size with a median value (x_{50}) of $9.91 \pm 0.15 \mu\text{m}$ ($n = 3$). Significantly larger particles are found with the

surrogate substance ACAM2 ($p < 0.05$) revealing a x_{50} of $125.86 \pm 4.13 \mu\text{m}$ ($n = 3$), while ACAM3 shows the highest x_{50} value of $216.12 \pm 2.84 \mu\text{m}$. Similarly, LM1–3 illustrate a significant gradual increase in particle size ($p < 0.05$), starting with LM1, which exhibits an x_{50} value of $28.96 \pm 0.21 \mu\text{m}$ ($n = 3$), followed by LM2 with $116.83 \pm 3.22 \mu\text{m}$ ($n = 3$) and LM3 with $188.31 \pm 2.04 \mu\text{m}$ ($n = 3$). These discrete particle fractions, differentiated into fine, medium, and coarse sizes, are also displayed in Fig. 4 confirming the fractionation by sieving.
(means \pm SD, $n = 3$).

Considering both, particle size and shape, the true densities of the samples are determined. The true densities of ACAM (1.2854 – 1.2942 g/cm^3) and of LM (1.5364 and 1.5395 g/cm^3) show negligible variation and are comparable. Investigation of the bulk densities reveals an increase from ACAM1 (0.34 g/cm^3) to ACAM3, with an intermediate value of 0.65 g/cm^3 for ACAM2. For LM, the bulk densities are determined to be $0.57 \pm 0.01 \text{ g/cm}^3$ (LM1), $0.62 \pm 0.01 \text{ g/cm}^3$ (LM2), and $0.56 \pm 0.0 \text{ g/cm}^3$ (LM3). The Hausner ratios and compressibility indices are then calculated by determination of the tapped densities, where an increase in particle size is accompanied a decrease of both values, a phenomenon that may be explained by a reduction in cohesive forces and a decrease in electrostatic charge. These interactions significantly affect the tendency of pharmaceutical powders to become airborne and to form dust by altering the adherence of the particles to each other as well as their attraction to or repulsion from surfaces, thus indirectly controlling the distribution of dust particles in the air.

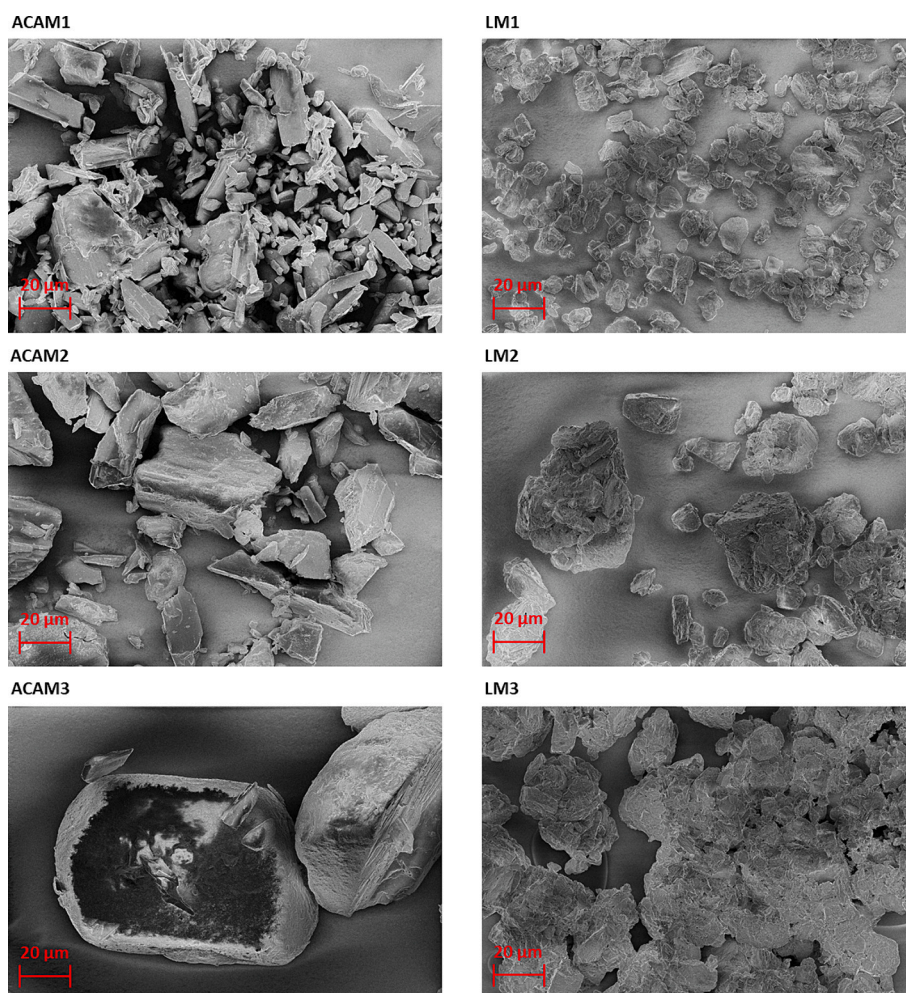
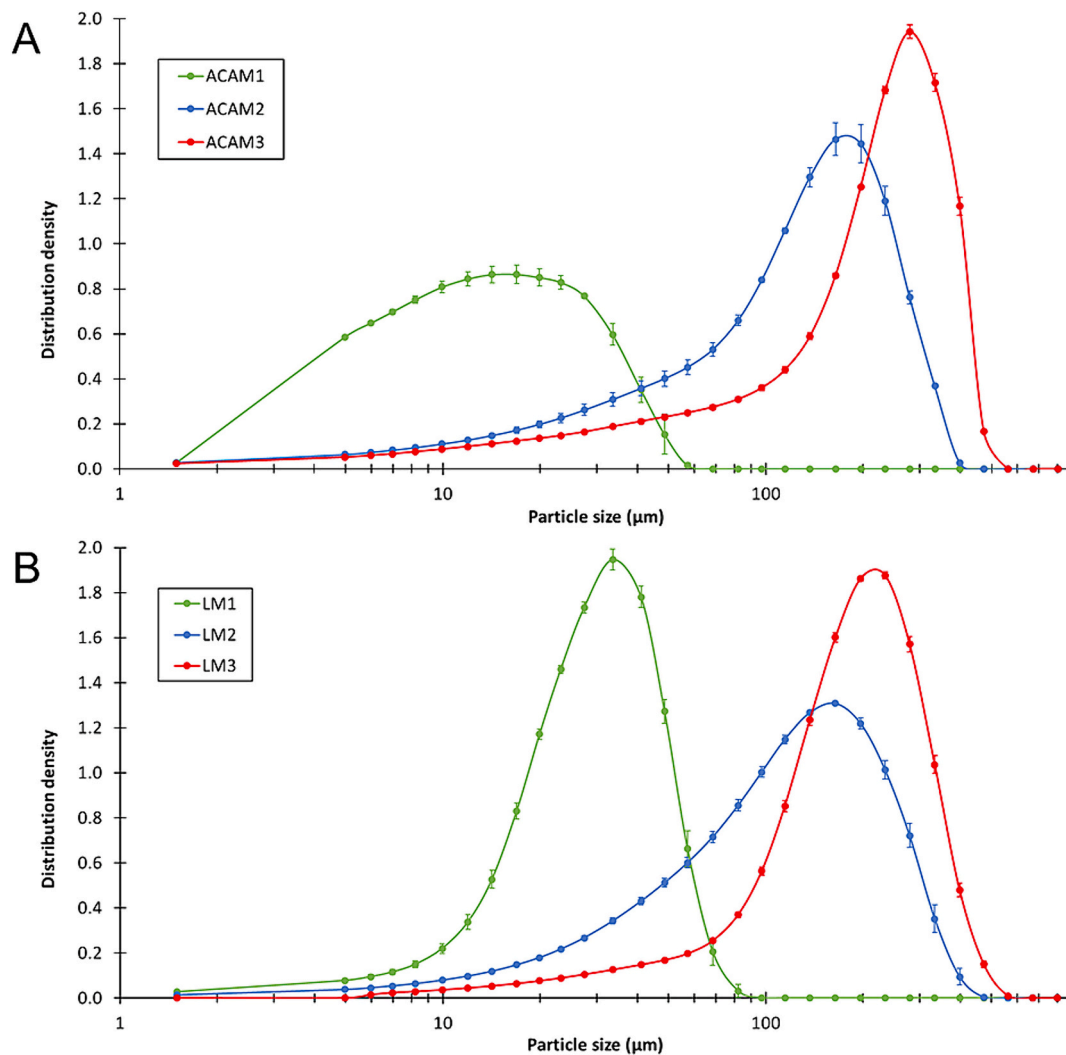


Fig. 3. SEM images of the fine, medium-size, and coarse fractions of ACAM and LM at a magnification of 250.

Table 2Physical properties of ACAM1,2, and 3 as well as LM1,2, and 3 (means \pm SD, $n = 3$; $n = 10$ for the true densities).

Physical properties	ACAM1	ACAM2	ACAM3	LM1	LM2	LM3
Particle size x_{10} (μm)	2.05 ± 0.09	20.08 ± 0.89	28.03 ± 0.70	12.25 ± 0.16	27.66 ± 0.77	68.98 ± 0.95
Particle size x_{50} (μm)	9.91 ± 0.15	125.86 ± 4.13	216.12 ± 2.84	28.96 ± 0.21	116.83 ± 3.22	188.31 ± 2.04
Particle size x_{90} (μm)	29.98 ± 1.26	248.34 ± 1.16	363.32 ± 1.96	48.48 ± 0.23	250.64 ± 6.34	326.25 ± 3.92
True density (g/cm^3)	1.2854 ± 0.0047	1.2942 ± 0.0023	1.2921 ± 0.0008	1.5364 ± 0.0033	1.5395 ± 0.0010	1.5392 ± 0.0008
Bulk density (g/cm^3)	0.34 ± 0.02	0.65 ± 0.01	0.67 ± 0.00	0.57 ± 0.01	0.62 ± 0.01	0.56 ± 0.00
Hausner ratio	1.59 ± 0.03	1.21 ± 0.01	1.16 ± 0.01	1.42 ± 0.01	1.24 ± 0.01	1.20 ± 0.01
Compressibility index (%)	37.30 ± 1.67	17.7 ± 0.49	14.1 ± 0.53	29.34 ± 0.47	19.08 ± 0.58	16.54 ± 0.55
Angle of repose ($^\circ$)	49.0 ± 0.8	48.6 ± 0.8	35.8 ± 0.4	41.5 ± 0.3	33.6 ± 0.0	27.9 ± 0.5
Residual moisture content (%)	0.14 ± 0.04	0.15 ± 0.02	0.14 ± 0.04	0.43 ± 0.05	0.36 ± 0.06	0.37 ± 0.03

**Fig. 4.** Mean particle size distribution of ACAM1,2, and 3 (A) and LM1, 2, and 3 (B).

3.2. Dustiness investigation

The investigation on dustiness is performed with binary powder blends of an active ingredient or surrogate substance ACAM and the excipient LM. For this purpose, the measured dust emissions of plain ACAM are compared with those of the binary powder blends. Special focus is placed on the adequate atomization of the powder samples to be investigated and on the diffusive transport of the airborne particles within the closed system of the TCS. In Fig. 5, the measured dust emissions of ACAM1, 2, and 3 are shown at amounts of 50, 100, 150, 200, and 250 mg each to adapt the ACAM fractions in the binary powder blends. In a previous study with the TCS, it was shown that there is a

linear relationship between the measured dust emission of ACAM and the atomized mass of ACAM up to a range of 400 mg. As expected, linearity is also observed for ACAM1, 2, and 3 in present investigations, with a coefficient of determination of 0.9868 for ACAM1, 0.9889 for ACAM2, and 0.9252 for ACAM3.

ACAM1 with the finest ACAM particles, shows significantly higher ($p < 0.05$) dust emissions at all atomized masses. Furthermore, ACAM2 with medium-size particles reveals a significantly ($p < 0.05$) higher dust emission than ACAM3 and a significantly lower emission ($p < 0.05$) than ACAM1. Apparently, differences in dust emission exist within the TCS if using ACAM with different particle sizes, with finer particles exhibiting a higher dust emission than coarser particles.

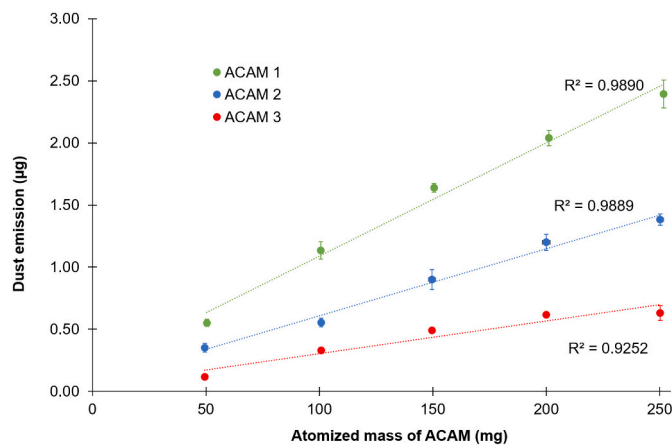


Fig. 5. Dust emissions of ACAM1, 2, and 3 (means \pm SD, $n = 3$).

The dust emissions of ACAM1 as well as of the binary powder blends of ACAM1 and either LM1, 2, or 3 at mixing ratios of 20:80, 40:60, 60:40, and 80:20 is displayed in Fig. 6. A decrease in dust emissions is observed with all examined binary powder blends. The lowest reduction in emissions is found with the blends of ACAM1 and LM3, with values between 23.0 % and 54.1 %. The highest reduction in emissions is observed with the ACAM1-LM1 and ACAM1-LM2 blends, with no significant difference ($p > 0.05$) between these two blends.

As expected, dust emissions increase with increasing ACAM fractions in the blends. The largest reductions in dust emissions are observed with blends of ACAM:LM (40:60). In contrast, smaller differences in dust emission are found between plain ACAM and its 80:20 binary powder blends.

A potential explanation for the relatively high dust emissions of the ACAM1-LM3 blend could be the significant differences in particle size between fine ACAM1 and coarse LM3. Apparently, blends of fine and coarse particles significantly decrease dust emissions under the given process parameters of the TCS. Such interactive powder blends are also used in powder inhalers to reduce the attraction between the micronized active pharmaceutical ingredient (API) and the coarse excipient, improving the release of the API during inhalation [60–62]. As mentioned in the introduction, other parameters also influence dustiness: Apart from different particle sizes, the type of atomization or the mechanism of energy transfer to the powder particles, also have a significant impact on dustiness.

In Fig. 7 the dust emissions of ACAM2 and its binary powder blends from ACAM2 are illustrated. Dust emissions are reduced by mixing

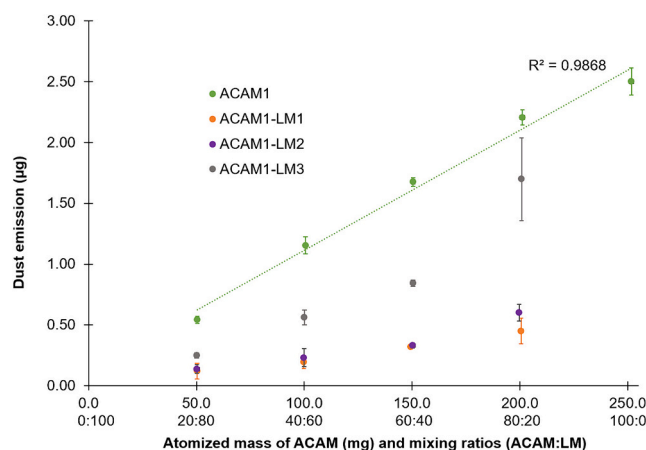


Fig. 6. Dust emissions of ACAM1 and binary powder blends of ACAM1 and either LM1, 2, or 3 (means \pm SD, $n = 3$).

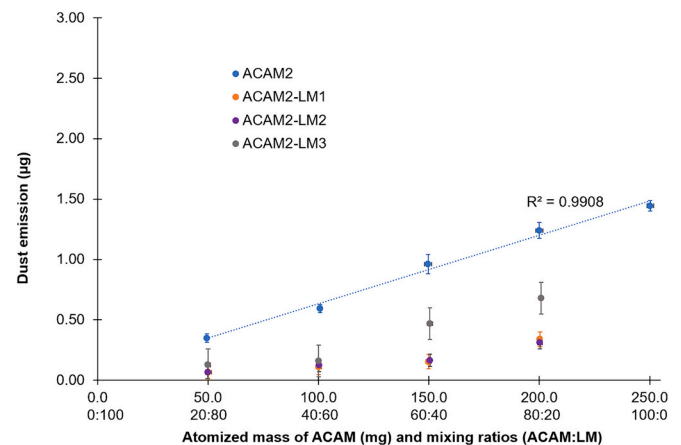


Fig. 7. Dust emissions of ACAM2 and binary powder blends of ACAM2 and either LM1, 2, or 3 (means \pm SD, $n = 3$).

ACAM2 with either LM1, 2, or 3, with the blend of ACAM2 and LM3 showing the highest emissions. Blends of ACAM2 and either LM1 or LM2 do not show significant differences ($p > 0.05$) in dust emission but exhibit significantly ($p < 0.05$) lower emissions compared to the blends of ACAM2 and LM3 at the 60:40 and 80:20 ratios. As already shown in Fig. 5, ACAM1 significantly higher dust emissions are obtained with ACAM2.

The resulting dust emissions of ACAM3 and its binary powder blends are shown in Fig. 8. As expected, all binary blends of ACAM3 also lead to a reduction in dust emission. Up to a mixing ratio 60:40 (ACAM:LM), a reduction in emissions is observed, but with no significant differences ($p > 0.05$). Only at a mixing ratio of 80:20, a significant difference in emissions is found. At this mixing ratio, the blends of ACAM3 and LM3 exhibit the highest dustiness, while its binary blends with LM2 or LM1 show lower emissions.

The results of this study indicate that the dust emission of the plain ACAM and its binary powder blends with LM in the closed system of the TCS with the selected process parameters were influenced by the particle size of the two powders. In particular, if mixing fine ACAM and coarse LM comparably high dust emissions are remarkable. Fine and medium-size LM particles seem to cause a raise of surface energy by increasing the surface area and thus the adsorption the ACAM particles to the LM surface area.

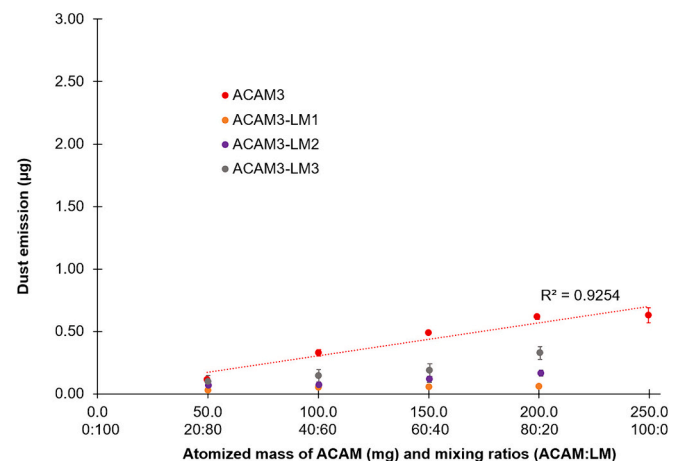


Fig. 8. Dust emissions of ACAM3 and binary powder blends of ACAM3 and either LM1, 2, or 3 (means \pm SD, $n = 3$).

4. Conclusion

The investigation of dust emissions of fine, medium-size, and coarse fractions of ACAM (ACAM1, 2, and 3) carried out with a two-chamber setup (TCS) reveals statistically significant differences in dust emissions. ACAM1 shows the highest dust emissions, while ACAM2 and ACAM3, with increased particle sizes, exhibit significantly lower emissions. In a previous study, a linear correlation between dust emissions and an atomized mass threshold of up to 400 mg ACAM was identified. Results of the presented investigations of binary powder blends using the TCS demonstrate a substantial and reproducible reduction in dust emissions when mixing ACAM with LM. The reduction in dust emissions is most pronounced at a mixing ratio of 40:60, especially if fine ACAM (ACAM1) is mixed with coarse LM (LM3). In contrast, the blend of fine ACAM with coarse LM shows the highest dust emission reduction, while the lowest reduction is observed with the blend of coarse ACAM and fine LM. The investigation of the dustiness of binary powder blends containing ACAM2 results in a significant reduction in dust emissions with all powder blends. The blend ACAM2-LM3 exhibits the lowest reduction in dust emission. ACAM3 shows the lowest dust emissions in comparison to ACAM2 and ACAM1, further reduced by mixing with LM. Significant differences in dust emissions are only observed between all binary powder blends of ACAM3 at a ratio of 80:20. At this mixing ratio, the blends of ACAM3 and LM3 exhibit the highest dust emissions.

In summary, the dust emissions of ACAM in the TCS are influenced by the mixing ratio with LM and the particle size. Fine particles exhibit higher dust emissions because of their larger specific surface area and lower bulk density, which enhance diffusive and convective transport within the TCS. Additionally, surface energies, adsorption phenomena, and particle shape significantly influence the results. The transport mechanisms and energy transfer during atomization also affect the dustiness of the binary powder blends.

However, it is important to recognize that while the investigations with the TCS provides valuable insights under controlled laboratory conditions, the transferability of these findings to industrial settings may be limited. The complexity and variability of industrial processes, as highlighted in the introduction, may require additional considerations and adaptations when transferring these results into practice.

Based on the presented results, it may be concluded that the dustiness of pharmaceutical powders, investigated with the TCS, depends on the surrogate and excipient properties. Consideration of other common pharmaceutical excipients like mannitol, starch, or microcrystalline cellulose may be of interest in this context. Additionally, examining β -lactose monohydrate, which differs in surface texture from α -lactose monohydrate, may further provide important knowledge. Furthermore, analyzing powder mixtures containing more than two components would be informative.

CRediT authorship contribution statement

Steffen Wirth: Writing – original draft, Visualization, Validation, Software, Project administration, Methodology, Investigation, Funding acquisition, Formal analysis, Data curation, Conceptualization. **Martin Schöler:** Writing – review & editing, Validation. **Claudia S. Leopold:** Writing – review & editing, Validation, Project administration.

Declaration of competing interest

The authors declare that they have no known competing financial interests or personal relationships that could have appeared to influence the work reported in this paper.

Data availability

The data that has been used is confidential.

Acknowledgments

The authors would like to express their gratitude to Petra Borbe and Kai Braunschweig, whose technical support made a significant contribution to this study. Special thanks are due to the electron microscopy team for taking the SEM pictures.

References

- [1] S. Haigney, HPAPI capacity challenges, *Pharm. Technol.* 2019 (4) (2019) 6–10.
- [2] International Society for Pharmaceutical Engineering (ISPE), ISPE D/A/CH Affiliate: Containment Manual, ISPE D/A/CH, Offenbach/Main, Germany, 2017.
- [3] P. Setty, Optimal Handling of Highly Active Pharmaceutical Ingredients during Milling and Blending Operations, Massachusetts Institute of Technology (Department of Chemical Engineering), Cambridge (USA), 2013.
- [4] R. Ronald, Bioprocessing challenges of antibody-drug conjugates, *Bioprocess Int.* 12 (2014) 6–10.
- [5] S. Wollowitz, Managing high-potency active pharmaceutical ingredients - a drug sponsor's guide, *Drug Dev. Res.* 71 (2010) 420–428, <https://doi.org/10.1002/ddr.20385>.
- [6] G. Franco, Ramazzini and workers' health, *Lancet* 354 (1999) 858–861, [https://doi.org/10.1016/S0140-6736\(99\)80042-7](https://doi.org/10.1016/S0140-6736(99)80042-7).
- [7] P. Tiwari, S.R. Chowdhury, Sustainable production of highly active pharmaceutical ingredients (HAPIs), *Int. J. Sci. Res. Publ.* 4 (2014) 2250–3153.
- [8] E. Dunny, I. O'Connor, J. Bones, Containment challenges in HPAPI manufacture for ADC generation, *Drug Discov. Today* 22 (2017) 947–951, <https://doi.org/10.1016/j.drudis.2017.02.003>.
- [9] G. Mari, A. Moccaldi, G. Ludovisi, Handling of high potency drugs: process and containment, *trans. Ecol. Environ.* 85 (1999) 257–265, <https://doi.org/10.2495/EEH050281>.
- [10] R. Denk, S. Ag, A. Flueckinger, H. Kisaka, R. Maeck, L. Restetzi, A. Schreiner, R. Schulze, L. Sachsen, Isolators key to preventing cross-contamination, *PDA Lett. LIII* (2017) 34–40.
- [11] J. Becker, T. Pohlmann, Development and implementation of a large-scale HPAPI manufacturing process, *Chim. Oggi-Chemistry Today* 35 (2019) 20–24.
- [12] International Society for Pharmaceutical Engineering (ISPE), Good Practice Guide: Assessing the Particulate Containment Performance of Pharmaceutical Equipment, ISPE, North Bethesda (USA), 2012. www.ispe.org.
- [13] A.W. Ader, J.P. Farris, R.H. Ku, Occupational health categorization and compound handling practice systems - roots, application and future, *Chem. Health Saf.* 12 (2005) 20–26, <https://doi.org/10.1016/j.chs.2005.01.016>.
- [14] J. Lanning, M.A.G. Boundy, D. Leith, Validating a model for the prediction of dust generation, *Part. Sci. Technol.* 13 (1995) 105–116, <https://doi.org/10.1080/02726359508906673>.
- [15] C. Champmartin, F. Clerc, Inhalable dust measurements as a first approach to assessing occupational exposure in the pharmaceutical industry, *J. Occup. Environ. Hyg.* 11 (2014) 85–92, <https://doi.org/10.1080/15459624.2013.843781>.
- [16] G. Lidén, Dustiness testing of materials handled at workplaces, *Ann. Occup. Hyg.* 50 (2006) 437–439, <https://doi.org/10.1093/annhyg/mel042>.
- [17] N.J. Adams, D.L. Johnson, R.A. Lynch, The effect of pressure differential and care provider movement on airborne infectious isolation room containment effectiveness, *Am. J. Infect. Control* 39 (2011) 91–97, <https://doi.org/10.1016/j.ajic.2010.05.025>.
- [18] H. Liu, S. Zhang, L. Liu, J. Yu, B. Ding, High-performance filters from biomimetic wet-adhesive nanoarchitected networks, *J. Mater. Chem. A* 8 (2020) 18955–18962, <https://doi.org/10.1039/d0ta06886a>.
- [19] J.H. Vincent, Aerosol Sampling: Science, Standards, Instrumentation and Applications, 2007.
- [20] R.H. Ku, An overview of setting occupational exposure limits (OELs) for pharmaceuticals, *Chem. Health Saf.* 7 (2000) 34–37, [https://doi.org/10.1016/S1074-9098\(99\)00070-2](https://doi.org/10.1016/S1074-9098(99)00070-2).
- [21] B.D. Naumann, E.V. Sargent, B.S. Starkman, W.J. Fraser, G.T. Becker, G.D. Kirk, Performance-based exposure control limits for pharmaceutical active ingredients, *Am. Ind. Hyg. Assoc. J.* 57 (1996) 33–42, <https://doi.org/10.1080/15428119691015197>.
- [22] J.H. Vincent, D. Mark, The basis of dust sampling in occupational hygiene: a critical review, *Ann. Occup. Hyg.* 24 (1981) 375–390, <https://doi.org/10.1093/annhyg/24.4.375>.
- [23] S. Bach, E. Schmidt, Determining the dustiness of powders - a comparison of three measuring devices, *Ann. Occup. Hyg.* 52 (2008) 717–725, <https://doi.org/10.1093/annhyg/men062>.
- [24] J. Stein, T. Fuchs, C. Mattern, Advanced milling and containment Technologies for Superfine Active Pharmaceutical Ingredients, *Chem. Eng. Technol.* 33 (2010) 1464–1470, <https://doi.org/10.1002/ceat.200900590>.
- [25] V. Kanjiyangat, M. Hareendran, Engineering intervention to reduce API dust exposure during milling operation, *J. Chem. Health Saf.* 25 (2018) 36–39, <https://doi.org/10.1016/j.jchas.2017.07.002>.
- [26] S. Armenta, M. Blanco, Ion mobility spectrometry: a comprehensive and versatile tool for occupational pharmaceutical exposure assessment, *Anal. Chem.* 84 (2012) 4560–4568, <https://doi.org/10.1021/ac300655t>.
- [27] Air quality — Particle Size Fraction Definitions for Health-Related Sampling (ISO 7708:1995), Geneva (Switzerland), 1995.

- [28] R.F. Phalen, W.C. Hinds, L. Angeles, W. John, I. Researcher, P.J. Liroy, Particle size-selective sampling in the workplace: rationale and recommended techniques, *Ann. Occup. Hyg.* 32 (1988) 403–411, <https://doi.org/10.1016/B978-0-08-034185-9.50046-2>.
- [29] T. Ohta, H. Maeda, R. Kubota, A. Koga, K. Terada, Establishment of powder dustiness evaluation method by dustmeter with small amount of pharmaceutical ingredients, *Int. J. Pharm.* 472 (2014) 251–256, <https://doi.org/10.1016/j.ijpharm.2014.05.067>.
- [30] M.A.E. Plinke, R. Maus, D. Leith, Experimental examination of factors that affect dust generation by using Heubach and mri testers, *Am. Ind. Hyg. Assoc. J.* 53 (1992) 325–330, <https://doi.org/10.1080/15298669291359726>.
- [31] T. Deng, K.A. Paul, M.S.A. Bradley, L. Immins, C. Preston, J.F. Scott, E.H. Welfare, Investigations on air induced segregation of pharmaceutical powders and effect of material flow functions, *Powder Technol.* 203 (2010) 354–358, <https://doi.org/10.1016/j.powtec.2010.05.028>.
- [32] K. Hjemsted, T. Schneider, Dustiness from powder materials, *J. Aerosol Sci.* 27 (1996) 485–486, [https://doi.org/10.1016/0021-8502\(96\)00315-1](https://doi.org/10.1016/0021-8502(96)00315-1).
- [33] P.T. O'Shaughnessy, M. Kang, D. Ellickson, A novel device for measuring respirable dustiness using low-mass powder samples, *J. Occup. Environ. Hyg.* 9 (2012) 129–139, <https://doi.org/10.1080/15459624.2011.652061>.
- [34] S. Chakravarty, O. Le Bihan, M. Fischer, M. Morgeneyer, Dust generation in powders: effect of particle size distribution, *EPJ Web Conf.* 140 (2017) 1–4, <https://doi.org/10.1051/epjconf/201714013018>.
- [35] S. Chakravarty, M. Fischer, P. García-Tríñanes, D. Parker, O. Le Bihan, M. Morgeneyer, Study of the particle motion induced by a vortex shaker, *Powder Technol.* 322 (2017) 54–64, <https://doi.org/10.1016/j.powtec.2017.08.026>.
- [36] M. Fischer, S. Chakravarty, O. Le Bihan, M. Morgeneyer, Parametric study of the particle motion induced by a vortex shaker, *Powder Technol.* 374 (2020) 70–81, <https://doi.org/10.1016/j.powtec.2020.06.060>.
- [37] C. Bressot, M. Morgeneyer, O. Aguerre-Chariol, J. Bouillard, K. Zaras, G.W. Visser, R.J. Meier, Sanding and analysis of dust from nano-silica filled composite resins for stereolithography, *Chem. Eng. Res. Des.* 156 (2020) 23–30, <https://doi.org/10.1016/j.cherd.2020.01.011>.
- [38] S. Chakravarty, M. Fischer, P. García-Tríñanes, M. Dalle, L. Meunier, O. Aguerre-Chariol, O. Le Bihan, M. Morgeneyer, Long-term dust generation from silicon carbide powders, *Process. Saf. Environ. Prot.* 116 (2018) 115–125, <https://doi.org/10.1016/j.psep.2018.01.021>.
- [39] M. Levin, I.K. Koponen, K.A. Jensen, Exposure assessment of four pharmaceutical powders based on dustiness and evaluation of damaged HEPA filters, *J. Occup. Environ. Hyg.* 11 (2014) 165–177, <https://doi.org/10.1080/15459624.2013.848038>.
- [40] A. Klippel, M. Schmidt, U. Krause, Dustiness in workplace safety and explosion protection - review and outlook, *J. Loss Prev. Process Ind.* 34 (2015) 22–29, <https://doi.org/10.1016/j.jlp.2015.01.011>.
- [41] S. Bach, U. Eickmann, E. Schmidt, Comparison of established systems for measuring the dustiness of powders with the UNC dustiness tester developed especially for pharmaceutical substances, *Ann. Occup. Hyg.* 57 (2013) 1078–1086, <https://doi.org/10.1093/annhyg/met022>.
- [42] K.H. Carlson, D.R. Herman, T.F. Markey, R.K. Wolff, M.A. Dorato, A comparison of two dustiness evaluation methods, *Am. Ind. Hyg. Assoc. J.* 53 (1992) 448–454, <https://doi.org/10.1080/15298669291359933>.
- [43] H. Chen, M.A. Jog, L.A. Turkevich, Computational fluid dynamics simulations of aerosol behavior in a high-speed (Heubach) rotating drum dustiness tester, *Particuology* 72 (2023) 68–80, <https://doi.org/10.1016/j.partic.2022.02.010>.
- [44] P. Dubey, U. Ghia, L.A. Turkevich, Computational fluid dynamics analysis of the Venturi dustiness tester, *Powder Technol.* 312 (2017) 310–320, <https://doi.org/10.1016/j.powtec.2017.02.030>.
- [45] K. Hjemsted, T. Schneider, Documentation of a dustiness drum test, *Ann. Occup. Hyg.* 40 (1996) 627–643, [https://doi.org/10.1016/S0003-4878\(96\)00024-5](https://doi.org/10.1016/S0003-4878(96)00024-5).
- [46] F. Hamelmann, E. Schmidt, Methods for characterizing the dustiness estimation of powders, *Chem. Eng. Technol.* 27 (2004) 844–847, <https://doi.org/10.1002/ceat.200403210>.
- [47] M. Boundy, D. Leith, T. Polton, Method to evaluate the dustiness of pharmaceutical powders, *Ann. Occup. Hyg.* 50 (2006) 453–458, <https://doi.org/10.1093/annhyg/mel004>.
- [48] D.E. Evans, L.A. Turkevich, C.T. Roettgers, G.J. Deye, P.A. Baron, Dustiness of fine and nanoscale powders, *Ann. Occup. Hyg.* 57 (2013) 261–277, <https://doi.org/10.1093/annhyg/mes060>.
- [49] S. Chakravarty, M. Fischer, O. Le Bihan, M. Morgeneyer, Towards a theoretical understanding of dustiness, *Granul. Matter* 21 (2019) 1–22, <https://doi.org/10.1007/s10035-019-0929-z>.
- [50] K. Saleh, M.T. Moufarej Abou Jaoude, M. Morgeneyer, E. Lefrançois, O. Le Bihan, J. Bouillard, Dust generation from powders: a characterization test based on stirred fluidization, *Powder Technol.* 255 (2014) 141–148, <https://doi.org/10.1016/j.powtec.2013.10.051>.
- [51] H. Salehi Kahrizsangi, D. Sofia, D. Barletta, M. Poletto, Dust generation in vibrated cohesive powders, *Chem. Eng. Trans.* 43 (2015) 769–774, <https://doi.org/10.3303/CET1543129>.
- [52] H. Salehi, N. Lotrecchiano, D. Barletta, M. Poletto, Dust release from aggregative cohesive powders subjected to vibration, *Ind. Eng. Chem. Res.* 56 (2017) 12326–12336, <https://doi.org/10.1021/acs.iecr.7b02241>.
- [53] S. Wirth, M. Schöler, J. Brüggemann, C.S. Leopold, A novel two-chamber setup for containment investigations with special focus on the dustiness of pharmaceutical powders depending on the airflow, *Pharmaceutics* 14 (2022) 2387, <https://doi.org/10.3390/pharmaceutics14112387>.
- [54] H. Hurychová, M. Kuentz, Z. Šklubalová, Fractal aspects of static and dynamic flow properties of pharmaceutical excipients, *J. Pharm. Innov.* 13 (2018) 15–26, <https://doi.org/10.1007/s12247-017-9302-0>.
- [55] O. Butler, J. Forster, J. Saunders, Analytical protocol for the sensitive determination of mannitol, sorbitol and glucose containing powders in pharmaceutical workplaces by ion chromatography using a pulsed amperometric detector, *J. Pharm. Biomed. Anal.* 106 (2015) 204–209, <https://doi.org/10.1016/j.jpba.2014.10.006>.
- [56] S. Wirth, M. Schöler, C.S. Leopold, Investigation on the Dustiness of a Binary Powder Mixture with a Newly Developed Two-Chamber Setup, 12th PBP World Meet, 2021.
- [57] S. Wirth, M. Schöler, C.S. Leopold, Dust emissions of surrogate substances resulting from diffusive and convective transport for containment investigations with a newly developed two-chamber setup, in: *PharmSci 360 Annu. Meet.*, 2022.
- [58] S. Wirth, M. Schöler, J. Brüggemann, C.S. Leopold, An investigation on the relationship between dust emission and air flow as well as particle size with a novel containment two-chamber setup, *Pharmaceutics* 16 (2024), <https://doi.org/10.3390/pharmaceutics16081088>.
- [59] European Pharmacopoeia 10.0, European Directorate for the Quality of Medicines & Health Care (EDQM), Strasbourg, France, 2019.
- [60] F. Podczek, The relationship between particulate properties of carrier materials and the adhesion force of drug particles in interactive powder mixtures, *J. Adhes. Sci. Technol.* 11 (1997) 1089–1104, <https://doi.org/10.1163/156856197X00859>.
- [61] H. Adi, I. Larson, H. Chiou, P. Young, D. Traini, P. Stewart, Agglomerate strength and dispersion of salmeterol xinafoate from powder mixtures for inhalation, *Pharm. Res.* 23 (2006) 2556–2565, <https://doi.org/10.1007/s11095-006-9082-6>.
- [62] F. Podczek, Adhesion forces in interactive powder mixtures of a micronized drug and carrier particles of various particle size distributions, *J. Adhes. Sci. Technol.* 12 (1998) 1323–1339, <https://doi.org/10.1163/156856198X00461>.

Discussion

The novel two-chamber system (TCS) developed in this thesis was applied in all three studies described in Chapters 3.1 to 3.3. First investigations with the TCS showed that by dividing the measuring process into an atomisation, transport, and detection phase, an investigation of the dustiness of pharmaceutical powders was possible and led to precise and reproducible results.

During the atomisation phase, the surrogate substance ACAM was atomised at sample quantities between 50 and 500 mg. The results revealed a linear correlation between the atomised sample quantity of ACAM up to 400 mg and the resulting dust emission. While the correlation coefficient of $R^2 = 0.984$ indicates a high reproducibility as well as a clear relationship between atomisation sample quantity and dust emission, the maximum relative standard deviation of 6.58 % underlines the reliability of the method. However, above an atomised sample quantity of 400 mg no further increase in dust emission was observed, indicating a saturation effect. This saturation effect may be explained by several factors, such as the limited volume of the emission chamber, the operational features of the atomisation process and/or the physicochemical properties of the surrogate substance ACAM. These factors may interact to create a threshold beyond which additional atomised material does not lead to a proportional increase of dust emission. However, the saturation effect only plays a minor role in this study, as the primary goal was to reproducibly atomise small quantities of pharmaceutical powders and to ensure consistent results. This knowledge was subsequently applied to further investigations with the TCS using sample masses below 400 mg to ensure an optimum reproducibility and compliance with the objectives of the study.

The transport phase was investigated by generating pressure differences and, thus, air flows between the detection and emission chambers. The pressure differences

ranged from 0 and 12 Pa, with plain diffusive transport of airborne particles occurring at a pressure difference of $\Delta p = 0$ Pa and an oppositely directed convective air flow taking place at pressure differences between 1 and 12 Pa. As expected, the highest dust emissions were measured during plain diffusive transport, as there was no flow against the diffusion of the particles. This observation corresponds to the theoretical principles according to which particles move independently during diffusion and are not influenced by external flow effects. However, the generation of pressure differences within the TCS always resulted in reduced dust emissions compared to those measured with plain diffusion. In the initial experiments, a pressure difference of 1 to 4 Pa showed a significant decrease in dust emissions, which further decreased with rising pressure difference. By modifications of the TCS, the pressure difference could be increased up to 12 Pa. Between 5 and 8 Pa dust emissions were only detected with very fine particles, whereas above 8 Pa, no dust emissions were detected at all.

Pressure differences and the resulting air flows are used in the pharmaceutical industry to minimise potential exposure to hazardous dust. The investigations with the TCS showed a good correlation with standard values that are established in industrial applications. For leaks, a minimum flow rate of 0.2 m/s ensures separation between the process zone and the environment. Recommended flow rates are between 0.4 and 0.5 m/s, comparable to those in the TCS.

The reduction in dust emissions caused by increasing pressure differences was also described using mathematical models. Exponential functions showed the best fit with R^2 values between 0.926 and 0.987, followed by quadratic functions ($R^2 = 0.863 - 0.977$). Linear functions showed the lowest fit ($R^2 = 0.674 - 0.882$). These results were confirmed by numerical flow simulations. The simulated average air velocities in the range of 0.09 to 0.37 m/s corresponded closely with the measured velocities (0.09 to 0.41 m/s). It may also be concluded from the mathematical functions used to describe

the reduction of dust emissions that an increase of the pressure differences is an effective means of minimising dust emissions. It is particularly remarkable that even low pressure differences with the resulting low average air velocities may lead to significant reductions in dust emissions. This emphasises the relevance of the pressure differences, even if they are relatively moderate.

The obtained results show that the TCS may serve as a model for a potential scenario in the pharmaceutical industry. However, it is important to note that dust emissions depend on a variety of factors that may significantly influence their extent. These factors include the material properties of the substances applied, the design of the TCS and the type of atomisation. They should be considered when transferring the results to industrial applications to implement realistic and effective emission reduction measures.

As already described in numerous studies, the particle size has a significant influence on dust emission. Therefore, this influence on dust emission was analysed in more detail using the TCS. The influence of particle size on dustiness was also investigated. At a pressure difference of 0 Pa, fine ACAM particle fractions exhibited a higher dustiness than coarse fractions. As expected, an increase in the pressure difference resulting in an oppositely directed convective flow led to a significant reduction in dust emissions. Coarse ACAM particle fractions showed no measurable dust emissions even at low pressure differences, while fine fractions required higher pressure differences. These results of the investigations with the TCS clearly show that the particle size has a significant influence on dust generation. Nevertheless, it should be noted that dust emissions are influenced by multiple factors. For example, other material-related factors, the type and transmission of the mechanical stimulus, or other external factors may also have an effect. Therefore, the transferability of the results to

other systems or scenarios in the pharmaceutical industry is only possible to a limited extent.

With regard to the investigated ACAM:LM powder blends, the blends of fine ($x_{50} = 9.91 \pm 0.15 \mu\text{m}$), medium-size ($x_{50} = 125.86 \pm 4.13 \mu\text{m}$) and coarse ($x_{50} = 216.12 \pm 2.84 \mu\text{m}$) ACAM particle fractions with fine ($x_{50} = 28.96 \pm 0.21 \mu\text{m}$), medium-size ($x_{50} = 116.83 \pm 3.22 \mu\text{m}$) and coarse ($x_{50} = 188.31 \pm 2.04 \mu\text{m}$) LM particle fractions resulted in a significant reduction in dust emissions compared to plain ACAM. Fine particles showed higher dust emissions than coarser particles. However, the emissions could be reduced by mixing with LM. Particularly fine ACAM in combination with coarse LM led to higher dust emissions than blends with fine or medium-size LM. Dust emissions increased as the percentage of ACAM in the mixtures increased. Blends of medium-size and coarse ACAM with LM also showed a reduction in emissions. The dust emissions within the TCS appear to depend on the mixing ratio and the particle size of the powder blends. The specific surface area as well as the bulk density also have an influence on the emissions. Furthermore, the particle shape and surface energies may affect the results. Mechanisms such as energy and mass transport during atomisation also play a role in dust generation of the powder blends.

The evacuation time in the detection phase was analysed by three different methods to ensure that the particles were detected in a reasonable time. CFD simulations showed that the pyramidal design of the detection chamber allows for efficient evacuation, with 540 s being sufficient to capture 99.99 % of the particles. These results were confirmed by smoke tests in which 99.51 ± 0.13 % of the particles were detected after the same time period. In addition, dustiness investigations verified these results, as over 99 % of the particles were also detected within 540 s. The results of the CFD simulation, smoke and dustiness tests show a high level of conformity, which

indicates their good transferability. The pyramidal design of the detection chamber contributes significantly to an effective airborne particle detection.

For all three studies, the investigated powders applied were characterised with regard to their material properties. The true density of ACAM was in the range between 1.282 and 1.301 g/cm³. The residual moisture content amounted to 0.14 - 0.15 %. However, parameters such as bulk and tapped density and derived parameters such as the Hausner ratio and the compressibility index showed significant differences depending on the particle size. The considerable differences in the particle sizes of the ACAM fractions allowed an investigation of the influence of the particle size on dustiness. For LM, which was used to investigate the dustiness of binary powder blends, the true density values were between 1.536 and 1.540 g/cm³. The residual moisture content amounted to 0.36 - 0.43 %. The powders were thoroughly characterised to ensure reliable and reproducible measurements of their dust emissions. Parameters such as particle size, bulk and tapped density, true density and moisture content were analysed and revealed significant differences regarding the two powder components. Thus, they enabled an accurate investigation of dustiness.

In summary, the TCS offers a comprehensive and precise way of analysing pharmaceutical powders, particularly regarding dust emissions. It allows a detailed investigation of influencing factors such as particle size, mixing ratios and pressure differences on dust generation. The combination of reproducible results, flexible adaptability to different conditions and the ability to simulate industrial scenarios makes the TCS a versatile tool.

References

1. G. Mari, A. Moccaldi, G. Ludovisi. Handling of high potency drugs: process and containment. *Trans Ecol Environ*. 1999;85:257–65.
 2. S. Wollowitz. Managing high-potency active pharmaceutical ingredients - A drug sponsor's guide. *Drug Dev Res*. 2010;71(7):420–8.
 3. P. Tiwari, S.R. Chowdhury. Sustainable Production of Highly Active Pharmaceutical Ingredients (HAPIs). *Int J Sci Res Publ*. 2014;4(1):2250–3153.
 4. G. Franco. Ramazzini and workers' health. *Lancet*. 1999;354(9181):858–61.
 5. ISPE D/A/CH Working Group Containment. Containment Manual. Mannheim, Deutschland: ISPE D/A/CH; 2016. 226 p.
 6. R.J.L. Heron, F.C. Pickering. Health effects of exposure to active pharmaceutical ingredients (APIs). *Occup Med (Chic Ill)*. 2003;53(6):357–62.
 7. E. Dunny, I. O'Connor, J. Bones. Containment challenges in HPAPI manufacture for ADC generation. *Drug Discov Today*. 2017;22(6):947–51.
 8. S. Haigney. HPAPI Capacity Challenges. *Pharm Technol*. 2019;2019(4)(4):6–10.
 9. E.L. Barle, G.C. Winkler, S. Glowienke, A. Elhajouji, J. Nunic, H.J. Martus. Setting occupational exposure limits for genotoxic substances in the pharmaceutical industry. *Toxicol Sci*. 2016;151(1):2–9.
 10. M. Glogovac, C. Paulson, A. Lambert, G.C. Winkler, E. Lovsin Barle. Disease area and mode of action as criteria to assign a default occupational exposure limit. *Regul Toxicol Pharmacol*. 2021;122(February):104891.
 11. K. Blum, R. FitzGerald, M.F. Wilks, E.L. Barle, N.B. Hopf. Use of the benchmark-dose (BMD) approach to derive occupational exposure limits (OELs) for genotoxic carcinogens: N-nitrosamines. *J Appl Toxicol*. 2023;43(8):1183–200.
 12. A.W. Ader, J.P. Farris, R.H. Ku. Occupational health categorization and compound handling practice systems - Roots, application and future. *Chem Heal Saf*. 2005;12(4):20–6.
 13. H. Stahl. How to make tablets from potent APIs. *Pharm Technol*. 2010;2010(3):34–9.
 14. I. Grayson, J. Becker, T. Pohlmann, K. Blumbach, K. McCleary, M. Van Hooiser. Development and implementation of a large-scale HPAPI manufacturing process. *Chim Oggi-Chemistry Today*. 2019;35(January):20–4.
-

-
15. R. Denk, S. Ag, A. Flueckinger, H. Kisaka, R. Maeck, L. Restetzki, et al. Isolators Key to Preventing Cross-Contamination. *PDA Lett.* 2017;LIII(10):34–40.
 16. C.A. Challener. Minimizing risk during HPAPI manufacture. *Pharm Technol.* 2015;39(3):50–5.
 17. D. Mark, J.H. Vincent. A new personal sampler for airborne total dust in workplaces. *Ann Occup Hyg.* 1986;30(1):89–102.
 18. L. Gridelet, P. Delbecq, L. Hervé, P. Boissolle, D. Fleury, S. Kowal, et al. Proposal of a new risk assessment method for the handling of powders and nanomaterials. *Ind Health.* 2015;53(1):56–68.
 19. J.A. Gómez, A. García. How to set up a Project for Handling High Potent Products under Isolator. *Ind Quim.* 2022;54–60.
 20. C. Champmartin, F. Clerc. Inhalable dust measurements as a first approach to assessing occupational exposure in the pharmaceutical industry. *J Occup Environ Hyg.* 2014;11(2):85–92.
 21. G. Lidén. Dustiness testing of materials handled at workplaces. *Ann Occup Hyg.* 2006;50(5):437–9.
 22. O. Lazzaro. Choosing containment strategies for highly potent APIs. *Pharm Technol* [Internet]. 2016;40(5):66–9. Available from: <https://www.pharmtech.com/view/choosing-containment-strategies-highly-potent-apis-0>
 23. A.C. Easty, N. Coakley, R. Cheng, M. Cividino, P. Savage, R. Tozer, et al. Safe handling of cytotoxics: Guideline recommendations. *Curr Oncol.* 2015;22(1):e27–37.
 24. S. Bach, E. Schmidt. Determining the dustiness of powders - A comparison of three measuring devices. *Ann Occup Hyg.* 2008;52(8):717–25.
 25. P. Setty. Optimal Handling of Highly Active Pharmaceutical Ingredients during Milling and Blending Operations. Massachusetts Institute of Technology (MIT), Cambridge, MA (USA); 2013.
 26. J. Stein, T. Fuchs, C. Mattern. Advanced Milling and Containment Technologies for Superfine Active Pharmaceutical Ingredients. *Chem Eng Technol.* 2010 Sep;33(9):1464–70.
 27. V. Kanjiyangat, M. Hareendran. Engineering intervention to reduce API dust exposure during milling operation. *J Chem Heal Saf.* 2018;25(1):36–9.
-

-
28. O. Macho, Ľ. Gabrišová, A. Gušťačík, K. Jezso, M. Juriga, J. Kabát, et al. The Influence of Wet Granulation Parameters on the Compaction Behavior and Tablet Strength of a Hydralazine Powder Mixture. *Pharmaceutics*. 2023;15(8).
 29. Z. Zhang, F. He, Y. Zhang, R. Yu, Y. Li, Z. Zheng, et al. Experiments and modelling of potassium release behavior from tablet biomass ash for better recycling of ash as eco-friendly fertilizer. *J Clean Prod*. 2018;170:379–87.
 30. S. Inghelbrecht, J.P. Remon. Reducing dust and improving granule and tablet quality in the roller compaction process. *Int J Pharm*. 1998;171(2):195–206.
 31. F.A. Alhusban, A.M. El-shaer, R.J. Jones, A.R. Mohammed. Recent Patents and Trends in Orally Disintegrating Tablets. *Recent Pat Drug Deliv Formul*. 2010;4(3):178–97.
 32. C. Cowhere, M.A. Grelinger, K.F. Wong. Dust Inhalation Exposures from the Handling of Small Volumes of Powders. *Am Ind Hyg Assoc J*. 1989;50(3):131–8.
 33. L. Kenny. Scientific principles and pragmatic solutions for the measurement of exposure to inhalable dust. *Ann Occup Hyg*. 2003;47(6):437–40.
 34. A. De Werk Neal, R.A. Wadden, W.L. Chiou. Exposure of hospital workers to airborne antineoplastic agents. *Am J Hosp Pharm*. 1983;40(4):597–601.
 35. N.F.J. Van Nimmen, K.L.C. Poels, H.A.F. Veulemans. Identification of exposure pathways for opioid narcotic analgesics in pharmaceutical production workers. *Ann Occup Hyg*. 2006;50(7):665–77.
 36. O. Butler, J. Forder, J. Saunders. Analytical protocol for the sensitive determination of mannitol, sorbitol and glucose containing powders in pharmaceutical workplaces by ion chromatography using a pulsed amperometric detector. *J Pharm Biomed Anal*. 2015;106:204–9.
 37. R.H. Ku. An overview of setting occupational exposure limits (OELs) for pharmaceuticals. *Chem Heal Saf*. 2000;9098(99):34–7.
 38. V. Ahuja, M. Krishnappa. Approaches for setting occupational exposure limits in the pharmaceutical industry. *J Appl Toxicol*. 2022;42(1):154–67.
 39. T. Calkins. Containment of high-potency products in a GMP environment. *Bioprocess Int*. 2010;8(8):14–8.
 40. E. V. Sargent, E. Faria, T. Pfister, R.G. Sussman. Guidance on the establishment of acceptable daily exposure limits (ADE) to support Risk-Based Manufacture of Pharmaceutical Products. *Regul Toxicol Pharmacol*. 2013;65(2):242–50.
-

-
41. G.D. Nielsen, S. Øvrebø. Background, approaches and recent trends for setting health-based occupational exposure limits: A minireview. *Regul Toxicol Pharmacol.* 2008;51(3):253–69.
 42. D.J. Paustenbach, D.M. Cowan, J. Sahmel. The History and Biological Basis of Occupational Exposure Limits for Chemical Agents. *Patty's Ind Hyg.* 2011;865–955.
 43. S. Karthikeyan, J.A. Inbaraj, P. Thangavel, D. Deepa, N. Saravanan, R. Karthikeyan. Selection of Containment System for Handling Cytotoxic Drugs in Pharmaceutical Industry. *Educ Adm Theory Pract.* 2024;30(4):6806–11.
 44. S.C. Hu, A. Shiue, H.Y. Liu, R. Ben Chiu. Validation of contamination control in rapid transfer port chambers for pharmaceutical manufacturing processes. *Int J Environ Res Public Health.* 2016;13(11).
 45. M. Levin, I.K. Koponen, K.A. Jensen. Exposure assessment of four pharmaceutical powders based on dustiness and evaluation of damaged HEPA filters. *J Occup Environ Hyg.* 2014;11(3):165–77.
 46. S.P. Binks. Occupational toxicology and the control of exposure to pharmaceutical agents at work. *Occup Med (Chic Ill).* 2003;53(6):363–70.
 47. International Society for Pharmaceutical Engineers. Good Practice Guide: Assessing the Particulate Containment Performance of Pharmaceutical Equipment. 2nd ed. Wood JP, editor. Tampa, Florida: ISPE (International Society for Pharmaceutical Engineering); 2012. 100 p.
 48. J.H. Vincent. Aerosol sampling: Science, Standards, Instrumentation and Applications. West Sussex: John Wiley & Sons, Inc; 2007. 0–470 p.
 49. B.D. Naumann, E. V. Sargent, B.S. Starkman, W.J. Fraser, G.T. Becker, G.D. Kirk. Performance-based exposure control limits for pharmaceutical active ingredients. *Am Ind Hyg Assoc J.* 1996;57(1):33–42.
 50. C.C. Cosner. Industrial Hygiene in the Pharmaceutical and Consumer Healthcare Industries. 1st Editio. Boca Raton: CRC Press; 2023. 178 p.
 51. E.P. Hayes, R.A. Jolly, E.C. Faria, E.L. Barle, J.P. Bercu, L.R. Molnar, et al. A harmonization effort for acceptable daily exposure application to pharmaceutical manufacturing – Operational considerations. *Regul Toxicol Pharmacol.* 2016;79:S39–47.
 52. D.A. Basketter, C. Broekhuizen, M. Fieldsend, S. Kirkwood, R. Mascarenhas, K. Maurer, et al. Defining occupational and consumer exposure limits for enzyme protein respiratory allergens under REACH. *Toxicology.* 2010;268(3):165–70.
-

-
53. J.A. Krajewski, S. Tarkowski, M. Cyprowski, J. Szarapińska-Kwaszewska, B. Dudkiewicz. Occupational exposure to organic dust associated with municipal waste collection and management. *Int J Occup Med Environ Health*. 2002;15(3):289–301.
 54. European Parliamentary Research Service. Protection of workers from exposure to carcinogens or mutagens. Brussels (Belgium): European Parliament; 2018.
 55. J.P. Bercu, E.J. Morinello, C. Sehner, B.K. Shipp, P.A. Weideman. Point of departure (PoD) selection for the derivation of acceptable daily exposures (ADEs) for active pharmaceutical ingredients (APIs). *Regul Toxicol Pharmacol*. 2016;79:S48–56.
 56. R.G. Sussman, B.D. Naumann, T. Pfister, C. Sehner, C. Seaman, P.A. Weideman. A harmonization effort for acceptable daily exposure derivation – Considerations for application of adjustment factors. *Regul Toxicol Pharmacol*. 2016;79:S57–66.
 57. M.J. Olson, E.C. Faria, E.P. Hayes, R.A. Jolly, E.L. Barle, L.R. Molnar, et al. Issues and approaches for ensuring effective communication on acceptable daily exposure (ADE) values applied to pharmaceutical cleaning. *Regul Toxicol Pharmacol*. 2016;79(2016):S19–27.
 58. J.F. Reichard, M.A. Maier, B.D. Naumann, A.M. Pecquet, T. Pfister, R. Sandhu, et al. Toxicokinetic and toxicodynamic considerations when deriving health-based exposure limits for pharmaceuticals. *Regul Toxicol Pharmacol*. 2016;79:S67–78.
 59. Volkmann GmbH. Handling von kritischen und toxischen Stoffen bis OEB 6 [Internet]. Handling von kritischen und toxischen Stoffen bis OEB 6. 2020 [cited 2025 Apr 29]. Available from: <https://volkmann.info/news/containment-oeb-5-handling-von-kritischen-und-toxischen-stoffen/>
 60. D.E. Evans, L.A. Turkevich, C.T. Roettgers, G.J. Deye, P.A. Baron. Dustiness of fine and nanoscale powders. *Ann Occup Hyg*. 2013 Mar;57(2):261–77.
 61. S. Chakravarty, M. Fischer, O. Le Bihan, M. Morgeneyer. Towards a theoretical understanding of dustiness. *Granul Matter*. 2019;21(4):1–22.
 62. G. Lidén, L.C. Kenny. Errors in inhalable dust sampling for particles exceeding 100 μm . *Ann Occup Hyg*. 1994;38(4):373–84.
 63. S. Hesse, S. Hahn, K. Schroeder, I. Mangelsdorf, J. Lamb, M. Van Tongeren. Evaluation of Tier 1 Exposure Assessment Models under REACH (eteam) Project - Substudy Report on Uncertainty of Tier 1 Models. 2015.
 64. T.L. Ogden, J.L. Birkett. An inhalable-dust sampler, for measuring the hazard from total airborne particulate. *Ann Occup Hyg*. 1978;21(1):41–50.
-

-
65. R.G. Sussman, A.R. Schatz, T.A. Kimmel, A. Ader, B.D. Naumann, P.A. Weideman. Identifying and assessing highly hazardous drugs within quality risk management programs. *Regul Toxicol Pharmacol.* 2016;79:S11–8.
 66. E. V. Sargent, A. Flueckiger, E.L. Barle, W. Luo, L.R. Molnar, R. Sandhu, et al. The regulatory framework for preventing cross-contamination of pharmaceutical products: History and considerations for the future. *Regul Toxicol Pharmacol.* 2016;79:S3–10.
 67. F. Hamelmann, E. Schmidt. Methods of estimating the dustiness of industrial powders – A review. *KONA Powder Part J.* 2003;21(March):7–18.
 68. J. Lanning, M.A.G. Boundy, D. Leith. Validating a model for the prediction of dust generation. *Part Sci Technol.* 1995;13(2):105–16.
 69. J.M. Berg, J.L. Tymoczko, G.J. Gatto, L. Stryer. *Biochemie*. 8th ed. Stryer *Biochemie*. Berlin (Germany): Springer Spektrum; 2018. 1401 p.
 70. A.M. Kaleem, J. Koilpillai, D. Narayanasamy. Mastering Quality: Uniting Risk Assessment With Quality by Design (QbD) Principles for Pharmaceutical Excellence. *Cureus.* 2024;16(8).
 71. R. Gowland. The accidental risk assessment methodology for industries (ARAMIS)/layer of protection analysis (LOPA) methodology: A step forward towards convergent practices in risk assessment? *J Hazard Mater.* 2006;130(3 SPEC. ISS.):307–10.
 72. R.F. Phalen, W.C. Hinds, L. Angeles, W. John, I. Researcher, P.J. Liroy. Particle Size-Selective Sampling in the Workplace: Rationale and Recommended Techniques. *Ann Occup Hyg.* 1988;32(December 2016):403–11.
 73. T. Ohta, H. Maeda, R. Kubota, A. Koga, K. Terada. Establishment of powder dustiness evaluation method by dustmeter with small amount of pharmaceutical ingredients. *Int J Pharm.* 2014;472(1–2):251–6.
 74. M.G. Plinke, M. A., Leith, D., Holstein, D. B., & Boundy. Experimental examination of factors that affect dust generation. *Am Ind Hyg Assoc J.* 1991;52(12):521–8.
 75. T. Deng, K.A. Paul, M.S.A. Bradley, L. Immins, C. Preston, J.F. Scott, et al. Investigations on air induced segregation of pharmaceutical powders and effect of material flow functions. *Powder Technol.* 2010;203(2):354–8.
 76. K. Hjemsted, T. Schneider. Dustiness from powder materials. *J Aerosol Sci.* 1996;27(SUPPL.1):S485–6.
 77. S. Chakravarty, O. Le Bihan, M. Fischer, M. Morgeneyer. Dust generation in powders: Effect of particle size distribution. *EPJ Web Conf.* 2017;140:1–4.
-

-
78. P.T. O'Shaughnessy, M. Kang, D. Ellickson. A novel device for measuring respirable dustiness using low-mass powder samples. *J Occup Environ Hyg.* 2012;9(3):129–39.
 79. S. Armenta, M. Blanco. Ion mobility spectrometry: A comprehensive and versatile tool for occupational pharmaceutical exposure assessment. *Anal Chem.* 2012;84(10):4560–8.
 80. M.A.E. Plinke, R. Maus, D. Leith. Experimental examination of factors that affect dust generation by using Heubach and MRI testers. *Am Ind Hyg Assoc J.* 1992;53(5):325–30.
 81. A. Klippel, M. Schmidt, U. Krause. Dustiness in workplace safety and explosion protection - Review and outlook. *J Loss Prev Process Ind.* 2015;34:22–9.
 82. J.W. Cherrie, A.T. Gillies, A. Sleuwenhoek, M. Van Tongeren, P. McDonnell, M. Coggins, et al. Modelling exposure to pharmaceutical agents. *J Phys Conf Ser.* 2009;151.
 83. H. Hurychová, M. Kuentz, Z. Šklubalová. Fractal Aspects of Static and Dynamic Flow Properties of Pharmaceutical Excipients. *J Pharm Innov.* 2018;13(1):15–26.
 84. F. Podczec. Adhesion forces in interactive powder mixtures of a micronized drug and carrier particles of various particle size distributions. *J Adhes Sci Technol.* 1998;12(12):1323–39.
 85. F. Hamelmann, E. Schmidt. Methods for characterizing the dustiness estimation of powders. *Chem Eng Technol.* 2004;27(8):844–7.
 86. S. Bach, U. Eickmann, E. Schmidt. Comparison of established systems for measuring the dustiness of powders with the UNC dustiness tester developed especially for pharmaceutical substances. *Ann Occup Hyg.* 2013;57(8):1078–86.
 87. C.P. Pujara, D.O. Kildsig. Effect of Individual Particle Characteristics on Airborne Emissions. In: Wood JP, editor. *Containment in the Pharmaceutical Industry*. 1st Editio. New York (USA): CRC Press; 2020. p. 29–53.
 88. M.A.E. Plinke, D. Leith, M.G. Boundy, F. Löffler. Dust generation from handling powders in industry. *Am Ind Hyg Assoc J.* 1995 Mar 1;56(3):251–7.
 89. I. Pensis, J. Mareels, D. Dahmann, D. Mark. Comparative evaluation of the dustiness of industrial minerals according to European standard EN 15051. *Ann Occup Hyg.* 2010;54(2):204–16.
-

-
90. C.P. Pujara. Determination of factors that affect the generation of airborne particles from bulk pharmaceutical powders. Dissertations and Theses. [West Lafayette, Indiana (USA)]: Purdue University; 1997.
 91. S. Chakravarty, M. Fischer, P. García-Triñanes, M. Dalle, L. Meunier, O. Aguerre-Chariol, et al. Long-term dust generation from silicon carbide powders. *Process Saf Environ Prot.* 2018;116:115–25.
 92. S.A. Sethi, T. Schneider. A gas fluidization dustiness tester. *J Aerosol Sci.* 1996;27(SUPPL.1):S305–6.
 93. D. Leith. Drag on nonspherical objects. *Aerosol Sci Technol.* 1987;6(2):153–61.
 94. X. Fu, D. Huck, L. Makein, B. Armstrong, U. Willen, T. Freeman. Effect of particle shape and size on flow properties of lactose powders. *Particuology.* 2012;10(2):203–8.
 95. T. Schneider, K.A. Jensen. Combined single-drop and rotating drum dustiness test of fine to nanosize powders using a small drum. *Ann Occup Hyg.* 2008;52(1):23–34.
 96. K.A. Jensen, I.K. Koponen, P.A. Clausen, T. Schneider. Dustiness behaviour of loose and compacted Bentonite and organoclay powders: What is the difference in exposure risk? *J Nanoparticle Res.* 2009;11(1):133–46.
 97. U. Bröckel, M. Wahl, R. Kirsch, H.J. Feise. Formation and growth of crystal bridges in bulk solids. *Chem Eng Technol.* 2006;29(6):691–5.
 98. M. Boundy, D. Leith, T. Polton. Method to evaluate the dustiness of pharmaceutical powders. *Ann Occup Hyg.* 2006;50(5):453–8.
 99. M. Morgeneyer, O. Le Bihan, A. Ustache, O. Aguerre-Chariol. Experimental study of the aerosolization of fine alumina particles from bulk by a vortex shaker. *Powder Technol.* 2013;246:583–9.
 100. J. Visser. Van der Waals and other cohesive forces affecting powder fluidization. *Powder Technol.* 1989;58(1):1–10.
 101. A. Santomaso, P. Lazzaro, P. Canu. Powder flowability and density ratios: The impact of granules packing. *Chem Eng Sci.* 2003;58(13):2857–74.
 102. E. Marring, A.C. Hoffmann, L.P.B.M. Janssen. The effect of vibration on the fluidization behaviour of some cohesive powders. *Powder Technol.* 1994;79(1):1–10.
-

-
103. G. Nichols, S. Byard, M.J. Bloxham, J. Botterill, N.J. Dawson, A. Dennis, et al. A review of the terms agglomerate and aggregate with a recommendation for nomenclature used in powder and particle characterization. *J Pharm Sci.* 2002;91(10):2103–9.
 104. X.L. Chen, C.A. Wheeler, T.J. Donohue, R. McLean, A.W. Roberts. Evaluation of dust emissions from conveyor transfer chutes using experimental and CFD simulation. *Int J Miner Process.* 2012;110–111:101–8.
 105. B. Stahlmecke, S. Wagener, C. Asbach, H. Kaminski, H. Fissan, T.A.J. Kuhlbusch. Investigation of airborne nanopowder agglomerate stability in an orifice under various differential pressure conditions. *J Nanoparticle Res.* 2009;11(7):1625–35.
 106. A. Castellanos. The relationship between attractive interparticle forces and bulk behaviour in dry and uncharged fine powders. *Adv Phys.* 2005;54(4):263–376.
 107. P.M. Young, A. Sung, D. Traini, P. Kwok, H. Chiou, H.K. Chan. Influence of humidity on the electrostatic charge and aerosol performance of dry powder inhaler carrier based systems. *Pharm Res.* 2007;24(5):963–70.
 108. T. Nomura, T. Satoh, H. Masuda. The environment humidity effect on the tribo-charge of powder. *Powder Technol.* 2003;135–136:43–9.
 109. P.C.L. Kwok, H.K. Chan. Effect of relative humidity on the electrostatic charge properties of dry powder inhaler aerosols. *Pharm Res.* 2008;25(2):277–88.
 110. A.G. Bailey. Electrostatic phenomena during powder handling. *Powder Technol.* 1984;37(1):71–85.
 111. O.L.C. Le Bihan, A. Ustache, D. Bernard, O. Aguerre-Chariol, M. Morgeneyer. Experimental study of the aerosolization from a carbon nanotube bulk by a vortex shaker. *J Nanomater.* 2014;2014.
 112. T.E. Gill, T.M. Zobeck, J.E. Stout. Technologies for laboratory generation of dust from geological materials. *J Hazard Mater.* 2006;132(1 SPEC. ISS.):1–13.
 113. K. Saleh, M.T. Moufarej Abou Jaoude, M. Morgeneyer, E. Lefrancois, O. Le Bihan, J. Bouillard. Dust generation from powders: A characterization test based on stirred fluidization. *Powder Technol.* 2014;255:141–8.
 114. K. Hjemsted, T. Schneider. Documentation of a dustiness drum test. *Ann Occup Hyg.* 1996;40(6):627–43.
 115. A.D. Maynard, P.A. Baron, M. Foley, A.A. Shvedova, E.R. Kisin, V. Castranova. Exposure to carbon nanotube material: Aerosol release during the handling of unrefined single-walled carbon nanotube material. *J Toxicol Environ Heal - Part A.* 2004;67(1):87–107.
-

-
116. I. Ogura, H. Sakurai, M. Gamo. Dustiness testing of engineered nanomaterials. *J Phys Conf Ser.* 2009;170:0–4.
 117. M. Duan, Y. Wang, X. Ren, X. Qu, Y. Cao, Y. Yang, et al. Correlation analysis of three influencing factors and the dust production rate for a free-falling particle stream. *Particuology.* 2017;34:126–33.
 118. Y. Wang, X. Ren, J. Zhao, Z. Chu, Y. Cao, Y. Yang, et al. Experimental study of flow regimes and dust emission in a free falling particle stream. *Powder Technol.* 2016;292:14–22.
 119. R. Ansart, A. de Ryck, J.A. Dodds. Dust emission in powder handling: Free falling particle plume characterisation. *Chem Eng J.* 2009;152(2–3):415–20.
 120. D.A. Lundgren. A measurement technique to quantitate fugitive dust emission from handling of granular products. *J Aerosol Sci.* 1986;17(3):632–4.
 121. R. Ansart, A. de Ryck, J.A. Dodds, M. Roudet, D. Fabre, F. Charru. Dust emission by powder handling: Comparison between numerical analysis and experimental results. *Powder Technol.* 2009;190(1–2):274–81.
 122. Y. Ding, B. Stahlmecke, H. Kaminski, Y. Jiang, T.A.J. Kuhlbusch, M. Riediker. Deagglomeration testing of airborne nanoparticle agglomerates: Stability analysis under varied aerodynamic shear and relative humidity conditions. *Aerosol Sci Technol.* 2016;50(11):1253–63.
 123. Y. Ding, M. Riediker. A system to assess the stability of airborne nanoparticle agglomerates under aerodynamic shear. *J Aerosol Sci.* 2015;88:98–108.
 124. J.C. Chow, J.G. Watson, J.E. Houck, L.C. Pritchett, C. Fred Rogers, C.A. Frazier, et al. A laboratory resuspension chamber to measure fugitive dust size distributions and chemical compositions. *Atmos Environ.* 1994;28(21):3463–81.
 125. European Committee for Standardization. Workplace atmospheres - Measurement of the dustiness of bulk materials - Requirements and reference test methods. Brussels (Belgium): European Committee for Standardization; 2006. 24 p.
 126. Air quality — Particle size fraction definitions for health-related sampling (ISO 7708:1995). Geneva (Switzerland); 1995.
 127. H. Chen, M.A. Jog, L.A. Turkevich. Computational fluid dynamics simulations of aerosol behavior in a high-speed (Heubach) rotating drum dustiness tester. *Particuology.* 2023;72:68–80.
 128. M. Gawol, G. Adrian. Permanently non-dusting pigment and dye preparations, method for producing them, and measuring device therefore. USA: United States Patent and Trademark Office; US4762523, 1988. p. 5.
-

-
129. W.A. Heitbrink, W.F. Todd, T.J. Fischbach. Correlation of tests for material dustiness with worker exposure from the bagging of powders. *Appl Ind Hyg*. 1989;4(1):12–6.
 130. A. Toman, Z. Dyduch, T. Skowronek. Prototype device for measuring the dustiness of stone and lime dust used in explosion prevention. *J Sustain Min*. 2024;23(3):327–36.
 131. T. Londershausen, E. Schmidt. Development of Forecast Formulas for Assessing the Dust Formation Tendency of Moist Bulk Materials Using the UNC Dustiness Tester. *Chem Eng Technol*. 2018;41(11):2259–65.
 132. P. Dubey, U. Ghia, L.A. Turkevich. Computational fluid dynamics analysis of the Venturi Dustiness Tester. *Powder Technol*. 2017;312(February):310–20.
 133. D.E. Evans, L.A. Turkevich, C.T. Roettgers, G.J. Deye. Comment on comparison of powder dustiness methods. *Ann Occup Hyg*. 2014;58(4):524–8.
 134. K.H. Carlson, D.R. Herman, T.F. Markey, R.K. Wolff, M.A. Dorato. A comparison of two dustiness evaluation methods. *Am Ind Hyg Assoc J*. 1992;53(7):448–54.
 135. V. Aizenberg, S.A. Grinshpun, K. Willeke, J. Smith, P.A. Baron. Performance characteristics of the button personal inhalable aerosol sampler. *Am Ind Hyg Assoc J*. 2000;61(3):398–404.
 136. Y. Zhou, Y.S. Cheng. Evaluation of IOM personal sampler at different flow rates. *J Occup Environ Hyg*. 2009;7(2):88–93.
 137. J.H. Vincent, D. Mark. The basis of dust sampling in occupational hygiene: A critical review. *Ann Occup Hyg*. 1981;24(4):375–90.
 138. R.M. Buchan, S.C. Soderholm, M.I. Tillery. Aerosol Sampling Efficiency of 37 mm Filter Cassettes. *Am Ind Hyg Assoc J*. 1986;47(12):825–31.
 139. D.L. Bartley. Inhalable aerosol samplers. *Appl Occup Environ Hyg*. 1998;13(5):274–8.
 140. SKC Ltd. IOM Sampler Instructions [Internet]. IOM Sampler Instructions. 2024 [cited 2025 May 29]. Available from: <https://www.skcltd.com/images/pdfs/007-05-003.pdf>
 141. N.P. Vaughan, C.P. Chalmers, R.A. Botham. Field comparison of personal samplers for inhalable dust. *Ann Occup Hyg*. 1990;34(6):553–73.
 142. M. Harper. A review of workplace aerosol sampling procedures and their relevance to the assessment of beryllium exposures. *J Environ Monit*. 2006;8(6):598–604.
-








-
143. J. Zheng. Formulation and analytical development for low-dose oral drug products. Hoboken (USA): John Wiley & Sons, Inc; 2009. 476 p.
 144. J. Abitha. The Containment Performance Verification and Determination of Surrogate Particles. *DJ Int J Adv Microbiol Microbiol Res.* 2016;1(1):14–21.
 145. A.S. Wilkinson, M.C. Allwood, C.P. Morris, A. Wallace, R. Finnis, E. Kaminska, et al. Performance testing protocol for closed-system transfer devices used during pharmacy compounding and administration of hazardous drugs. *PLoS One.* 2018;13(10):1–15.
 146. A. Sayma. Computational Fluid Dynamics. Computational Fluid Dynamics. Copenhagen: Ventus Publishing ApS / BookBoon; 2009. 133 p.
 147. J. Wendt. Computational Fluid Dynamics. John F. Wendt, editor. New York (USA): McGraw-Hill; 1995.
 148. Griffith. Immersed Methods for Fluid–Structure Interaction. *Physiol Behav.* 2016;176(1):100–106.
 149. G. Hou, J. Wang, A. Layton. Numerical methods for fluid-structure interaction - A review. *Commun Comput Phys.* 2012;12(2):337–77.
 150. H. Bandringa. Immersed boundary methods. *International Journal for Numerical Methods in Fluids.* University of Groningen; 2010.
 151. N. Lavanya, S. Bhattacharyya. Computational fluid dynamics-the futuristic innovation in pharmaceutical industry. *Indian J Pharm Educ Res.* 2021;55(4):930–8.
 152. H.S. Pordal, C.J. Matice, T.J. Fry. The role of computational fluid dynamics in the pharmaceutical industry. *Pharm Technol.* 2002;26(2):72–9.
 153. G. Tian, M. Hindle, S. Lee, P.W. Longest. Validating CFD Predictions of Pharmaceutical Aerosol Deposition with in Vivo Data. *Pharm Res.* 2015;32(10):3170–87.
 154. C.A. Ruzycki, E. Javaheri, W.H. Finlay. The use of computational fluid dynamics in inhaler design. *Expert Opin Drug Deliv.* 2013;10(3):307–23.
 155. W. Longest, D. Farkas. Development of a New Inhaler for High-Efficiency Dispersion of Spray-Dried Powders Using Computational Fluid Dynamics (CFD) Modeling. *AAPS J.* 2019;21(2).
 156. Q. Zhu, M. Kakhi, C. Jayasundara, R. Walenga, S.R.B. Behara, H.K. Chan, et al. CFD-DEM investigation of the effects of aperture size for a capsule-based dry powder inhaler. *Int J Pharm.* 2023;647(July):123556.
-

-
157. L.C. Almeida, R. Bharadwaj, A. Eliahu, C.R. Wassgren, K. Nagapudi, A.R. Muliadi. Capsule-Based dry powder inhaler evaluation using CFD-DEM simulations and next generation impactor data. *Eur J Pharm Sci.* 2022;175(May):106226.
 158. A. Kritikos, R. Singh, G. Tsilomelekis, F.J. Muzzio. A Novel CFD Model of SMX Static Mixer Used in Advanced Continuous Manufacturing of Active Pharmaceutical Ingredients (API). *J Pharm Innov.* 2024;19(2).
 159. K. Ahookhosh, M. Saidi, H. Aminfar, M. Mohammadpourfard, H. Hamishehkar, S. Yaqoubi. Dry powder inhaler aerosol deposition in a model of tracheobronchial airways: Validating CFD predictions with in vitro data. *Int J Pharm.* 2020;587(June):119599.
 160. A. Pohar. A Review of Computational Fluid Dynamics (CFD) Simulations of Mixing in the Pharmaceutical Industry. *Biomed J Sci Tech Res.* 2020;27(3):20732–6.
 161. P.W. Longest, D. Farkas, A. Hassan, M. Hindle. Computational Fluid Dynamics (CFD) Simulations of Spray Drying: Linking Drying Parameters with Experimental Aerosolization Performance. *Pharm Res.* 2020;37(6):1–20.
 162. H. Aziz, S.N. Ahsan, G. De Simone, Y. Gao, B. Chaudhuri. Computational Modeling of Drying of Pharmaceutical Wet Granules in a Fluidized Bed Dryer Using Coupled CFD-DEM Approach. *AAPS PharmSciTech.* 2022;23(1):1–19.
 163. N.K. Palakurthi. Aerodynamics of Particle Detachment from Surfaces – A Numerical Study. University of Cincinnati; 2013.
 164. S. Hemamanjushree, V.K. Tippavajhala. Simulation of Unit Operations in Formulation Development of Tablets Using Computational Fluid Dynamics. *AAPS PharmSciTech.* 2020;21(3):1–13.
 165. H. Pan, X.Z. Chen, X.F. Liang, L.T. Zhu, Z.H. Luo. CFD simulations of gas-liquid-solid flow in fluidized bed reactors - A review. *Powder Technol.* 2016;299:235–58.
 166. L. Liu, Y. Huang. HVAC Design Optimization for Pharmaceutical Facilities with BIM and CFD. *Buildings.* 2024;14(6).
 167. H. Metwally, E.E. Khalil, T. Abou. Air Quality and Flow Regimes at Clean Room. *Jt Thermophys Heat Transf Conf.* 2018;1–13.
 168. L. Lestari, R. Permatasari. Return Air Grille Position in a Cleanroom for Medicinal Packaging Using CFD Method. *J Phys Conf Ser.* 2024;2739(1).
-

-
169. F.Y. Zhao, J. Cheng, B. Liu, Z.R. Huang, Y.J. Zhang, X. Li. Regional flow motion and heat energy balance analysis of a 10,000 class pharmaceutical cleanroom with secondary return air conditioning system. *Int J Refrig.* 2021;129:237–49.
 170. S. Wirth, M. Schöler, J. Brüggmann, C.S. Leopold. A Novel Two-Chamber Setup for Containment Investigations with Special Focus on the Dustiness of Pharmaceutical Powders Depending on the Airflow. *Pharmaceutics.* 2022;14(11):2387.
 171. S. Wirth, M. Schöler, J. Brüggmann, C.S. Leopold. An Investigation on the Relationship between Dust Emission and Air Flow as Well as Particle Size with a Novel Containment Two-Chamber Setup. *Pharmaceutics.* 2024;16(8).
 172. S. Wirth, M. Schöler, C.S. Leopold. Investigations on the dustiness of binary acetaminophen - lactose monohydrate powder blends. *Powder Technol.* 2024;448(September).
-

Appendix

Hazardous materials

Substance	Supplier	Danger symbol	Hazard statements	Precautionary statements
Methanol	VRW, USA	  	H225, H301, H311, H331, H370	P210, P233, P260, P280, P303+P361+P353, P304+P340, P310
Acetonitrile	VRW, USA	 	H225, H302, H312, H332	P210, P280, P301+P312, P304+P340, P403+P233
Acetaminophen	Caelo, Germany Fagron, Germany		H373	P260, P314, P501
Lactose Monohydrate	Meggle, Germany		None	P261, P280
Sulfuric Acid	Dräger, Germany		H290, H314	P260, P280, P303+P361+P353, P305+P351+P338, P310, P405

List of figures

Figure 1: Overview of OEBs, OELs and ADEs and their relationship.	6
Figure 2: Schematic illustration of the Continuous Drop Test Apparatus.	14
Figure 3: Simplified illustration of the Heubach Dustmeter, highlighting its main components.	15
Figure 4: Illustration of the Palas Dustview with its setup and operational principle.	16
Figure 5: Schematic illustration of the UNC Dustiness Tester.	18
Figure 6: Design of an IOM sampler.	20
Figure 7: Illustrative summary of methodology and main outcomes of the study.	32
Figure 8: Comprehensive depiction of the study design and key results.	53
Figure 9: Visual representation of the essential features and outcome of the study.	72

List of tables

Table 1: OEB classification system.	5
Table 2: Overview of methods and devices for measuring dust emission.	13
Table 3: Challenges during handling HPAPIs.	22
Table 4: Criteria for selecting surrogate substances.	23
Table 5: Summarised properties of potential surrogate substances.	24

Curriculum vitae

Name:	Wirth, Steffen	Date of birth:	Sep 5 th , 1992
Marital status:	unmarried	Place of birth:	Oldenburg

Education	since 11/2018	Ph.D. student, Division of Pharmaceutical Technology Universität Hamburg Supervisor: Prof. Dr. Dr. h.c. C.S. Leopold
	07/2018	Licensure as a pharmacist (Approbation)
	04/2013 - 05/2017	Study of Pharmacy, Christian-Albrechts-Universität zu Kiel
Specialization	since 2019	„Fachapotheker für Pharmazeutische Analytik und Technologie“
Internships	12/2017	Intern, antares-apotheken oHG im Struensee-Haus
	06/2017	Intern, University of Copenhagen - Department of Pharmacy
School	2011	A-level diploma, Jade-Gymnasium, Jaderberg

Acknowledgements

This dissertation was conducted at the University of Hamburg, in the Department of Chemistry, within the division of Pharmaceutical Technology. It was initiated and supervised by Professor Dr. Dr. h.c. Claudia S. Leopold. At this point, I would like to express my gratefulness to all those who supported and enriched this work.

My special thanks go to Prof. Dr. Dr. h.c. Claudia S. Leopold for providing this challenging and fascinating research topic and for welcoming me into her research group. Her expertise and inspiring discussions significantly contributed to the success of this dissertation.

I am deeply grateful to Dr. Martin Schöler for his dedicated co-supervision and constructive collaboration. His support and valuable advice were indispensable for this work.

I want to extend my thanks to Dr. Albrecht Sakmann for his assistance and the fruitful exchange regarding the organisation and implementation of teaching activities. I am also grateful to Petra Borbe and Kai Braunschweig for their technical expertise and support in conducting and analysing various experiments.

Special thanks go to Jonas Brüggmann for his guidance and patient introduction to the methodology of CFD simulations. His assistance greatly facilitated my engagement with this complex field.

I would also like to thank the entire research group of Pharmaceutical Technology for the collegial and supportive environment. Working with them has been both productive and personally enriching.

My heartfelt thanks go to Cristian Kulcitki, Simon Schulte-Herbrüggen, Hendrik Küllmar, and Daniel Lutz for carefully proofreading this dissertation. Their feedback and suggestions have significantly enhanced the quality of this work.

I deeply appreciate my friends for their understanding and patience throughout the past years.

Finally, I am deeply indebted to my parents for their unwavering support and trust throughout this journey. I would also like to extend my heartfelt thanks to Svenja Giese. Her patience, encouragement, and support have been invaluable over the past years and crucial in completing this work.

Declaration on oath / Eidesstattliche Versicherung

Hiermit versichere ich an Eides statt, die vorliegende Dissertationsschrift selbst verfasst und keine anderen als die angegebenen Quellen und Hilfsmittel benutzt zu haben. Sofern im Zuge der Erstellung der vorliegenden Dissertationsschrift generative Künstliche Intelligenz (gKI) basierte elektronische Hilfsmittel verwendet wurden, versichere ich, dass meine eigene Leistung im Vordergrund stand und dass eine vollständige Dokumentation aller verwendeten Hilfsmittel gemäß der Guten wissenschaftlichen Praxis vorliegt. Ich trage die Verantwortung für eventuell durch die gKI generierte fehlerhafte oder verzerrte Inhalte, fehlerhafte Referenzen, Verstöße gegen das Datenschutz- und Urheberrecht oder Plagiate

Datum, Unterschrift
